ABSTRACT

Title of dissertation: A CLASS OF EFFICIENT, STABLE NAVIER-STOKES SOLVERS

Jie Liu, Doctor of Philosophy, 2006

Dissertation directed by: Dr. Jian-Guo Liu
Department of Mathematics

We study a class of numerical schemes for Navier-Stokes equations (NSE) or Stokes equations (SE) for incompressible fluids in a bounded domain with given boundary value of velocity.

The incompressibility constraint and non-slip boundary condition have made this problem very challenging. Their treatment by finite element method leads to the well-known inf-sup compatibility condition. Their treatment by finite difference method leads to the very popular projection method, which suffers from low resolution near the boundary.

In [LLP], the authors propose an unconstrained formulation of NSE or SE, which replace the divergence-free constraint by a pressure equation with an appropriate boundary condition. All of the schemes in this thesis are based on this new formulation. In contrast to traditional methods, these schemes do not need to fulfill the traditional inf-sup compatibility condition between velocity space and pressure space. More importantly, they can achieve high-order accuracy very easily and are very efficient due to the decoupling of the update of velocity and pressure. They

can even be proved to be unconditionally stable.

There are two ways to analyze the schemes that we propose. The first is based upon the sharp estimate of the pressure in [LLP]. The second relies on a nice identity.

Using the pressure estimates, we propose and study a C^1 finite element (FE) scheme for the steady-state SE as well as for the time-dependent NSE. For steady-state SE, we can either use an iterative scheme or solve velocity and pressure together.

Using the nice identity, we prove that the semi-discrete iterative scheme for the steady-state SE converges ("semi-discrete" means that the spatial variable are kept continuous). This identity will also be crucial for our proofs of the stability and error estimates of the time-dependent C^0 FE schemes.

Associated numerical computations demonstrate stability and accuracy of these schemes.

We also present the numerical results of yet another C^0 FE scheme ([JL]) for the time-dependent NSE for which the theory of the fully discrete case is yet lacking.

A CLASS OF STABLE, EFFICIENT NAVIER-STOKES SOLVERS

by

Jie Liu

Dissertation submitted to the Faculty of the Graduate School of the
University of Maryland, College Park in partial fulfillment
of the requirements for the degree of
Doctor of Philosophy
2006

Advisory Committee:
Dr. Jian-Guo Liu, Chair/Advisor
Dr. Stuart Antman
Dr. David Levermore
Dr. Ugo Piomelli
Dr. Eitan Tadmor
Dr. Athanasios Tzavaras

ACKNOWLEDGMENTS

First of all, I would like to take this opportunity to thank Dr. Liu for all his teaching and helping through all these years. Thank him for taking so much time to teach me from which I learned almost every mathematics I have working knowledge of. Thank him for showing me through his own work on how to work on a mathematics problem, for telling me to "put my heart into it when working on a problem" and for making me to believe that "nothing is impossible" and feel confident when searching for the solution.

Thanks are due to the teaching of Drs Antman, Levermore, Liu, Piomelli and Tadmor which led me onto the road of computational fluid dynamics — Dr. Antman taught me elasticity, fluid mechanics and electro-magnetism; Dr. Levermore taught me my first numerical PDE course and for the first time showed me the Leray theory of NSE in his kinetic theory course; Dr. Piomelli taught me my first fluid mechanics course as well as my first computational fluid dynamics course. Dr. Tadmor taught me hyperbolic equations, both theoretical and numerical, which I might continue to work on. For Dr. Tadmor, I would also like to express my deep appreciation for his constant encouragement and help on my most difficult times.

I would like to thank Dr. Tzavaras for agreeing to serve on my thesis committee and for sparing his invaluable time reviewing the manuscript.

Although not able to serve on my dissertation committee, Dr. Pego in many

sense is my co-advisor on this project. I thank him for all that he has taught me and given to me.

I thank my colleagues at Maryland, in particular Bin Chen, Zhiwei Chen, Shibin Dai, Ning Jiang, Weiran Sun, Dongming Wei, Linbao Zhang and Dianwen Zhu, for discussing with me and teaching me various kind of mathematics.

Finally and most importantly, I thank my parents for everything they have done for me.

TABLE OF CONTENTS

LIST OF FIGURES

Chapter 1

Introduction

We want to study numerical methods for solving Navier-Stokes equations (NSE) in a bounded domain with given velocity boundary condition. The pressure has long been a source of difficulty. The pressure is a Lagrange multiplier that enforces the incompressibility constraint. This leads to computational difficulties related to the lack of useful boundary conditions for determining the pressure by solving boundary-value problems.

There are several ways to cope with this problem but each has its own drawbacks: Finite element (FE) solvers for this problem require special care to arrange that the approximation spaces for velocity and pressure satisfy a compatibility condition to enforce an inf-sup condition (or Ladyzhenskaya-Babuška-Brezzi condition). Ways of circumventing the compatibility condition have been developed (e.g., stabilized finite-element methods [BBGS]), but at the cost of additional complexity. Projection methods suffers from low resolution near boundaries [OID] (see the Appendix for more details). The vorticity-stream function formulation only works well for simply connected domain in $\mathbb{R}^2$.

In [LLP], a pressure equation is proposed which when combined with the momentum equation, enforces $\nabla \cdot \boldsymbol{u} = 0$ automatically. Hence, one can use this pressure equation to replace the divergence free constraint. Based on this new formulation, a

class of numerical methods for NSE can be designed which are very efficient due to the decoupling of the update of pressure and velocity. Although these new methods treat both pressure and nonlinear convection term explicitly, they are still able to achieve unconditional stability. Equally important, this class of methods can achieve high order accuracy (like 4th order accuracy in time and spectral accuracy in space) very easily, which used to be extremely difficult. Moreover, FE schemes based on this new formulation are able to disregard the traditional compatibility condition.

We will only focus on FE schemes in this thesis and show their mathematical theory as well as numerical results. Let us now start with the simpler steady-state NSE. Later, we will turn to the time-dependent NSE.

1.1 Steady state equations

Consider the steady-state NSE for incompressible fluid flow in a domain Ω in $\mathbb{R}^N$ ($N = 2$ or 3) with given boundary conditions on $\Gamma := \partial\Omega$:

$$\boldsymbol{u}\cdot\nabla\boldsymbol{u} + \nabla p = \nu\Delta\boldsymbol{u} + \boldsymbol{f} \quad \text{in } \Omega, \tag{1.1}$$

$$\nabla\cdot\boldsymbol{u} = 0 \quad \text{in } \Omega, \tag{1.2}$$

$$\boldsymbol{u} = \boldsymbol{g} \quad \text{on } \Gamma. \tag{1.3}$$

Here $\boldsymbol{u}$ is the fluid velocity, p the pressure, and $\nu = 1/\mathrm{Re}$ is the kinematic viscosity coefficient with Re the Reynolds number, assumed to be a fixed positive constant. For consistency, we need to assume

$$\int_\Gamma \boldsymbol{n}\cdot\boldsymbol{g} = 0. \tag{1.4}$$

From (1.1), we see that

$$\nabla p = \nu \Delta \boldsymbol{u} + \boldsymbol{f} - \boldsymbol{u} \cdot \nabla \boldsymbol{u}.$$

In [LLP], an equation for the pressure is proposed

$$\nabla p = \nu (I - \mathcal{P})(\Delta \boldsymbol{u} - \nabla \nabla \cdot \boldsymbol{u}) + (I - \mathcal{P})(\boldsymbol{f} - \boldsymbol{u} \cdot \nabla \boldsymbol{u}), \tag{1.5}$$

which when combined with (1.1) and (1.3) leads to (1.2) (see Lemma 1). In other words, we can replace (1.2) with (1.5); Equations (1.5),(1.1),(1.3) are called unconstrained formulation of NSE. In (1.5), we have used the Helmholtz-Hodge projection operator $\mathcal{P}$ which is defined as follows: By the Poincaré inequality, one can show that $\nabla H^1(\Omega) = \{\nabla g \mid g \in H^1(\Omega)\}$ is a closed subspace of $L^2(\Omega, \mathbb{R}^N)$ and hence we have the orthogonal decomposition

$$L^2(\Omega, \mathbb{R}^N) = (\nabla H^1(\Omega))^\perp \oplus \nabla H^1(\Omega). \tag{1.6}$$

It is the projection from $L^2(\Omega, \mathbb{R}^N)$ onto $(\nabla H^1(\Omega))^\perp$ that is called the Helmholtz-Hodge projetction and is denoted by $\mathcal{P}$.

Note that $(\nabla H^1(\Omega))^\perp$ is composed of those functions which are divergence free and have zero normal component on the boundary. Hence, in strong form, (1.5) can be rewritten as

$$\Delta p = \nabla \cdot (\boldsymbol{f} - \boldsymbol{u} \cdot \nabla \boldsymbol{u}) \qquad \text{in } \Omega, \tag{1.7}$$

$$\boldsymbol{n} \cdot \nabla p = \nu (\Delta \boldsymbol{u} - \nabla \nabla \cdot \boldsymbol{u}) + \boldsymbol{n} \cdot (\boldsymbol{f} - \boldsymbol{u} \cdot \nabla \boldsymbol{u}) \qquad \text{on } \Gamma. \tag{1.8}$$

The unconstrained formulation (1.5),(1.1),(1.3) opens the door to a new class of Navier-Stokes solvers. One advantage of the FE schemes based on this new

formulation is that they do not require the inf-sup compatibility conditions between the FE spaces for the velocity and pressure.

In Chapter 3, we will study those FE schemes for the steady-state SE which either solve for $(\boldsymbol{u}, p)$ together or iteratively. As one can see from the statement of Theorem 4 or Theorem 5, the error estimates of those scheme do not require the inf-sup compatibility conditions.

1.2 Time dependent equations

What is more important about the pressure equation (1.5) is that based on it, one can easily design high-order method (in both time and space) for the time-dependent NSE:

$$\partial_t \boldsymbol{u} + \boldsymbol{u}\cdot\nabla\boldsymbol{u} + \nabla p = \nu\Delta\boldsymbol{u} + \boldsymbol{f} \quad \text{in } \Omega, \tag{1.9}$$

$$\nabla\cdot\boldsymbol{u} = 0 \quad \text{in } \Omega, \tag{1.10}$$

$$\boldsymbol{u} = 0 \quad \text{on } \Gamma, \qquad \boldsymbol{u}(0,x) = \boldsymbol{u}_{\text{in}}(x) \quad \text{in } \Omega. \tag{1.11}$$

Here, for simplicity, we consider no-slip boundary condition. Boundary conditions like (1.3) can be handled similarly [LLP, section 7]. Naturally, we need the following compatibility condition

$$\nabla\cdot\boldsymbol{u}_{\text{in}} = 0 \tag{1.12}$$

As in the steady-state case, one can replace (1.10) with (1.5) and hence obtain the unconstrained formulation of NSE (1.5),(1.9),(1.11) (see Lemma 2).

When solving the time-dependent NSE (1.9)–(1.11), one can achieve simplicity and efficiency through decoupling updates of velocity and pressure by using

projection methods. But projection methods have suffered from low resolution near boundaries, particulary for pressure, a key quantity involved in creating lift, drag, boundary-layer separation, and other phenomena of prime physical interest.

Recently, several groups of researchers have devised schemes that achieve separation of velocity and pressure updates without generating numerical boundary layers, in ways that turn out to be closely related (see [TMV, WL, BCM, HP, Pe, EL, GS1, JL, LLP].) As explained in [LLP] (see also the Appendix), these schemes all emerge, through different means of spatial discretization and higher-order time stepping, from a prototypical first-order time discretization scheme for the unconstrained formulation of NSE (1.5),(1.9),(1.11) and is described as follows: Given an approximation $\boldsymbol{u}^n \in H^2 \cap H_0^1(\Omega, \mathbb{R}^N)$ to the velocity at time $t_n = n\Delta t$, determine $\nabla p^n \in L^2(\Omega, \mathbb{R}^N)$ from (1.5), namely, by solving

$$\langle \nabla p^n, \nabla q \rangle = \langle \boldsymbol{f}^n - \boldsymbol{u}^n \cdot \nabla \boldsymbol{u}^n + \nu \Delta \boldsymbol{u}^n - \nu \nabla \nabla \cdot \boldsymbol{u}^n, \nabla q \rangle \quad \forall q \in H^1(\Omega), \tag{1.13}$$

where $\boldsymbol{f}^n = \boldsymbol{f}(t_n)$, then determine $\boldsymbol{u}^{n+1} \in H^2 \cap H_0^1(\Omega, \mathbb{R}^N)$ from the elliptic boundary-value problem

$$\frac{\boldsymbol{u}^{n+1} - \boldsymbol{u}^n}{\Delta t} - \nu \Delta \boldsymbol{u}^{n+1} = \boldsymbol{f}^n - \boldsymbol{u}^n \cdot \nabla \boldsymbol{u}^n - \nabla p^n, \tag{1.14}$$

$$\boldsymbol{u}^{n+1}\big|_\Gamma = 0. \tag{1.15}$$

1.2.1 C^0 and C^1 FE schemes for time-dependent problem

To facilitate the spatial discretization, equation (1.13) can be reformulated to involve only first-order derivatives of $\boldsymbol{u}^n$, using the vector identity

$$\Delta \boldsymbol{u} - \nabla \nabla \cdot \boldsymbol{u} = -\nabla \times \nabla \times \boldsymbol{u}, \tag{1.16}$$

and the fact that by Green's formula,

$$-\langle \nabla \times \nabla \times \boldsymbol{u}, \nabla q \rangle_\Omega = \langle \nabla \times \boldsymbol{u}, \boldsymbol{n} \times \nabla q \rangle_\Gamma, \tag{1.17}$$

where $\boldsymbol{n}$ is the outward unit normal to $\Gamma = \partial\Omega$. This naturally leads to a class of C^0 finite-element discretizations for the pressure Poisson equation. Let $Y_h \subset H^1(\Omega)/\mathbb{R}$ be a space of C^0 finite elements for pressure, where $h > 0$ is a bounded discretization parameter. Given an approximation $\boldsymbol{u}_h^n$ to $\boldsymbol{u}^n$, we determine $p_h^n \in Y_h$ by requiring that

$$\langle \nabla p_h^n, \nabla q_h \rangle = \langle \boldsymbol{f}^n - \boldsymbol{u}_h^n \cdot \nabla \boldsymbol{u}_h^n, \nabla q_h \rangle + \nu \langle \nabla \times \boldsymbol{u}_h^n, \boldsymbol{n} \times \nabla q_h \rangle_\Gamma \tag{1.18}$$

for all $q_h \in Y_h$.

To discretize the momentum equation (1.14), as proposed in [JL] (also see [GS1]) we can look for the approximate velocity $\boldsymbol{u}_h^{n+1}$ in a standard C^0 finite-element space $X_{0,h} \subset H_0^1(\Omega, \mathbb{R}^N)$, and require

$$\left\langle \frac{\boldsymbol{u}_h^{n+1} - \boldsymbol{u}_h^n}{\Delta t}, \boldsymbol{v}_h \right\rangle + \nu \langle \nabla \boldsymbol{u}_h^{n+1}, \nabla \boldsymbol{v}_h \rangle = \langle -\nabla p_h^n + \boldsymbol{f}^n - \boldsymbol{u}_h^n \cdot \nabla \boldsymbol{u}_h^n, \boldsymbol{v}_h \rangle \tag{1.19}$$

for all $\boldsymbol{v}_h \in X_{0,h}$. This C^0 scheme (1.18),(1.19) is easy to implement and efficient. As noted in [JL], for the most general $\boldsymbol{u}_h^n \in H_0^1(\Omega, \mathbb{R}^N)$ and $q_h \in H^1(\Omega)$, the boundary integral in (1.18) does not make sense. But for piecewise polynomial finite-element spaces, $\nabla \times \boldsymbol{u}_h^n$ and $\boldsymbol{n} \times \nabla q_h$ are also piecewise polynomials on Γ, and therefore in practice there is no trouble to implement that term.

As we report below in section 4.4, the C^0 scheme (1.18),(1.19) appears to be unconditionally stable and convergent in numerical experiments, with no compatibility condition imposed on $X_{0,h}$ and Y_h. The results for driven cavity flow and flow

over a back-facing step achieve high quality with low cost and complexity. But so far, we are unable to provide a rigorous analysis for this scheme. Numerical results for a Legendre-Galerkin method based on (1.18) and (1.19) were reported in [JL].

Using C^1 finite elements for velocity instead yields schemes far more accessible to analysis (though less attractive for computation). Taking $X_{0,h} \subset H^2 \cap H_0^1(\Omega, \mathbb{R}^N)$, we discretize (1.14) by requiring that $\boldsymbol{u}_h^{n+1}$ satisfy

$$\begin{aligned} \left\langle \frac{\nabla \boldsymbol{u}_h^{n+1} - \nabla \boldsymbol{u}_h^n}{\Delta t}, \nabla \boldsymbol{v}_h \right\rangle + \nu \langle \Delta \boldsymbol{u}_h^{n+1}, \Delta \boldsymbol{v}_h \rangle \\ = \langle \nabla p_h^n - \boldsymbol{f}^n + \boldsymbol{u}_h^n \cdot \nabla \boldsymbol{u}_h^n, \Delta \boldsymbol{v}_h \rangle \end{aligned} \tag{1.20}$$

for all $\boldsymbol{v}_h \in X_{0,h}$. This scheme has the attractive feature that the convection and pressure terms are treated explicitly, and moreover the spaces $X_{0,h}$ and Y_h are not required to satisfy any compatibility requirement related to the inf-sup condition. It is rather surprising, then, that this scheme is unconditionally stable, at least with the provision that Ω has a C^3 boundary and one can manage to construct the spaces $X_{0,h}$ and Y_h. This stability result was proved in [LLP]; key parts of the argument will be revisited below. Moreover, we have the following error estimate for (1.18),(1.20).

Theorem 1 *Assume that Ω is a bounded domain in $\mathbb{R}^N$ (N=2,3) with C^3 boundary. Let $M_0, \nu > 0$, and let $T_* > 0$ be given by the stability theorem 6 below. Let $m \geq 2$, $m' \geq 1$ be integers, and assume that*

(i) The spaces $X_{0,h} \subset H^2 \cap H_0^1(\Omega, \mathbb{R}^N)$ and $Y_h \subset H^1(\Omega)$ have the property that

whenever $0 < h < 1$, $\boldsymbol{v} \in H^{m+1} \cap H_0^1(\Omega, \mathbb{R}^N)$ *and* $q \in H^{m'}(\Omega)$,

$$\inf_{\boldsymbol{v}_h \in X_{0,h}} \|\Delta(\boldsymbol{v} - \boldsymbol{v}_h)\| \le C_0 h^{k-1} \|\boldsymbol{v}\|_{H^{k+1}} \quad \text{for } 2 \le k \le m, \tag{1.21}$$

$$\inf_{q_h \in Y_h} \|\nabla(q - q_h)\| \le C_0 h^{m'-1} \|q\|_{H^{m'}}, \tag{1.22}$$

where $C_0 > 0$ *is independent of* $\boldsymbol{v}$, q *and* h.

(ii) $\boldsymbol{f} \in C^1([0,T], L^2(\Omega, \mathbb{R}^N))$, $T > 0$, *and a given solution of (1.9)–(1.11) satisfies*

$$(\boldsymbol{u}, p) \in C^1([0,T]; H^{m+1}(\Omega, \mathbb{R}^N)) \times C^1([0,T]; H^{m'}(\Omega)/\mathbb{R}).$$

Then there exists a $C_1 > 0$ *with the following property: Whenever* $\boldsymbol{u}_h^0 \in X_{0,h}$, $0 < h < 1$, $0 < n\Delta t \le \min(T, T_*)$, *and*

$$\|\nabla \boldsymbol{u}_h^0\|^2 + \nu \Delta t \|\Delta \boldsymbol{u}_h^0\|^2 + \sum_{k=0}^{n} \|\boldsymbol{f}(t_k)\|^2 \Delta t \le M_0, \tag{1.23}$$

then the velocity and pressure errors $\boldsymbol{e}^n = \boldsymbol{u}(t_n) - \boldsymbol{u}_h^n$, $r^n = p(t_n) - p_h^n$ *for the solution to the finite-element scheme (1.18) and (1.20) satisfy*

$$\begin{aligned} &\sup_{0 \le k \le n} \|\nabla \boldsymbol{e}^k\|^2 + \sum_{k=0}^{n} \left(\|\Delta \boldsymbol{e}^k\|^2 + \|\nabla r^k\|^2 \right) \Delta t \\ &\qquad \le C_1 (\Delta t^2 + h^{2m-2} + h^{2m'-2} + \|\nabla \boldsymbol{e}^0\|^2 + \|\Delta \boldsymbol{e}^0\|^2 \Delta t). \end{aligned} \tag{1.24}$$

1.2.2 Another C^0 finite element scheme for the time-dependent problem

Although we can prove the stability and obtain error estimates, there are two main drawbacks of scheme (1.18),(1.20). First, it requires C^1 finite elements which in real computation are more expensive than C^0 finite elements. Second, there is

an annoying C^3 boundary requirement in Theorem 1 which is not satisfied for most interesting applications. Although in practice we have found that this condition is not necessary, but it is still there in the mathematical theory.

Attempts to get rid of these two restrictions have been taken. In this thesis, a new C^0 finite element scheme is proposed which is both practically easy to implement and mathematically guaranteed to perform well. It is motivated by Guermond and Shen's work on projection methods [GS2]. We can prove that it is unconditional stable for SE. Moreover, as long as the solution is regular enough, we have error estimates. Unlike the C^1 scheme, we do not require Γ to be of class C^3. The scheme is as follows: Choose finite element spaces $X_{0,h} \subset C^0 \cap H_0^1(\Omega, \mathbb{R}^3)$ and $Y_h \subset C^0 \cap H^1(\Omega)$. Given $\boldsymbol{u}_h^0$ and $\boldsymbol{u}_h^1$, find $\boldsymbol{u}_h^n$ $(n \geq 2)$ satisfying

$$\begin{aligned} &\left\langle \frac{\boldsymbol{u}_h^{n+1} - \boldsymbol{u}_h^n}{\Delta t}, \boldsymbol{v}_h \right\rangle + \nu \big\langle \nabla \boldsymbol{u}_h^{n+1}, \nabla \boldsymbol{v}_h \big\rangle - \nu \big\langle \nabla \times \boldsymbol{u}_h^n, \nabla \times \boldsymbol{v}_h \big\rangle \\ =&\left\langle \mathcal{P}_h \left(\frac{\boldsymbol{u}_h^n - \boldsymbol{u}_h^{n-1}}{\Delta t} + \boldsymbol{F}^n - \boldsymbol{F}^{n-1} \right), \boldsymbol{v}_h \right\rangle \end{aligned} \tag{1.25}$$

for any $\boldsymbol{v}_h \in X_{0,h}$, where $\boldsymbol{F}^n = \boldsymbol{f}^n - \boldsymbol{u}_h^n \cdot \nabla \boldsymbol{u}_h^n$ for NSE and $\boldsymbol{F}^n = \boldsymbol{f}^n$ for SE. The discrete Helmholtz-Hodge projection $\mathcal{P}_h$ in (1.25) is defined as follows: For any $\boldsymbol{a} \in L^2(\Omega, \mathbb{R}^N)$, define $q_h \in Y_h$ by solving

$$\big\langle \nabla q_h, \nabla \phi_h \big\rangle = \big\langle \boldsymbol{a}, \nabla \phi_h \big\rangle \qquad \forall \phi_h \in Y_h. \tag{1.26}$$

Then $\mathcal{P}_h \boldsymbol{a} := \boldsymbol{a} - \nabla q_h$. If one need the pressure, it can be recovered from (1.18).

For the C^0 FE scheme (1.25), we will prove stability and obtain error estimates in Chapter 5.

1.3 Outline of the thesis

The thesis is organized as follows. In the next chapter, we give a short review of the unconstrained formulation of NSE based upon which we have proposed all of our FE schemes. We will also recall the pressure estimates from [LLP], which is crucial for the analysis of our C^1 FE scheme. The rest of the thesis is divided into three parts, one for steady-state computation and two for time-dependent problems. Each of them contain both mathematical theorems as well as numerical computations. We first study the steady-state problem in Chapter 3 and show that these schemes do not require the inf-sup compatibility condition. In Chapter 4, we study the time-dependent problem using the C^1 FE scheme (1.18),(1.20) as well as C^0 FE scheme (1.18),(1.19). We will show the stability and error estimates of the C^1 scheme. After mentioning some practical issue that we need to pay attention to when implementing the code, we present numerical results for these two schemes. In particular, we demonstrate numerically that with this consistent discretization of NSE, we can achieve high accuracy in both space and time. Finally, in Chapter 5, we try to show that we can manage to design a C^0 FE scheme whose stability and error estimates results do not require the boundary to be C^3 (Lipschitz domain is enough). Finally, the thesis ends up with a conclusion chapter as well as an appendix chapter addressing the connection between this new method and projection methods

that exist in the literature.

Chapter 2

The unconstrained formulation and pressure estimates

In this chapter, we show that the unconstrained formulation for both the steady-state NSE and the time-dependent NSE do leads to $\nabla \cdot \boldsymbol{u} = 0$ and hence the unconstrained formulation is equivalent to the original formulation.

We will then recall the estimate for the pressure which is proved in [LLP]. Most of the analysis of the C^1 finite element scheme will depend on this estimate.

2.1 Steady-state NSE

Lemma 1 *If $(\boldsymbol{u}, p) \in H^2(\Omega, \mathbb{R}^N) \times H^1(\Omega)$ satisfies (1.5)+(1.1)+(1.3) with $\boldsymbol{g}$ satisfying (1.4), then $\nabla \cdot \boldsymbol{u} = 0$.*

Proof: From (1.1) and (1.5), we see ∇p has two different representations. After making them equal, we get

$$\nu(I - \mathcal{P})(\Delta \boldsymbol{u} - \nabla\nabla \cdot \boldsymbol{u}) + (I - \mathcal{P})(\boldsymbol{f} - \boldsymbol{u} \cdot \nabla \boldsymbol{u}) = \nu \Delta \boldsymbol{u} + \boldsymbol{f} - \boldsymbol{u} \cdot \nabla \boldsymbol{u}.$$

Dotting both sides with $\nabla\phi$ for any $\phi \in H^1(\Omega)$ and recalling that by definition $\mathcal{P}\boldsymbol{v} \in (\nabla H^1)^\perp$ for any $\boldsymbol{v} \in L^2(\Omega, \mathbb{R}^N)$ (i.e. $\langle \mathcal{P}\boldsymbol{v}, \nabla\phi \rangle = 0$), we have

$$\langle \nu(\Delta \boldsymbol{u} - \nabla\nabla \cdot \boldsymbol{u}) + \boldsymbol{f} - \boldsymbol{u} \cdot \nabla \boldsymbol{u}, \nabla\phi \rangle = \langle \nu \Delta \boldsymbol{u} + \boldsymbol{f} - \boldsymbol{u} \cdot \nabla \boldsymbol{u}, \nabla\phi \rangle.$$

Hence

$$\langle \nabla\nabla \cdot \boldsymbol{u}, \nabla\phi \rangle = 0.$$

By taking $\phi = \nabla \cdot \boldsymbol{u}$, we see that

$$\nabla \cdot \boldsymbol{u} = \text{Constant}.$$

Integrating both sides over Ω and using the compatibility condition (1.4), we get

$$\int_\Omega \text{Constant} = \int_\Gamma \boldsymbol{n} \cdot \boldsymbol{g} = 0.$$

Hence $\nabla \cdot \boldsymbol{u} = 0$. $\square$

2.2 Time-dependent NSE

Lemma 2 *If* $(\boldsymbol{u}, p) \in L^2(0,T; H^2(\Omega, \mathbb{R}^N)) \cap H^1(0,T; L^2(\Omega, \mathbb{R}^N)) \times L^2(0,T; H^1(\Omega)/\mathbb{R})$ *satisfies (1.5),(1.9),(1.11) with* $\boldsymbol{u}_{\text{in}}$ *satisfying (1.12), then* $\nabla \cdot \boldsymbol{u} = 0$.

Proof: As in the steady-state case, we get

$$\big\langle \nabla \nabla \cdot \boldsymbol{u}, \nabla \phi \big\rangle = \big\langle \partial_t \boldsymbol{u}, \nabla \phi \big\rangle.$$

Note the fact that the mapping $t \mapsto \|\nabla \cdot \boldsymbol{u}\|^2$ is absolute continuous and

$$\big\langle \partial_t \boldsymbol{u}, \nabla \nabla \cdot \boldsymbol{u} \big\rangle = -\frac{1}{2} \frac{d}{dt} \|\nabla \cdot \boldsymbol{u}\|^2. \tag{2.1}$$

To prove (2.1), we should consider the time mollified function $\boldsymbol{u}_\varepsilon = \boldsymbol{u}(x, \cdot) * \varphi_\varepsilon(\cdot)$. We first prove (2.1) for $\boldsymbol{u}_\varepsilon$, then write it into weak form and let ε goes to zero.

Now, letting $\phi = \nabla \cdot \boldsymbol{u}$, we get

$$\frac{1}{2} \frac{d}{dt} \|\nabla \cdot \boldsymbol{u}\|^2 + \|\nabla \nabla \cdot \boldsymbol{u}\|^2 = 0$$

Since initially $\nabla \cdot \boldsymbol{u} = 0$, we have $\nabla \cdot \boldsymbol{u} = 0$ for all later time. $\square$

2.3 Pressure estimates

It is not difficult to show [LLP, Lemma 1] that for any vector field $\boldsymbol{u} \in L^2(\Omega)^N$,

$$\nabla\nabla\cdot\boldsymbol{u} = \Delta(I-\mathcal{P})\boldsymbol{u}. \tag{2.2}$$

Using this, we see that

$$(\Delta\mathcal{P}-\mathcal{P}\Delta)\boldsymbol{u} = (I-\mathcal{P})\Delta\boldsymbol{u} - \nabla\nabla\cdot\boldsymbol{u} = (I-\mathcal{P})(\Delta\boldsymbol{u}-\nabla\nabla\cdot\boldsymbol{u}) =: \nabla p_{\mathrm{S}}, \tag{2.3}$$

where p_{S} is called the *Stokes pressure*, which is part of the pressure in (1.5). One might expect this commutator to be "small" in some sense. Indeed, it vanishes in the case when the domain is $\mathbb{R}^N$ or a box with periodic boundary conditions. With no-slip boundary conditions, the key estimate of Liu *et al.* [LLP] is that this commutator is strictly bounded in the L^2-norm by the Laplacian term, up to lower order terms:

Theorem 2 *Let $\Omega \subset \mathbb{R}^N$ ($N \geq 2$) be a connected bounded domain with C^3 boundary. Then for any $\varepsilon > 0$, there exists a $C \geq 0$ such that for all vector fields $\boldsymbol{u} \in H^2 \cap H^1_0(\Omega, \mathbb{R}^N)$,*

$$\int_\Omega |(\Delta\mathcal{P}-\mathcal{P}\Delta)\boldsymbol{u}|^2 \leq \left(\frac{1}{2}+\varepsilon\right)\int_\Omega |\Delta\boldsymbol{u}|^2 + C\int_\Omega |\nabla\boldsymbol{u}|^2. \tag{2.4}$$

This estimate turns out to be crucial for our analysis of C^1 FE schemes for both steady and time-dependent problems.

Chapter 3

Steady-state Stokes equations

In this section, we will study a FE solver for the steady-state SE. We start with a semi-discrete iterative solver. Then we study the C^1 FE scheme which solves $(\boldsymbol{u}, p)$ together. Finally, we study the C^1 FE iterative solver.

3.1 Semi-discrete iterative solver for steady-state Stokes equations

Consider steady-state SE

$$\nabla p = \nu \Delta \boldsymbol{u} + \boldsymbol{f}, \qquad \nabla \cdot \boldsymbol{u} = 0, \qquad \boldsymbol{u}|_\Gamma = 0. \tag{3.1}$$

Since this is a linear equation, we can take $\nu = 1$. Using Lemma 1, we can rewrite it as the following unconstrained SE:

$$\nabla p = \Delta \boldsymbol{u} + \boldsymbol{f}, \tag{3.2}$$

$$\nabla p = (I - \mathcal{P})\Delta \boldsymbol{u} - \nabla\nabla \cdot \boldsymbol{u} + (I - \mathcal{P})\boldsymbol{f}, \quad \boldsymbol{u}|_\Gamma = 0. \tag{3.3}$$

Let $\nabla p_{\mathrm{s}} = \nabla p - (I - \mathcal{P})\boldsymbol{f}$. Then the above equations can be rewritten as

$$\nabla p_{\mathrm{s}} = \Delta \boldsymbol{u} + \mathcal{P}\boldsymbol{f}, \tag{3.4}$$

$$\nabla p_{\mathrm{s}} = (I - \mathcal{P})\Delta \boldsymbol{u} - \nabla\nabla \cdot \boldsymbol{u}, \quad \boldsymbol{u}|_\Gamma = 0. \tag{3.5}$$

Theorem 3 *Let $\boldsymbol{f} \in L^2(\Omega, \mathbb{R}^N)$. Consider the iteration:*

$$\nabla p^{n-1} = \Delta \boldsymbol{u}^n + \mathcal{P}\boldsymbol{f}, \qquad \boldsymbol{u}^n|_\Gamma = 0, \tag{3.6}$$

$$\nabla p^n = (I - \mathcal{P})\Delta \boldsymbol{u}^n - \nabla\nabla \cdot \boldsymbol{u}^n. \tag{3.7}$$

Then there is a $\boldsymbol{u} \in H_0^1(\Omega, \mathbb{R}^N)$ so that

$$\boldsymbol{u}^n \rightharpoonup \boldsymbol{u} \quad \textit{weakly in } H_0^1(\Omega, \mathbb{R}^N)$$

and $\boldsymbol{u}$ is the Leray weak solution of the steady-state SE (3.1).

Proof: To start, we can take $p^0 = 0$ and $\Delta \boldsymbol{u}^1 + \mathcal{P}\boldsymbol{f} = 0$. Operating on both side of (3.6) with $\mathcal{P}$, we get

$$\mathcal{P}\Delta \boldsymbol{u}^n + \mathcal{P}\boldsymbol{f} = 0. \tag{3.8}$$

From (3.6) and (3.7), we get

$$(I - \mathcal{P})\Delta \boldsymbol{u}^n - \nabla\nabla \cdot \boldsymbol{u}^n = \Delta \boldsymbol{u}^{n+1} + \mathcal{P}\boldsymbol{f}.$$

for $n \geq 1$. We use (3.8) to write the last equation as

$$\Delta(\boldsymbol{u}^{n+1} - \boldsymbol{u}^n) + \nabla\nabla \cdot \boldsymbol{u}^n = 0. \tag{3.9}$$

We can further rewrite (3.9) as

$$-\nabla \times \nabla \times (\boldsymbol{u}^{n+1} - \boldsymbol{u}^n) + \nabla\nabla \cdot \boldsymbol{u}^{n+1} = 0. \tag{3.10}$$

Dotting this equation with $-2\boldsymbol{u}^{n+1}$, we find that

$$\|\nabla \times \boldsymbol{u}^{n+1}\|^2 - \|\nabla \times \boldsymbol{u}^n\|^2 + \|\nabla \times (\boldsymbol{u}^{n+1} - \boldsymbol{u}^n)\|^2 + 2\|\nabla \cdot \boldsymbol{u}^{n+1}\|^2 = 0. \tag{3.11}$$

Summing on n, we find that

$$\|\nabla \times \boldsymbol{u}^n\| \leq \|\nabla \times \boldsymbol{u}^1\| \quad \text{for all } n \geq 1, \tag{3.12}$$

$$\|\nabla \cdot \boldsymbol{u}^n\| \to 0 \quad \text{as } n \to \infty. \tag{3.13}$$

Therefore the $\boldsymbol{u}^n$ are uniformly bounded in $H_0^1(\Omega, \mathbb{R}^N)$ and hence there is a $\boldsymbol{u} \in H_0^1(\Omega, \mathbb{R}^N)$ such that

$$\boldsymbol{u}^n \rightharpoonup \boldsymbol{u} \quad \text{weakly in } H^1(\Omega, \mathbb{R}^N),$$

and hence

$$\nabla \cdot \boldsymbol{u}^n \rightharpoonup \nabla \cdot \boldsymbol{u} \quad \text{weakly in } L^2(\Omega, \mathbb{R}^N),$$

which implies $\nabla \cdot \boldsymbol{u} = 0$.

Take any $\boldsymbol{v} \in H_0^1(\Omega, \mathbb{R}^N)$ with $\nabla \cdot \boldsymbol{v} = 0$ and dot it with (3.6). Since $\mathcal{P}\boldsymbol{v} = \boldsymbol{v}$, we find that

$$0 = -\big\langle \nabla \boldsymbol{u}^n, \nabla \boldsymbol{v} \big\rangle + \big\langle \boldsymbol{f}, \boldsymbol{v} \big\rangle.$$

Passing to the limit, we find that $\boldsymbol{u}$ is the (Leray) weak solution of steady-state SE. So, the iterated $\boldsymbol{u}^n$ converges strongly in L^2 and weakly in H^1 to the solution. □

Remark 1: An identity similar to (3.11) will appear again in the analysis of the C^0 FE scheme (1.25). For example, see how we go from (5.14) to (5.15). Like what happens here, using this identity will be the key for our analysis of scheme (1.25).

Remark 2: As a by-product, we have proved the existence of solution to the steady-state SE. The traditional existence proof relies on the diffusivity of the Stokes operator $\mathcal{P}\Delta$ in $V = \{\boldsymbol{v} \in H_0^1(\Omega, \mathbb{R}^N) \mid \nabla \cdot \boldsymbol{v} = 0\}$ [Te] which eventually leads to an inf-sup compatibility condition in the traditional FE schemes. This new existence

proof on the PDE level may imply that by using this unconstrained formulation, we might eventually circumvent the inf-sup compatibility condition on the discrete level. Indeed, when trying to generalize the above analysis to time-dependent problem, one can end up with scheme (1.25) naturally.

3.2 FE solver for steady-state SE which solves $(\boldsymbol{u}, p)$ together

We will need Theorem 2 for the analysis of the C^1 FE scheme. Due to the lower-order term in (2.4), we need the following two tricks to help out. First, we can add $(I - \mathcal{P})\boldsymbol{u}$ to the velocity equation of Stokes problem and write it as

$$\nabla p = \Delta \boldsymbol{u} + \mathcal{P}\boldsymbol{f} - \gamma(I - \mathcal{P})\boldsymbol{u}, \tag{3.14}$$

$$\nabla p = (I - \mathcal{P})\Delta \boldsymbol{u} - \nabla\nabla \cdot \boldsymbol{u}, \quad \boldsymbol{u}|_\Gamma = 0, \tag{3.15}$$

where $\gamma \geq 0$. Exactly as in Lemma 1, we can prove that (3.14),(3.15) is equivalent to the traditional steady-state SE. Moreover, notice the identity

$$\big\langle \Delta \boldsymbol{u} - \gamma(I - \mathcal{P})\boldsymbol{u}, \Delta \boldsymbol{u} - \gamma \mathcal{P}\boldsymbol{u} \big\rangle = \|\Delta \boldsymbol{u}\|^2 + \gamma \|\nabla \boldsymbol{u}\|^2. \tag{3.16}$$

So, dotting both sides of (3.14) with $\Delta \boldsymbol{v} - \gamma \mathcal{P}\boldsymbol{v}$, we get the weak form of steady-state SE:

$$\big\langle \nabla p, \Delta \boldsymbol{v} \big\rangle = \big\langle \Delta \boldsymbol{u} + \mathcal{P}\boldsymbol{f}, \Delta \boldsymbol{v} - \gamma \mathcal{P}\boldsymbol{v} \big\rangle - \gamma \big\langle (I - \mathcal{P})\boldsymbol{u}, \Delta \boldsymbol{v} \big\rangle \tag{3.17}$$

$$\big\langle \nabla p, \nabla q \big\rangle = \big\langle \Delta \boldsymbol{u} - \nabla\nabla \cdot \boldsymbol{u}, \nabla q \big\rangle. \tag{3.18}$$

After rewriting (3.17) appropriately, based on the above weak formulation, we propose the following C^1 FE scheme for steady-state SE:

$$\begin{aligned}
&\langle \Delta \boldsymbol{u}_h, \Delta \boldsymbol{v}_h \rangle - \gamma \langle \boldsymbol{u}_h, \Delta \boldsymbol{v}_h \rangle + \gamma \left(\langle \mathcal{P}_h \boldsymbol{u}_h, \Delta \boldsymbol{v}_h \rangle - \langle \Delta \boldsymbol{u}_h, \mathcal{P}_h \boldsymbol{v}_h \rangle \right) \\
&\qquad - \langle \nabla p_h, \Delta \boldsymbol{v}_h \rangle = - \langle \mathcal{P}_h \boldsymbol{f}, \Delta \boldsymbol{v}_h - \gamma \boldsymbol{v}_h \rangle \qquad \forall \boldsymbol{v}_h \in X_{0,h}, \qquad (3.19) \\
&\langle \nabla p_h, \nabla q_h \rangle - \langle \Delta \boldsymbol{u}_h - \nabla \nabla \cdot \boldsymbol{u}_h, \nabla q_h \rangle = 0 \qquad \forall q_h \in Y_h. \qquad (3.20)
\end{aligned}$$

The discrete Helmholtz-Hodge projection $\mathcal{P}_h$ in (3.19) is defined as in (1.26).

We can choose $\gamma \geq 0$ so that this system is coercive. Hence we succeed in replacing the inf-sup condition by Lax-Milgram, and solvability and error estimates follow.

Theorem 4 *Assume Ω is a bounded domain in $\mathbb{R}^N$ (N=2,3) with a C^3 boundary. Let $m \geq 2$, $m' \geq 1$ be integers, and assume*

(i) The spaces $X_{0,h} \subset H^2 \cap H_0^1(\Omega, \mathbb{R}^N)$ and $Y_h \subset H^1(\Omega)$ have the property that whenever $0 < h < 1$, $\boldsymbol{v} \in H^{m+1} \cap H_0^1(\Omega, \mathbb{R}^N)$ and $q \in H^{m'}(\Omega)$,

$$\inf_{\boldsymbol{v}_h \in X_{0,h}} \|\Delta(\boldsymbol{v} - \boldsymbol{v}_h)\| \leq C_0 h^{k-1} \|\boldsymbol{v}\|_{H^{k+1}} \quad \text{for } 2 \leq k \leq m, \qquad (3.21)$$

$$\inf_{q_h \in Y_h} \|\nabla(q - q_h)\| \leq C_0 h^{m'-1} \|q\|_{H^{m'}}, \qquad (3.22)$$

where $C_0 > 0$ is independent of $\boldsymbol{v}$, q and h.

(ii) $\boldsymbol{f} \in H^{m'-1}(\Omega, \mathbb{R}^N)$ and the exact solution of (3.2),(3.3) satisfies

$$(\boldsymbol{u}, p) \in H^{m+1} \cap H^{m'+1}(\Omega, \mathbb{R}^N) \times H^{m'}(\Omega)/\mathbb{R}.$$

Then the velocity and pressure errors $\boldsymbol{e} = \boldsymbol{u} - \boldsymbol{u}_h$, $r = p - p_h$ *for the solution to the finite-element scheme (3.19) and (3.20) satisfy*

$$\|\Delta \boldsymbol{e}_h\| + \|\nabla r_h\| \leq C(h^{m-1} + h^{m'-1}) \tag{3.23}$$

For the proof of Theorem 4, we need the following two lemmas:

Lemma 3 *For any* $\boldsymbol{a}$, $\boldsymbol{b} \in L^2(\Omega, \mathbb{R}^N)$,

$$\big\langle \boldsymbol{a}, \mathcal{P}_h \boldsymbol{b} \big\rangle = \big\langle \mathcal{P}_h \boldsymbol{a}, \boldsymbol{b} \big\rangle = \big\langle \mathcal{P}_h \boldsymbol{a}, \mathcal{P}_h \boldsymbol{b} \big\rangle, \tag{3.24}$$

$$\|\mathcal{P}_h \boldsymbol{a}\|^2 + \|(I - \mathcal{P}_h)\boldsymbol{a}\|^2 = \|\boldsymbol{a}\|^2. \tag{3.25}$$

Proof: Let $\mathcal{P}_h \boldsymbol{a} = \boldsymbol{a} - \nabla q_h$ and $\mathcal{P}_h \boldsymbol{b} = \boldsymbol{b} - \nabla p_h$.

$$\big\langle \boldsymbol{a}, \mathcal{P}_h \boldsymbol{b} \big\rangle = \big\langle \boldsymbol{a}, \boldsymbol{b} - \nabla p_h \big\rangle = \big\langle \boldsymbol{a} - \nabla q_h, \boldsymbol{b} - \nabla p_h \big\rangle = \big\langle \boldsymbol{a} - \nabla q_h, \boldsymbol{b} \big\rangle = \big\langle \mathcal{P}_h \boldsymbol{a}, \boldsymbol{b} \big\rangle,$$

$$\|\boldsymbol{a} - \nabla q_h\|^2 = \big\langle \boldsymbol{a} - \nabla q_h, \boldsymbol{a} \big\rangle = \|\boldsymbol{a}\|^2 - \|\nabla q_h\|^2. \qquad \square$$

Lemma 4

$$\|(\mathcal{P} - \mathcal{P}_h)\boldsymbol{a}\| \leq C h^{m'-1} \|\boldsymbol{a}\|_{H^{m'-1}} \tag{3.26}$$

with m' *coming from (3.22).*

Proof: Let $\mathcal{P}\boldsymbol{a} = \boldsymbol{a} - \nabla q$ and $\mathcal{P}_h \boldsymbol{a} = \boldsymbol{a} - \nabla q_h$, where

$$\big\langle \nabla q_h, \nabla \phi_h \big\rangle = \big\langle a, \nabla \phi_h \big\rangle = \big\langle \nabla q, \nabla \phi_h \big\rangle.$$

So, we can get

$$\|(\mathcal{P} - \mathcal{P}_h)\boldsymbol{a}\| = \|\nabla(q - q_h)\| \leq \inf_{\phi_h \in Y_h} \|\nabla(q - \phi_h)\| \leq C h^{m'-1} \|q\|_{H^{m'}}.$$

Proof of Theorem 4 Consider the H^2 projection $\mathbf{\Pi}_h \boldsymbol{u}$ and H^1 projection $\mathbf{P}_h p$. From the pressure equation, we have

$$\left\langle \nabla \mathbf{P}_h p, \nabla q_h \right\rangle - \left\langle (\Delta - \nabla\nabla\cdot)\mathbf{\Pi}_h \boldsymbol{u}, \nabla q_h \right\rangle = \ell_1$$

where $\ell_1 = \left\langle (\Delta - \nabla\nabla\cdot)(I - \mathbf{\Pi}_h)\boldsymbol{u}, \nabla q_h \right\rangle$ and hence

$$|\ell_1| \leq C h^{m-1} \|\nabla q_h\|.$$

For the momentum equation, we have

$$\begin{aligned} \left\langle \Delta \mathbf{\Pi}_h \boldsymbol{u}, \Delta \boldsymbol{v}_h \right\rangle - \gamma \left\langle \mathbf{\Pi}_h \boldsymbol{u}, \Delta \boldsymbol{v}_h \right\rangle + \gamma \left(\left\langle \mathcal{P}_h \mathbf{\Pi}_h \boldsymbol{u}, \Delta \boldsymbol{v}_h \right\rangle - \left\langle \Delta \mathbf{\Pi}_h \boldsymbol{u}, \mathcal{P}_h \boldsymbol{v}_h \right\rangle \right) \\ - \left\langle \nabla \mathbf{P}_h p, \Delta \boldsymbol{v}_h \right\rangle = - \left\langle \mathcal{P}_h \boldsymbol{f}, \Delta \boldsymbol{v}_h - \gamma \boldsymbol{v}_h \right\rangle + \ell_2 \end{aligned}$$

where

$$\begin{aligned} \ell_2 =& \gamma \left\langle (I - \mathbf{\Pi}_h)\boldsymbol{u}, \Delta \boldsymbol{v}_h \right\rangle - \gamma \left\langle (\mathcal{P} - \mathcal{P}_h + \mathcal{P}_h - \mathcal{P}_h \mathbf{\Pi}_h)\boldsymbol{u}, \Delta \boldsymbol{v}_h \right\rangle \\ &+ \gamma \left\langle \Delta (I - \mathbf{\Pi}_h)\boldsymbol{u}, \mathcal{P}_h \boldsymbol{v}_h \right\rangle + \gamma \left\langle \Delta \boldsymbol{u}, (\mathcal{P} - \mathcal{P}_h)\boldsymbol{v}_h \right\rangle \\ &+ \left\langle \nabla (I - \mathbf{P}_h) p, \Delta \boldsymbol{v}_h \right\rangle - \left\langle (I - \mathcal{P}_h)\boldsymbol{f}, \Delta \boldsymbol{v}_h - \gamma \boldsymbol{v}_h \right\rangle. \end{aligned}$$

So,

$$|\ell_2| \leq C \|\Delta \boldsymbol{v}_h\| (h^{m-1} + h^{m'-1})$$

Letting $r_h = \mathbf{P}_h p - p_h$ and $\boldsymbol{e}_h = \mathbf{\Pi}_h \boldsymbol{u} - \boldsymbol{u}_h$, we get

$$\begin{aligned} \left\langle \Delta \boldsymbol{e}_h, \Delta \boldsymbol{v}_h \right\rangle - \gamma \left\langle \boldsymbol{e}_h, \Delta \boldsymbol{v}_h \right\rangle + \gamma \left(\left\langle \mathcal{P}_h \boldsymbol{e}_h, \Delta \boldsymbol{v}_h \right\rangle - \left\langle \Delta \boldsymbol{e}_h, \mathcal{P}_h \boldsymbol{v}_h \right\rangle \right) \\ - \left\langle \nabla r_h, \Delta \boldsymbol{v}_h \right\rangle = \ell_2, \end{aligned} \tag{3.27}$$

$$\left\langle \nabla r_h, \nabla q_h \right\rangle - \left\langle \Delta \boldsymbol{e}_h - \nabla\nabla \cdot \boldsymbol{e}_h, \nabla q_h \right\rangle = \ell_1. \tag{3.28}$$

Now, rewrite (3.28) as

$$\big\langle \nabla r_h, \nabla q_h \big\rangle = \big\langle (I-\mathcal{P})(\Delta \boldsymbol{e}_h - \nabla\nabla\cdot \boldsymbol{e}_h), \nabla q_h \big\rangle + \ell_1$$

and let $q_h = r_h$ in (3.28). Using Theorem 2, we get

$$\|\nabla r_h\| \le \sqrt{1/2+\varepsilon}\|\Delta \boldsymbol{e}_h\| + C_\varepsilon \|\nabla \boldsymbol{e}_h\| + h^{m-1}.$$

Letting $\boldsymbol{v}_h = \boldsymbol{e}_h$ in (3.27) and noticing that $\big\langle \mathcal{P}_h \boldsymbol{e}_h, \Delta \boldsymbol{e}_h \big\rangle - \big\langle \Delta \boldsymbol{e}_h, \mathcal{P}_h \boldsymbol{e}_h \big\rangle = 0$, we get

$$\|\Delta \boldsymbol{e}_h\|^2 + \gamma \|\nabla \boldsymbol{e}_h\|^2 \le \frac{1}{2}\|\nabla r_h\|^2 + \frac{1}{2}\|\Delta \boldsymbol{e}_h\|^2 + C\|\Delta \boldsymbol{e}_h\|(h^{m-1} + h^{m'-1}).$$

Taking $\gamma = C_\varepsilon$, we find that

$$\|\Delta \boldsymbol{e}_h\|^2 + \gamma_1 \|\nabla \boldsymbol{e}_h\|^2 \le C(h^{2m-2} + h^{2m'-2}). \qquad \square$$

3.3 Iterative FE solver for steady-state SE

Motivated by (3.17) and (3.18), we propose the following iterative C^1 FE scheme for the steady-state SE:

$$\begin{aligned} &\big\langle \Delta \boldsymbol{u}_h^n, \Delta \boldsymbol{v}_h \big\rangle - \gamma \big\langle \boldsymbol{u}_h^n, \Delta \boldsymbol{v}_h \big\rangle + \gamma \left(\big\langle \mathcal{P}_h \boldsymbol{u}_h^n, \Delta \boldsymbol{v}_h \big\rangle - \big\langle \Delta \boldsymbol{u}_h^n, \mathcal{P}_h \boldsymbol{v}_h \big\rangle \right) \\ &\quad - \big\langle \nabla p_h^{n-1}, \Delta \boldsymbol{v}_h \big\rangle = -\big\langle \mathcal{P}_h \boldsymbol{f}, \Delta \boldsymbol{v}_h - \gamma \boldsymbol{v}_h \big\rangle, \qquad \forall \boldsymbol{v}_h \in X_{0,h} \end{aligned} \tag{3.29}$$

$$\big\langle \nabla p_h^n, \nabla q_h \big\rangle - \big\langle \Delta \boldsymbol{u}_h^n - \nabla\nabla\cdot \boldsymbol{u}_h^n, \nabla q_h \big\rangle = 0, \qquad \forall q_h \in Y_h \tag{3.30}$$

For this iterative solver, we have the following error estimates. Their proofs are very similar to (and much simpler than) the proof of Theorem 1 and are accordingly omitted.

Theorem 5 *Assume Ω is a bounded domain in $\mathbb{R}^N$ (N=2,3) with a C^3 boundary. Let $m \ge 2$, $m' \ge 1$ be integers, and assume*

(i) The spaces $X_{0,h} \subset H^2 \cap H_0^1(\Omega, \mathbb{R}^N)$ *and* $Y_h \subset H^1(\Omega)$ *have the property that whenever* $0 < h < 1$, $\boldsymbol{v} \in H^{m+1} \cap H_0^1(\Omega, \mathbb{R}^N)$ *and* $q \in H^{m'}(\Omega)$,

$$\inf_{\boldsymbol{v}_h \in X_{0,h}} \|\Delta(\boldsymbol{v} - \boldsymbol{v}_h)\| \le C_0 h^{k-1} \|\boldsymbol{v}\|_{H^{k+1}} \quad \text{for } 2 \le k \le m, \tag{3.31}$$

$$\inf_{q_h \in Y_h} \|\nabla(q - q_h)\| \le C_0 h^{m'-1} \|q\|_{H^{m'}}, \tag{3.32}$$

where $C_0 > 0$ *is independent of* $\boldsymbol{v}$, q *and* h.

(ii) $\boldsymbol{f} \in H^{m'-1}(\Omega, \mathbb{R}^N)$ *and the exact solution of (3.2),(3.3) satisfies*

$$(\boldsymbol{u}, p) \in H^{m+1} \cap H^{m'+1}(\Omega, \mathbb{R}^N) \times H^{m'}(\Omega)/\mathbb{R}.$$

Then the velocity and pressure errors $\boldsymbol{e}^n = \boldsymbol{u} - \boldsymbol{u}_h^n$, $r^n = p - p_h^n$ *for the solution to the finite-element scheme (3.29) and (3.30) satisfy*

$$\sum_{n=M}^{M+L} \|\Delta \boldsymbol{e}_h^n\| + \|\nabla r_h^n\| \le CL(h^{m-1} + h^{m'-1}) + C\|\Delta \boldsymbol{e}_h^M\| \tag{3.33}$$

for any positive integers M *and* L.

Remark: Note that unless $\gamma = 0$, the matrix in (3.19) or (3.29) is not sparse, which is mainly due to the matrix $A = \gamma(a_{i,j})$ with $a_{i,j} = \langle \mathcal{P}_h \phi_i, \Delta \phi_j \rangle - \langle \Delta \phi_i, \mathcal{P}_h \phi_j \rangle$. But notice that

$$\langle \mathcal{P}\boldsymbol{u}, \Delta \boldsymbol{v} \rangle - \langle \Delta \boldsymbol{u}, \mathcal{P}\boldsymbol{v} \rangle = 0 \qquad \text{when } \mathrm{suppt}\boldsymbol{u} \cap \Gamma = \emptyset \ \text{ and } \ \mathrm{suppt}\boldsymbol{v} \cap \Gamma = \emptyset.$$

Hence we can neglect those $a_{i,j}$ when both ϕ_i and ϕ_j are supported strictly inside Ω. After this modification, the remained matrix A is still skew-symmetric and the resulted matrix in (3.19) or (3.29) is sparse, although is not as sparse as the $\gamma = 0$ case. In a real computation, we can take $\gamma = 0$ and obtain the sparse matrix automatically.

3.4 Numerics for steady-state computation

We choose the C^1 finite element to be of Fraeijs de Veubeke-Sander (FVS) type C^1 finite elements (see [FV], [Ci, Exercises 6.1.5] and [LS]). And we use it for both velocity and pressure.

We take the domain to be $[-1,1]\times[-1,1]$ and let the exact solution be

$$u_{\text{ex}}(x,y,t) = \cos^2(\pi x/2)\sin(\pi y), \tag{3.34}$$

$$v_{\text{ex}}(x,y,t) = -\sin(\pi x)\cos^2(\pi y/2), \tag{3.35}$$

$$p_{\text{ex}}(x,y,t) = \quad \cos(\pi x/2)\sin(\pi y/2). \tag{3.36}$$

The forcing term $\boldsymbol{f}$ is chosen so that (3.34)–(3.36) is a solution of SE (3.1). Note that the domain we have used does not satisfy the C^3 boundary requirement; Moreover, in our computation, we will choose $\gamma = 0$ so that we do not need to compute the global projection for each test function, which hence makes the matrix sparse. We first show the results for (3.19),(3.20). In Figure 3.1, we plot the error as we vary h, which is the side length of the FVS element and we use uniform mesh. We have implemented the code with $\gamma > 0$ and the results are similar. Then we show the numeric results for (3.29),(3.30). In Figure 3.2, we plot the error as we vary h. We use uniform mesh and the stopping criteria we have used is $\max\{\|\boldsymbol{u}^{n+1}-\boldsymbol{u}^n\|_{W^{1,\infty}}, \|p^{n+1}-p^n\|_{W^{1,\infty}}\} < 10^{-8}$. As h becomes smaller, the number of iterations to reach the stopping criteria are listed at the top of Figure 3.2.

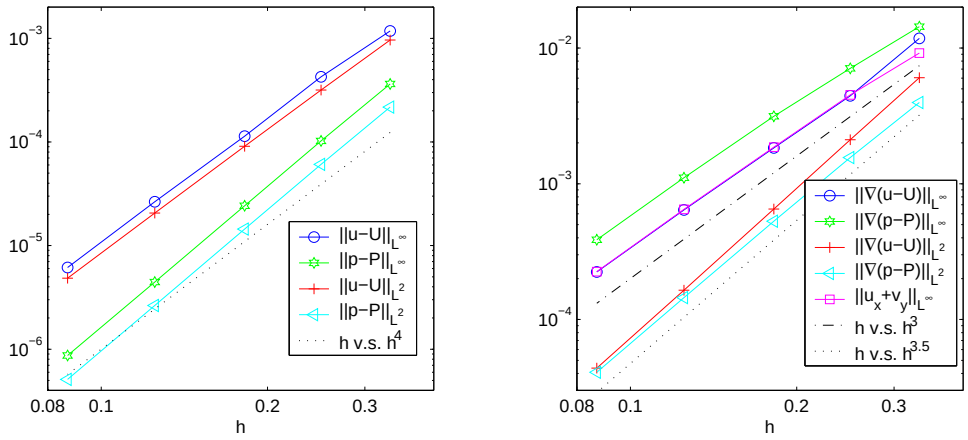

Figure 3.1: Scheme (3.19),(3.20). FVS/FVS. $\gamma = 0$.

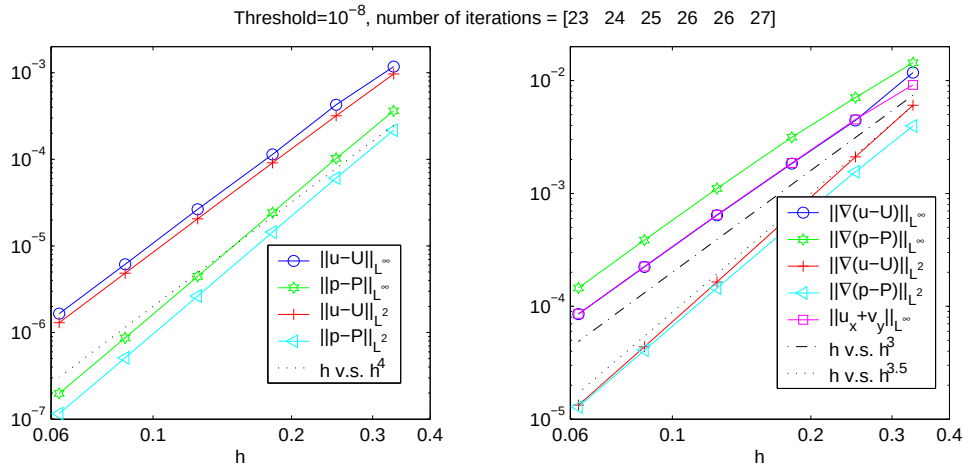

Figure 3.2: Scheme (3.29),(3.30). FVS/FVS. $\gamma = 0$.

Chapter 4

Time dependent problems: Part I

In this chapter, we turn to the time-dependent NSE. We will study C^1 FE schemes (1.18),(1.20). We prove both stability and error estimates for it. Then we will exhibit the numerical results for this scheme as well as $for the C^0$ FE scheme (1.18),(1.19), for which the mathematical theory in the fully discrete case is yet lacking.

4.1 Stability for C^1 FE scheme (1.18),(1.20)

For the C^1 scheme (1.18)+(1.20), we have the following stability results from Theorem 2 of [LLP]. (Note that the forcing term $\boldsymbol{f}^n$ in the scheme is averaged over $[t_n, t_{n+1}]$ in [LLP] rather than the value $\boldsymbol{f}(t_n)$ taken here, but the estimate below holds due to the stronger regularity now assumed for $\boldsymbol{f}$.)

Theorem 6 *Assume Ω is a bounded domain in $\mathbb{R}^N$ (N=2,3) with a C^3 boundary and let $M_0, \nu > 0$. Then, there exist positive constants T_* and C_* depend only on Ω, M_0, ν and have the following property. Suppose $X_{0,h} \subset H^2 \cap H_0^1(\Omega, \mathbb{R}^N)$, $Y_h \subset H^1(\Omega)$, $\boldsymbol{u}_h^0 \in X_{0,h}$, $\boldsymbol{f} \in C^1([0,T], L^2(\Omega, \mathbb{R}^N))$ for some $T > 0$, and suppose $0 < n\Delta t \leq \min(T, T_*)$ and*

$$\|\nabla \boldsymbol{u}_h^0\|^2 + \nu \Delta t \|\Delta \boldsymbol{u}_h^0\|^2 + \sum_{k=0}^{n} \|\boldsymbol{f}^k\|^2 \Delta t \leq M_0. \tag{4.1}$$

Then the solution to the finite element scheme (1.18),(1.20) satisfies

$$\sup_{0\le k\le n}\|\nabla \boldsymbol{u}_h^k\|^2+\sum_{k=0}^{n}\left(\|\Delta \boldsymbol{u}_h^k\|^2+\|\nabla p_h^k\|^2\right)\Delta t\le C_*. \tag{4.2}$$

Proof: For the reader's convenience, we recall here the key parts of the proof. Using (1.17), we rewrite (1.18) as

$$\begin{aligned}\left\langle \nabla p_h^n,\nabla q_h\right\rangle &=\left\langle \boldsymbol{f}(t_n)-\boldsymbol{u}_h^n\cdot\nabla \boldsymbol{u}_h^n,\nabla q_h\right\rangle-\nu\left\langle \nabla\times\nabla\times \boldsymbol{u}_h^n,\nabla q_h\right\rangle \qquad (4.3)\\ &=\left\langle \boldsymbol{f}(t_n)-\boldsymbol{u}_h^n\cdot\nabla \boldsymbol{u}_h^n,\nabla q_h\right\rangle-\nu\left\langle (I-\mathcal{P})\nabla\times\nabla\times \boldsymbol{u}_h^n,\nabla q_h\right\rangle,\\ &=\left\langle \boldsymbol{f}(t_n)-\boldsymbol{u}_h^n\cdot\nabla \boldsymbol{u}_h^n,\nabla q_h\right\rangle+\nu\left\langle \nabla p_{\rm s}(\boldsymbol{u}_h^n),\nabla q_h\right\rangle, \qquad (4.4)\end{aligned}$$

where

$$\nabla p_{\rm s}(\boldsymbol{u}_h^n)=-(I-\mathcal{P})\nabla\times\nabla\times \boldsymbol{u}_h^n=(I-\mathcal{P})\Delta \boldsymbol{u}_h^n-\nabla\nabla\cdot \boldsymbol{u}_h^n \tag{4.5}$$

is the Stokes pressure associated with $\boldsymbol{u}_h^n$.

Taking $q_h=p_h^n$, we get

$$\|\nabla p_h^n\|\le\|\boldsymbol{f}(t_n)-\boldsymbol{u}_h^n\cdot\nabla \boldsymbol{u}_h^n\|+\nu\|\nabla p_{\rm s}(\boldsymbol{u}_h^n)\|. \tag{4.6}$$

Let $\boldsymbol{v}_h=\boldsymbol{u}_h^{n+1}$ in (1.20) and use (4.6). We get

$$\begin{aligned}&\frac{1}{2\Delta t}\Big(\|\nabla \boldsymbol{u}_h^{n+1}\|^2-\|\nabla \boldsymbol{u}_h^n\|^2+\|\nabla \boldsymbol{u}_h^{n+1}-\nabla \boldsymbol{u}_h^n\|^2\Big)+\nu\|\Delta \boldsymbol{u}_h^{n+1}\|^2\\ &\quad\le\|\Delta \boldsymbol{u}_h^{n+1}\|\Big(2\|\boldsymbol{f}(t_n)-\boldsymbol{u}_h^n\cdot\nabla \boldsymbol{u}_h^n\|+\nu\|\nabla p_{\rm s}(\boldsymbol{u}_h^n)\|\Big)\\ &\quad\le\frac{\varepsilon_1}{2}\|\Delta \boldsymbol{u}_h^{n+1}\|^2+\frac{2}{\varepsilon_1}\|\boldsymbol{f}(t_n)-\boldsymbol{u}_h^n\cdot\nabla \boldsymbol{u}_h^n\|^2+\frac{\nu}{2}\big(\|\Delta \boldsymbol{u}_h^{n+1}\|^2+\|\nabla p_{\rm s}(\boldsymbol{u}_h^n)\|^2\big)\end{aligned} \tag{4.7}$$

for any $\varepsilon_1>0$. This gives

$$\begin{aligned}&\frac{1}{\Delta t}\Big(\|\nabla \boldsymbol{u}_h^{n+1}\|^2-\|\nabla \boldsymbol{u}_h^n\|^2\Big)+(\nu-\varepsilon_1)\|\Delta \boldsymbol{u}_h^{n+1}\|^2\\ &\qquad\le\frac{8}{\varepsilon_1}\left(\|\boldsymbol{f}(t_n)\|^2+\|\boldsymbol{u}_h^n\cdot\nabla \boldsymbol{u}_h^n\|^2\right)+\nu\|\nabla p_{\rm s}(\boldsymbol{u}_h^n)\|^2.\end{aligned} \tag{4.8}$$

Fix any β with $\frac{1}{2} < \beta < 1$. Using Theorem 2, one obtains

$$\begin{aligned}
&\frac{1}{\Delta t}\Big(\|\nabla \boldsymbol{u}_h^{n+1}\|^2 - \|\nabla \boldsymbol{u}_h^n\|^2\Big) + (\nu - \varepsilon_1)\big(\|\Delta \boldsymbol{u}_h^{n+1}\|^2 - \|\Delta \boldsymbol{u}_h^n\|^2\big) \\
&\qquad + (\nu - \varepsilon_1 - \nu\beta)\|\Delta \boldsymbol{u}_h^n\|^2 \\
&\qquad \le \frac{8}{\varepsilon_1}\big(\|\boldsymbol{f}(t_n)\|^2 + \|\boldsymbol{u}_h^n \cdot \nabla \boldsymbol{u}_h^n\|^2\big) + \nu C_\beta \|\nabla \boldsymbol{u}_h^n\|^2. \qquad (4.9)
\end{aligned}$$

At this point the pressure has been dealt with. Then, it is rather straightforward and standard to derive from Ladyzhenskaya's inequalities (see [LLP]) that for any $\varepsilon_2 > 0$, there exists a $C > 0$ such that

$$\|\boldsymbol{u}_h^n \cdot \nabla \boldsymbol{u}_h^n\|^2 \le \varepsilon_2 \|\Delta \boldsymbol{u}_h^n\|^2 + \frac{C}{\varepsilon_2}\|\nabla \boldsymbol{u}_h^n\|^6. \qquad (4.10)$$

Plug this into (4.9) and take ε_1, $\varepsilon_2 > 0$ satisfying $\nu - \varepsilon_1 > 0$ and $\varepsilon := \nu - \varepsilon_1 - \nu\beta - 8\varepsilon_2/\varepsilon_1 > 0$. We get

$$\begin{aligned}
&\frac{1}{\Delta t}\big(\|\nabla \boldsymbol{u}_h^{n+1}\|^2 - \|\nabla \boldsymbol{u}_h^n\|^2\big) + (\nu - \varepsilon_1)\big(\|\Delta \boldsymbol{u}_h^{n+1}\|^2 - \|\Delta \boldsymbol{u}_h^n\|^2\big) + \varepsilon\|\Delta \boldsymbol{u}_h^n\|^2 \\
&\qquad \le \frac{8}{\varepsilon_1}\|\boldsymbol{f}(t_n)\|^2 + \frac{8C}{\varepsilon_1\varepsilon_2}\|\nabla \boldsymbol{u}_h^n\|^6 + \nu C_\beta \|\nabla \boldsymbol{u}_h^n\|^2. \qquad (4.11)
\end{aligned}$$

The last step of the proof is a Gronwall-type argument that goes as follows: Put

$$z_n = \|\nabla \boldsymbol{u}_h^n\|^2 + (\nu - \varepsilon_1)\Delta t\|\Delta \boldsymbol{u}_h^n\|^2, \quad w_n = \varepsilon\|\Delta \boldsymbol{u}_h^n\|^2, \quad b_n = \|\boldsymbol{f}(t_n)\|^2. \qquad (4.12)$$

Then by (4.11),

$$z_{n+1} + w_n\Delta t \le z_n + C\Delta t(b_n + z_n + z_n^3), \qquad (4.13)$$

where we have replaced $\max\{8/\varepsilon_1, 8C/(\varepsilon_1\varepsilon_2), \nu C_\beta\}$ by C. Summing from 0 to $n-1$ and using (4.1) yields

$$z_n + \sum_{k=0}^{n-1} w_k\Delta t \le CM_0 + C\Delta t\sum_{k=0}^{n-1}(z_k + z_k^3) =: y_n. \qquad (4.14)$$

The quantities y_n increase with n and satisfy

$$y_{n+1} - y_n = C\Delta t(z_n + z_n^3) \leq C\Delta t(y_n + y_n^3). \tag{4.15}$$

Now set $F(y) = \ln(y/\sqrt{1+y^2})$ so that $F'(y) = (y+y^3)^{-1}$. Then on $(0,\infty)$, F is negative, increasing and concave, and we have

$$F(y_{n+1}) - F(y_n) \leq F'(y_n)(y_{n+1} - y_n) = \frac{y_{n+1} - y_n}{y_n + y_n^3} \leq C\Delta t, \tag{4.16}$$

whence

$$F(y_n) \leq F(y_0) + Cn\Delta t = F(CM_0) + Cn\Delta t. \tag{4.17}$$

Choosing any $T_* > 0$ so that $C_* := F(CM_0) + CT_* < 0$, we infer that as long as $n\Delta t \leq T_*$ we have $y_n \leq F^{-1}(C_*)$, and this together with (4.14) yields the stability estimate (4.2). □

4.1.1 CFL condition for convection diffusion equation

The aim of this subsection is to show that for the convection diffusion equation without any regularity assumption on the boundary Γ, if we treat viscous part with backward Euler and convection part with explicit Euler, no matter we use finite difference, C^0 finite element or C^1 finite element, there is no CFL constraint. Indeed, it is unconditionally stable.

To illustrate the point, let us simply consider the convection diffusion equation

$$u_t + cu_x = \nu u_{xx}$$

on $\mathbb{R}$.

In the finite element case, the proof is like above with discrete Gronwall inequality. We can also use energy estimate in the finite difference case, or we can use von Neumann analysis as follows: In finite difference, the scheme is like

$$\frac{u_m^{n+1}-u_m^n}{\Delta t}+c\frac{u_{m+1}^n-u_{m-1}^n}{2\Delta x}=\nu\frac{u_{m+1}^{n+1}-2u_m^{n+1}+u_{m-1}^{n+1}}{\Delta x^2}. \tag{4.18}$$

Let $\hat{u}(\xi)=\frac{1}{\sqrt{2\pi}}\sum_{m=-\infty}^{\infty}e^{-im\xi}u_m$ with $\xi\in(-\pi,\pi)$. From the above equation, we get

$$\frac{\hat{u}^{n+1}(\xi)-\hat{u}^n(\xi)}{\Delta t}+c\frac{e^{i\xi}-e^{-i\xi}}{2\Delta x}\hat{u}^n(\xi)=\nu\frac{e^{i\xi}-2+e^{-i\xi}}{\Delta x^2}\hat{u}^{n+1}(\xi).$$

The characteristic equation is

$$\lambda-1+\frac{c\Delta t}{\Delta x}i\sin(\xi)=-\frac{4\nu\Delta t}{\Delta x^2}\sin^2(\frac{\xi}{2})\lambda.$$

Hence

$$|\lambda|^2=\frac{1+(\frac{c\Delta t}{\Delta x})^2\sin^2(\xi)}{(1+\frac{4\nu\Delta t}{\Delta x^2}\sin^2(\frac{\xi}{2}))^2}\leq\frac{1+\frac{c^2\Delta t}{\nu}\frac{4\nu\Delta t}{\Delta x^2}\sin^2(\frac{\xi}{2})}{1+\frac{4\nu\Delta t}{\Delta x^2}\sin^2(\frac{\xi}{2})}\leq 1+\frac{c^2}{\nu}\Delta t.$$

Therefore the scheme (4.18) is stable without any restriction on Δt.

4.2 Error estimates for C^1 FE scheme (1.18),(1.20)

In this section we prove Theorem 1. Let $M_0,\nu>0$ and let T_*,C_* be given by Theorem 6. Fix integers $m\geq 2$ and $m'\geq 1$, let $C_0>0$ and suppose that $X_{0,h}$ and Y_h satisfy assumption (i) of the theorem. Suppose that T, $\boldsymbol{f}$, $\boldsymbol{u}$ and p satisfy assumption (ii), so that (1.9) and (1.10) hold. By Lemma 2, we can suppose that $\boldsymbol{u}$ and p satisfy the unconstrained system (1.9),(1.11),(1.5), without (1.10).

In what follows, C denotes a generic constant independent of Δt and h, whose value may change from case to case. (The value of C will depend on the solution,

so it may depend on quantities such as ν in ways that we will not attempt to track here.)

4.2.1 Approximation error

We first project the solution onto the finite element spaces and estimate the resulting approximation error. Define projections $\mathbf{\Pi}_h$ on $H^2 \cap H_0^1(\Omega, \mathbb{R}^N)$ and $\mathbf{P}_h$ on $H^1(\Omega)/\mathbb{R}$ as follows: Given any $\boldsymbol{a} \in H^2 \cap H_0^1(\Omega, \mathbb{R}^N)$ and $b \in H^1(\Omega)/\mathbb{R}$, we define

$$\boldsymbol{a}_h = \mathbf{\Pi}_h \boldsymbol{a} \in X_{0,h}, \qquad b_h = \mathbf{P}_h b \in Y_h, \tag{4.19}$$

as the solutions of the following weak-form Poisson equations:

$$\left\langle \Delta \boldsymbol{a}_h, \Delta \boldsymbol{v}_h \right\rangle = \left\langle \Delta \boldsymbol{a}, \Delta \boldsymbol{v}_h \right\rangle \qquad \forall \boldsymbol{v}_h \in X_{0,h}, \tag{4.20}$$

$$\left\langle \nabla b_h, \nabla q_h \right\rangle = \left\langle \nabla b, \nabla q_h \right\rangle \qquad \forall q_h \in Y_h. \tag{4.21}$$

Notice that since $\left\langle \Delta(\boldsymbol{a} - \boldsymbol{a}_h), \Delta \boldsymbol{a}_h \right\rangle = 0$,

$$\|\Delta \boldsymbol{a}\|^2 = \|\Delta \boldsymbol{a}_h\|^2 + \|\Delta(\boldsymbol{a} - \boldsymbol{a}_h)\|^2. \tag{4.22}$$

Moreover, we have the following basic estimates.

Lemma 5 *For any $\boldsymbol{a} \in H^2 \cap H_0^1(\Omega, \mathbb{R}^N)$, $b \in H^1(\Omega)/\mathbb{R}$,*

$$\|\Delta(\boldsymbol{a} - \boldsymbol{a}_h)\| \leq \inf_{\boldsymbol{v}_h \in X_{0,h}} \|\Delta(\boldsymbol{a} - \boldsymbol{v}_h)\|, \tag{4.23}$$

$$\|\nabla(b - b_h)\| \leq \inf_{q_h \in Y_h} \|\nabla(b - q_h)\|, \tag{4.24}$$

$$\|\nabla(\boldsymbol{a} - \boldsymbol{a}_h)\| \leq Ch \|\Delta(\boldsymbol{a} - \boldsymbol{a}_h)\|. \tag{4.25}$$

Proof: For any $\boldsymbol{v}_h \in X_{0,h}$,

$$\big\langle \Delta(\boldsymbol{a}-\boldsymbol{a}_h), \Delta(\boldsymbol{a}-\boldsymbol{a}_h)\big\rangle = \big\langle \Delta(\boldsymbol{a}-\boldsymbol{a}_h), \Delta(\boldsymbol{a}-\boldsymbol{v}_h)\big\rangle + \big\langle \Delta(\boldsymbol{a}-\boldsymbol{a}_h), \Delta(\boldsymbol{v}_h-\boldsymbol{a}_h)\big\rangle.$$

The last term is zero because of (4.20). Hence the Cauchy-Schwarz inequality gives (4.23). Similarly one can prove (4.24).

To prove (4.25), because $\nabla H_0^1(\Omega,\mathbb{R}^N) \subset L^2(\Omega,\mathbb{R}^N)$ is closed we have

$$\|\nabla(\boldsymbol{a}-\boldsymbol{a}_h)\| = \sup_{\boldsymbol{v}\in H_0^1} \frac{\big\langle \nabla(\boldsymbol{a}-\boldsymbol{a}_h), \nabla(-\boldsymbol{v})\big\rangle}{\|\nabla \boldsymbol{v}\|} = \sup_{\boldsymbol{v}\in H_0^1} \frac{\big\langle \Delta(\boldsymbol{a}-\boldsymbol{a}_h), \boldsymbol{v}\big\rangle}{\|\nabla \boldsymbol{v}\|}. \tag{4.26}$$

Given any $\boldsymbol{v} \in H_0^1$, define $\boldsymbol{w}_v \in H^3 \cap H_0^1$ to be the solution of

$$\Delta \boldsymbol{w}_v = \boldsymbol{v}. \tag{4.27}$$

By assumption (1.21), since $m \geq 2$ there exists $\boldsymbol{w}_{v,h} \in X_{0,h}$ such that

$$\|\Delta(\boldsymbol{w}_v - \boldsymbol{w}_{v,h})\| \leq Ch\|\boldsymbol{w}_v\|_{H^3} \leq Ch\|\nabla \boldsymbol{v}\|,$$

where we have used elliptic regularity for (4.27). Now from (4.26) we get

$$\begin{aligned}\|\nabla(\boldsymbol{a}-\boldsymbol{a}_h)\| &= \sup_{\boldsymbol{v}\in H_0^1} \frac{\big\langle \Delta(\boldsymbol{a}-\boldsymbol{a}_h), \Delta \boldsymbol{w}_v\big\rangle}{\|\nabla \boldsymbol{v}\|} \\ &= \sup_{\boldsymbol{v}\in H_0^1} \frac{\big\langle \Delta(\boldsymbol{a}-\boldsymbol{a}_h), \Delta(\boldsymbol{w}_v - \boldsymbol{w}_{v,h})\big\rangle}{\|\nabla \boldsymbol{v}\|} \leq Ch\|\Delta(\boldsymbol{a}-\boldsymbol{a}_h)\|.\end{aligned}$$

This proves the Lemma. □

Given our regularity and approximation assumptions (i) and (ii), we can conclude that with the notation

$$\boldsymbol{u}_h(t_n) = \boldsymbol{\Pi}_h \boldsymbol{u}(t_n), \qquad p_h(t_n) = \mathbf{P}_h p(t_n), \tag{4.28}$$

the error of approximating the solution by its projection is estimated by

$$\|\Delta(\boldsymbol{u}(t_n) - \boldsymbol{u}_h(t_n))\| \leq Ch^{m-1}, \qquad \|\nabla(p(t_n) - p_h(t_n))\| \leq Ch^{m'-1}. \tag{4.29}$$

4.2.2 Discretization error for pressure

It remains to estimate the discretization or scheme errors

$$\boldsymbol{e}_h^n = \boldsymbol{u}_h(t_n) - \boldsymbol{u}_h^n, \qquad r_h^n = p_h(t_n) - p_h^n. \tag{4.30}$$

We first focus on estimating the pressure error r_h^n in this subsection. Our aim is to show that for any $\varepsilon_0 > 0$ there exists $C > 0$ such that whenever $0 < n\Delta t \leq \min(T, T_*)$ we have

$$\|\nabla r_h^n\|^2 \leq \left(\frac{1}{2} + \varepsilon_0\right) \nu^2 \|\Delta \boldsymbol{e}_h^n\|^2 + C\|\nabla \boldsymbol{e}_h^n\|^2 + Ch^{2m-2}. \tag{4.31}$$

Recall that for any $q_h \in H^1(\Omega)$, the exact pressure satisfies

$$\big\langle \nabla p(t_n), \nabla q_h \big\rangle = \big\langle \boldsymbol{f}(t_n) - \boldsymbol{u}(t_n) \cdot \nabla \boldsymbol{u}(t_n), \nabla q_h \big\rangle - \nu \big\langle \nabla \times \nabla \times \boldsymbol{u}(t_n), \nabla q_h \big\rangle,$$

which can be rewritten as

$$\begin{aligned} \big\langle \nabla p_h(t_n), \nabla q_h \big\rangle =& \big\langle \boldsymbol{f}(t_n) - \boldsymbol{u}_h(t_n) \cdot \nabla \boldsymbol{u}_h(t_n), \nabla q_h \big\rangle \\ & - \nu \big\langle \nabla \times \nabla \times \boldsymbol{u}_h(t_n), \nabla q_h \big\rangle - \ell_n, \end{aligned} \tag{4.32}$$

where

$$\begin{aligned} \ell_n =& \big\langle (I - \boldsymbol{\Pi}_h)\boldsymbol{u}(t_n) \cdot \nabla \boldsymbol{u}(t_n) + \boldsymbol{u}_h(t_n) \cdot \nabla (I - \boldsymbol{\Pi}_h)\boldsymbol{u}(t_n), \nabla q_h \big\rangle \\ & + \nu \big\langle \nabla \times \nabla \times (I - \boldsymbol{\Pi}_h)\boldsymbol{u}(t_n), \nabla q_h \big\rangle. \end{aligned}$$

By Lemma 5,

$$|\ell_n| \leq C(h^m + \nu h^{m-1}) \|\nabla q_h\| \leq Ch^{m-1} \|\nabla q_h\|. \tag{4.33}$$

Rewrite (1.18) as (4.3) and then subtract it from (4.32). We get

$$\begin{aligned} \big\langle \nabla r_h^n, \nabla q_h \big\rangle =& - \big\langle \boldsymbol{e}_h^n \cdot \nabla \boldsymbol{u}_h(t_n) + \boldsymbol{u}_h^n \cdot \nabla \boldsymbol{e}_h^n, \nabla q_h \big\rangle \\ & - \nu \big\langle (I - \mathcal{P}) \nabla \times \nabla \times \boldsymbol{e}_h^n, \nabla q_h \big\rangle - \ell_n, \end{aligned} \tag{4.34}$$

where we have used $\left\langle \mathcal{P}\nabla\times\nabla\times \boldsymbol{e}_h^n, \nabla q_h\right\rangle = 0$. Take $q_h = r_h^n$ and let

$$I_1 = \nu\|(I-\mathcal{P})\nabla\times\nabla\times\boldsymbol{e}_h^n\|, \quad I_2 = \|\boldsymbol{e}_h^n\cdot\nabla\boldsymbol{u}_h(t_n)\|, \quad I_3 = \|\boldsymbol{u}_h^n\cdot\nabla\boldsymbol{e}_h^n\|.$$

By the Cauchy-Schwarz inequality we get that for any $\varepsilon_1 > 0$,

$$\|r_h^n\|^2 \le (I_1+I_2+I_3+Ch^{m-1})^2 \le I_1^2(1+\varepsilon_1) + \frac{1}{\varepsilon_1}(I_2+I_3+Ch^{m-1})^2. \tag{4.35}$$

We estimate terms as follows. By the vector identity (1.16) and (2.3) we have

$$-(I-\mathcal{P})\nabla\times\nabla\times\boldsymbol{e}_h^n = (\Delta\mathcal{P}-\mathcal{P}\Delta)\boldsymbol{e}_h^n.$$

Therefore by Theorem 2 we get the estimate

$$\|(I-\mathcal{P})\nabla\times\nabla\times\boldsymbol{e}_h^n\|^2 \le \left(\frac{1}{2}+\varepsilon_1\right)\|\Delta\boldsymbol{e}_h^n\|^2 + C\|\nabla\boldsymbol{e}_h^n\|^2. \tag{4.36}$$

Next recall that, as in [LLP], by the Sobolev embedding theorems and Ladyzhenskaya's inequalities we have

$$\int_\Omega |\boldsymbol{u}\cdot\nabla\boldsymbol{v}|^2 \le \left(\int_\Omega |\boldsymbol{u}|^6\right)^{\frac{1}{3}}\left(\int_\Omega |\nabla\boldsymbol{v}|^3\right)^{\frac{2}{3}} \le C\|\nabla\boldsymbol{u}\|^2\|\nabla\boldsymbol{v}\|\|\nabla\boldsymbol{v}\|_{H^1}. \tag{4.37}$$

We can use the regularity assumption (ii) together with the approximation bounds (4.29) to bound terms involving $\boldsymbol{u}_h(t_n)$, and the stability result from Theorem 6 to conclude that as long as (1.23) holds and $0 < n\Delta t \le \min(T, T_*)$, we have $\|\nabla\boldsymbol{u}_h^n\| \le C$ and hence

$$\|\boldsymbol{e}_h^n\cdot\nabla\boldsymbol{u}_h(t_n)\|^2 \le C\|\nabla\boldsymbol{e}_h^n\|^2\|\nabla\boldsymbol{u}_h(t_n)\|\|\nabla\boldsymbol{u}_h(t_n)\|_{H^1} \le C\|\nabla\boldsymbol{e}_h^n\|^2, \tag{4.38}$$

$$\|\boldsymbol{u}_h^n\cdot\nabla\boldsymbol{e}_h^n\|^2 \le C\|\nabla\boldsymbol{u}_h^n\|^2\|\nabla\boldsymbol{e}_h^n\|\|\nabla\boldsymbol{e}_h^n\|_{H^1} \le C\|\nabla\boldsymbol{e}_h^n\|\|\Delta\boldsymbol{e}_h^n\|. \tag{4.39}$$

In particular, we obtain

$$\frac{2}{\varepsilon_1}I_3^2 \le \frac{2C}{\varepsilon_1}\|\nabla\boldsymbol{e}_h^n\|\|\Delta\boldsymbol{e}_h^n\| \le \varepsilon_1\nu^2\|\Delta\boldsymbol{e}_h^n\|^2 + \frac{C^2}{\varepsilon_1^3\nu^2}\|\nabla\boldsymbol{e}_h^n\|^2. \tag{4.40}$$

Combining this with (4.38) and (4.36), from (4.35) we see that if ε_1 is chosen sufficiently small we get (4.31).

4.2.3 Discretization error for velocity

If we integrate (1.9) from t_n to t_{n+1}, and use the regularity assumption (ii), we see that the exact solution satisfies, for any $\boldsymbol{v}_h \in X_{0,h}$,

$$\begin{aligned}\left\langle \frac{1}{\Delta t}(\nabla \boldsymbol{u}(t_{n+1}) - \nabla \boldsymbol{u}(t_n)), \nabla \boldsymbol{v}_h \right\rangle + \nu \big\langle \Delta \boldsymbol{u}(t_{n+1}), \Delta \boldsymbol{v}_h \big\rangle \\ = \big\langle \nabla p(t_n) + \boldsymbol{u}(t_n) \cdot \nabla \boldsymbol{u}(t_n) - \boldsymbol{f}(t_n) + \boldsymbol{g}^n \Delta t, \Delta \boldsymbol{v}_h \big\rangle, \end{aligned} \tag{4.41}$$

where $\|\boldsymbol{g}^n\|$ is uniformly bounded in n. Using the projections in (4.28), we can rewrite this as

$$\begin{aligned}\left\langle \frac{1}{\Delta t}(\nabla \boldsymbol{u}_h(t_{n+1}) - \nabla \boldsymbol{u}_h(t_n)), \nabla \boldsymbol{v}_h \right\rangle + \nu \big\langle \Delta \boldsymbol{u}_h(t_{n+1}), \Delta \boldsymbol{v}_h \big\rangle \\ = \big\langle \nabla p_h(t_n) + \boldsymbol{u}_h(t_n) \cdot \nabla \boldsymbol{u}_h(t_n) - \boldsymbol{f}(t_n) + \boldsymbol{g}^n \Delta t, \Delta \boldsymbol{v}_h \big\rangle + \hat{\ell}^n, \end{aligned} \tag{4.42}$$

where, due to (4.20),

$$\begin{aligned}\hat{\ell}^n = &- \frac{1}{\Delta t} \big\langle \nabla (I - \boldsymbol{\Pi}_h)(\boldsymbol{u}(t_{n+1}) - \boldsymbol{u}(t_n)), \nabla v_h \big\rangle + \big\langle \nabla (I - \mathbf{P}_h) p(t_n), \Delta \boldsymbol{v}_h \big\rangle \\ &+ \big\langle \, ((I - \boldsymbol{\Pi}_h)\boldsymbol{u}(t_n)) \cdot \nabla \boldsymbol{u}(t_n) + (\boldsymbol{\Pi}_h \boldsymbol{u}(t_n)) \cdot \nabla (I - \boldsymbol{\Pi}_h)\boldsymbol{u}(t_n), \Delta \boldsymbol{v}_h \big\rangle. \end{aligned} \tag{4.43}$$

By the regularity assumptions (ii), (4.29) and (4.25), and estimates like (4.38)–(4.39) (and the elliptic regularity estimate $\|\nabla \boldsymbol{v}_h\| \leq \|\boldsymbol{v}_h\|_{H^2} \leq C\|\Delta \boldsymbol{v}_h\|$), we have

$$|\hat{\ell}^n| \leq C h^m \|\nabla \boldsymbol{v}_h\| + C(h^{m'-1} + h^{m-1/2})\|\Delta \boldsymbol{v}_h\| \leq \varepsilon_2 \|\Delta \boldsymbol{v}_h\|^2 + C(h^{2m'-2} + h^{2m-1}),$$

$$|\langle \boldsymbol{g}^n \Delta t, \Delta \boldsymbol{v}_h \rangle| \leq \varepsilon_2 \|\Delta \boldsymbol{v}_h\|^2 + C\Delta t^2.$$

Subtracting (1.20) from (4.42), we find that the scheme errors $\boldsymbol{e}_h^n$, r_h^n satisfy

$$\left\langle \frac{\nabla \boldsymbol{e}_h^{n+1} - \nabla \boldsymbol{e}_h^n}{\Delta t}, \nabla \boldsymbol{v}_h \right\rangle + \nu \langle \Delta \boldsymbol{e}_h^{n+1}, \Delta \boldsymbol{v}_h \rangle = \langle \nabla r_h^n, \Delta \boldsymbol{v}_h \rangle + \left\langle \boldsymbol{e}_h^n \cdot \nabla \boldsymbol{u}_h(t_n) + \boldsymbol{u}_h^n \cdot \nabla \boldsymbol{e}_h^n, \Delta \boldsymbol{v}_h \right\rangle + \left\langle \boldsymbol{g}^n \Delta t, \Delta \boldsymbol{v}_h \right\rangle + \hat{\ell}^n. \tag{4.44}$$

We will take $\boldsymbol{v}_h = \boldsymbol{e}_h^{n+1}$ and estimate terms on the right-hand side as follows. First, using (4.31) we get

$$\begin{aligned} \left| \langle \nabla r_h^n, \Delta \boldsymbol{e}_h^{n+1} \rangle \right| &\le \frac{\nu}{2} \|\Delta \boldsymbol{e}_h^{n+1}\|^2 + \frac{1}{2\nu} \|\nabla r_h^n\|^2 \\ &\le \frac{\nu}{2} \|\Delta \boldsymbol{e}_h^{n+1}\|^2 + \left(\frac{\nu}{4} + \frac{\varepsilon_0 \nu}{2} \right) \|\Delta \boldsymbol{e}_h^n\|^2 + C \|\nabla \boldsymbol{e}_h^n\|^2 + C h^{2m-2}. \end{aligned} \tag{4.45}$$

Using (4.38) and (4.39), we get

$$\begin{aligned} &\left| \left\langle \boldsymbol{e}_h^n \cdot \nabla \boldsymbol{u}_h(t_n) + \boldsymbol{u}_h^n \cdot \nabla \boldsymbol{e}_h^n, \Delta \boldsymbol{e}_h^{n+1} \right\rangle \right| \\ &\quad \le \varepsilon_2 \|\Delta \boldsymbol{e}_h^{n+1}\|^2 + \frac{C}{\varepsilon_2} \left(\|\nabla \boldsymbol{e}_h^n\|^2 + \|\nabla \boldsymbol{e}_h^n\| \|\Delta \boldsymbol{e}_h^n\| \right) \\ &\quad \le \varepsilon_2 \|\Delta \boldsymbol{e}_h^{n+1}\|^2 + \varepsilon_2 \|\Delta \boldsymbol{e}_h^n\|^2 + \frac{C}{\varepsilon_2^3} \|\nabla \boldsymbol{e}_h^n\|^2. \end{aligned} \tag{4.46}$$

Therefore we find that

$$\begin{aligned} &\frac{1}{2\Delta t} \left(\|\nabla \boldsymbol{e}_h^{n+1}\|^2 - \|\nabla \boldsymbol{e}_h^n\|^2 \right) + \left(\nu - \frac{\nu}{2} - 3\varepsilon_2 \right) \|\Delta \boldsymbol{e}_h^{n+1}\|^2 \\ &\le \left(\frac{\nu}{4} + \frac{\varepsilon_0 \nu}{2} + \varepsilon_2 \right) \|\Delta \boldsymbol{e}_h^n\|^2 + C \|\nabla \boldsymbol{e}_h^n\|^2 + C(\Delta t^2 + h^{2m'-2} + h^{2m-2}). \end{aligned} \tag{4.47}$$

Now, we can choose ε_0 and ε_2 sufficiently small so that the quantities

$$\tilde{\varepsilon}_1 = \nu - 6\varepsilon_2, \qquad \tilde{\varepsilon}_2 = \frac{\nu}{2} - \varepsilon_0 \nu - 8\varepsilon_2,$$

are positive. Then we can rewrite (4.47) as

$$\begin{aligned} &\frac{1}{\Delta t} \left(\|\nabla \boldsymbol{e}_h^{n+1}\|^2 - \|\nabla \boldsymbol{e}_h^n\|^2 \right) + \tilde{\varepsilon}_1 \left(\|\Delta \boldsymbol{e}_h^{n+1}\|^2 - \|\Delta \boldsymbol{e}_h^n\|^2 \right) + \tilde{\varepsilon}_2 \|\Delta \boldsymbol{e}_h^n\|^2 \\ &\quad \le \; C \|\nabla \boldsymbol{e}_h^n\|^2 + C(\Delta t^2 + h^{2m'-2} + h^{2m-2}). \end{aligned} \tag{4.48}$$

By a Gronwall-type argument similar to (4.12)–(4.15) above but without the cubic nonlinear terms, we deduce that if (1.23) holds and $0 \le n\Delta t \le \min(T, T_*)$, then

$$\sup_{0\le k\le n} \|\nabla \boldsymbol{e}_h^k\|^2 + \tilde{\varepsilon}_1 \sum_{k=0}^{n} \|\Delta \boldsymbol{e}_h^k\|^2 \Delta t$$
$$\le C(\Delta t^2 + h^{2m-2} + h^{2m'-2} + \|\nabla \boldsymbol{e}_h^0\|^2 + \tilde{\varepsilon}_2 \|\Delta \boldsymbol{e}_h^0\|^2 \Delta t). \tag{4.49}$$

Going back to (4.31), we get

$$\sum_{k=0}^{n} \|\nabla r_h^k\|^2 \Delta t \le C(\Delta t^2 + h^{2m-2} + h^{2m'-2} + \|\nabla \boldsymbol{e}_h^0\|^2 + \tilde{\varepsilon}_2 \|\Delta \boldsymbol{e}_h^0\|^2 \Delta t). \tag{4.50}$$

Finally, using (4.29) we can replace $\boldsymbol{e}_h^k$ and r_h^k in the two inequalities above by $\boldsymbol{e}^k$ and r^k respectively. This finishes the proof of the theorem. □

4.3 Practical issues

4.3.1 Divergence damping

Although it is satisfying to have a rigorous mathematical proof of stability and error estimates, the hypothesis that the domain is C^3 will fail to hold in many practical problems. Computational domains are commonly polygonal, and the smoothness of solutions can be limited by corner singularities. Our numerical experiments reported in section 4.4 below indicate that near corners where the solution may have a strong singularity, such as in a driven cavity or near a backward-facing step, the finite-element scheme (1.18),(1.20) may not perform well. One possible reason is that the divergence error is large near the corner and may diffuse out and pollute the solution downstream (see Figure 4.11).

There is, however, a way to alleviate this difficulty with divergence error. As was done by Petersson [Pe], we can add a lower-order term to damp the divergence. Instead of (1.5), we require

$$\nabla p = (I - \mathcal{P})(\boldsymbol{f} - \boldsymbol{u} \cdot \nabla \boldsymbol{u}) + \nu(I - \mathcal{P})(\Delta \boldsymbol{u} - \nabla \nabla \cdot \boldsymbol{u}) + \lambda(I - \mathcal{P})\boldsymbol{u}. \tag{4.51}$$

Using this in the NSE (1.9), we get

$$\partial_t \boldsymbol{u} + \mathcal{P}(\boldsymbol{u} \cdot \nabla \boldsymbol{u} - \boldsymbol{f} - \nu \Delta \boldsymbol{u}) = \nu \nabla(\nabla \cdot \boldsymbol{u}) - \lambda(I - \mathcal{P})\boldsymbol{u}. \tag{4.52}$$

Taking the divergence on both sides when λ does not depend on the space variable, we immediately see we have additionally a local damping term; the divergence $w = \nabla \cdot \boldsymbol{u}$ satisfies $\partial_t w = \nu \Delta w - \lambda w$.

Notice that $(I - \mathcal{P})\boldsymbol{u}$ in (4.51) is absent if $\boldsymbol{u}$ is already divergence-free. When $\lambda = O(1)$, it is a lower-order term, and the proofs of Theorem 1, 2 and 6 are easily extended to yield stability and error estimates of the same form for the modified schemes with $\boldsymbol{u} = 0$ on Γ.

4.3.2 Obtuse corners and C^1 finite elements

Another possible reason for poor performance of the C^1 scheme (1.18),(1.20) in domains with corners may be the presence of a corner singularity in the exact solution. In the following, we will first illustrate what kind of trouble we are facing and further describe the way that we propose to overcome it. In short, our approach is to add a small number of basis functions ("corner elements") to the finite-element space for velocity, to allow jumps in directional derivatives near the corner.

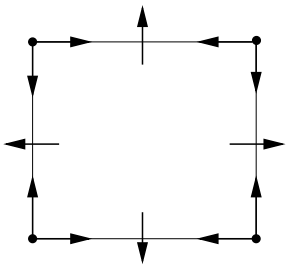

Figure 4.1: FVS finite element

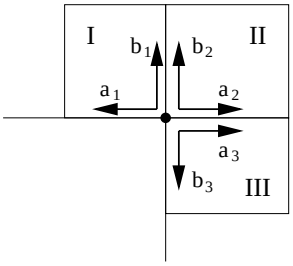

Figure 4.2: FEs around the corner

We will illustrate the problem in 2D with a particular kind of C^1 finite element that we have used in our computation, namely, the Fraeijs de Veubeke-Sander (FVS) type C^1 finite elements. They are piecewise 3rd-order polynomials that satisfy assumption (i) in Theorem 1 with $m = 3$ and $m' = 4$. There are 16 degrees of freedom in each FVS element. See Figure 4.1 for a descriptive diagram—the arrows stand for evaluating directional derivatives and the dots mean taking values at the associated points.

If we have an obtuse corner, we need to put three elements around the corner. See Figure 4.2 for an illustration. For globally C^1 functions in the finite-element space, there are three degrees of freedom at the vertex of the corner: one value and two directional derivatives. The problem comes from the directional derivatives, which we will denote by a and b for the horizontal and vertical velocity components, respectively. In Figure 4.2, we intentionally use a_i and b_i $(i = 1, 2, 3)$ to denote the a and b degrees of freedom evaluated separately in different elements at the vertex.

No-slip boundary conditions require that $a_1 = b_3 = 0$. To use C^1 finite elements in the standard way, since derivatives are continuous, one must set $a_i = b_i = 0$ for $i = 1, 2, 3$. As reported below in section 4.4.2, this leads to poor results

for flow over a backward-facing step.

A simple way to seek an improvement is to allow for the possibility of a discontinuity in directional derivatives near the corner. A method that we have implemented works as follows. Let $U_{0,h}$ denote the FVS finite-element space of piecewise polynomials that are C^1 in Ω and vanish on the boundary. The corresponding C^1 finite-element space for velocity is $X_{0,h} = U_{0,h} \times U_{0,h}$. Let $\{\phi_i\}_{i=1}^D$ be a basis for $U_{0,h}$, such that each function $u_h \in U_h$ is represented by

$$u_h = \sum_{i=1}^{D} u_i \phi_i, \tag{4.53}$$

where the number u_i is either the value or a directional derivative of u at some point on the element. (See Figure 4.1.) We augment this basis by including two additional basis functions or corner elements ϕ_a and ϕ_b, which are C^0 but not C^1 across the boundaries between the elements in Figure 4.2. To be more specific, the functions ϕ_a and ϕ_b are constructed inside each FVS element such that at the corner point P,

$$\partial_x \phi_a = 1 = a_2 = a_3 \quad \text{at } P \text{ in elements II and III,}$$

$$\partial_y \phi_b = 1 = b_1 = b_2 \quad \text{at } P \text{ in elements I and II,}$$

and all other degrees of freedom of these functions vanish in every element. In particular, $\phi_a \equiv 0$ in element I, so $\partial_x \phi_a$ is discontinuous across the boundary between elements I and II, and similarly $\phi_b \equiv 0$ in element III and $\partial_y \phi_b$ is discontinuous across the boundary between elements II and III. These additional basis functions are crude truncations of some FVS basis functions that are in $H^2(\Omega, \mathbb{R}^N)$ but not in $X_{0,h}$, so the necessary modifications are not difficult to implement in practice.

With the basis augmented by these obtuse corner elements, we get an augmented FVS finite-element space

$$\tilde{U}_{0,h} = U_{0,h} \oplus \text{span}\{\phi_a, \phi_b\}$$

and a new finite-element space for velocity, $\tilde{X}_{0,h} = \tilde{U}_{0,h} \times \tilde{U}_{0,h}$. We can then use the same equations, namely (1.20) and (1.18), to solve for velocity and pressure. The space Y_h remains unchanged. However, terms containing second derivatives of $\boldsymbol{u}_h^n$, $\boldsymbol{u}_h^{n+1}$ and $\boldsymbol{v}_h$ are now being computed and integrated element-wise. For example, the term $\left\langle \boldsymbol{u}_h^n \cdot \nabla \boldsymbol{u}_h^n, \Delta \boldsymbol{v}_h \right\rangle_\Omega$ is now replaced by $\sum_k \left\langle \boldsymbol{u}_h^n \cdot \nabla \boldsymbol{u}_h^n, \Delta \boldsymbol{v}_h \right\rangle_{\mathcal{T}_k}$ where $\{\mathcal{T}_k\}$ is the triangulation of Ω associated with $\tilde{X}_{0,h}$. (We do not add jump terms on the element boundaries. Numerical experiments we performed including such jump terms showed no essential difference.) Note that the matrix that we need to invert in order to solve for $\boldsymbol{u}_h^{n+1}$ remains symmetric positive-definite when corners are handled in this way.

Finally, we remark that in our scheme (1.18),(1.19) that uses C^0 finite elements for velocity, we do not require any special accommodation for the corner. In this case, derivatives are no longer degrees of freedom and the scheme performs well without modifications.

4.3.3 Non-homogeneous boundary conditions

We handle non-homogeneous boundary conditions for the velocity in the way described in [LLP]. Suppose the no-slip boundary condition (1.11) is replaced by

$$\boldsymbol{u} = \boldsymbol{g} \quad \text{on } \Gamma. \tag{4.54}$$

The boundary data $\boldsymbol{g}$ is required to satisfy the compatibility condition

$$\int_\Gamma \boldsymbol{n}\cdot\boldsymbol{g} = 0 \quad \text{for } t > 0.$$

Paper [LLP] proved unconditional stability and convergence of the following time-discrete scheme for the NSE (1.9),(1.10) and (4.54), under appropriate conditions on regularity and initial compatibility for the data. Given $\boldsymbol{u}^n \in H^2(\Omega,\mathbb{R}^N)$, determine $\nabla p^n \in L^2(\Omega,\mathbb{R}^N)$ so that for all $q \in H^1(\Omega)$,

$$\begin{aligned}\langle \nabla p^n, \nabla q\rangle &= \langle \boldsymbol{f}^n - \boldsymbol{u}^n\cdot\nabla\boldsymbol{u}^n + \nu\Delta\boldsymbol{u}^n - \nu\nabla\nabla\cdot\boldsymbol{u}^n, \nabla q\rangle \\ &\quad - \left\langle \frac{\boldsymbol{n}\cdot(\boldsymbol{g}^{n+1}-\boldsymbol{g}^n)}{\Delta t}, q\right\rangle_\Gamma ,\end{aligned} \tag{4.55}$$

then determine $\boldsymbol{u}^{n+1} \in H^2(\Omega,\mathbb{R}^N)$ from the boundary value problem

$$\frac{\boldsymbol{u}^{n+1}-\boldsymbol{u}^n}{\Delta t} - \nu\Delta\boldsymbol{u}^{n+1} = \boldsymbol{f}^n - \boldsymbol{u}^n\cdot\nabla\boldsymbol{u}^n - \nabla p^n, \tag{4.56}$$

$$\boldsymbol{u}^{n+1}\big|_\Gamma = \boldsymbol{g}^{n+1}. \tag{4.57}$$

We discretize these equations as before, modifying (1.18) to allow for a divergence damping term as in (4.51): Let $Y_h \subset H^1(\Omega)/\mathbb{R}$ be a space of C^0 finite elements for pressure. Given an approximation $\boldsymbol{u}_h^n$ to $\boldsymbol{u}^n$, determine $p_h^n \in Y_h$ so that

$$\begin{aligned}\langle \nabla p_h^n, \nabla q_h\rangle &= \langle \boldsymbol{f}^n - \boldsymbol{u}_h^n\cdot\nabla\boldsymbol{u}_h^n, \nabla q_h\rangle + \nu\langle \nabla\times\boldsymbol{u}_h^n, \boldsymbol{n}\times\nabla q_h\rangle_\Gamma \\ &\quad - \left\langle \frac{\boldsymbol{n}\cdot(\boldsymbol{g}^{n+1}-\boldsymbol{g}^n)}{\Delta t}, q_h\right\rangle_\Gamma - \lambda\langle\nabla\cdot\boldsymbol{u}_h^n, q_h\rangle\end{aligned} \tag{4.58}$$

for all $q_h \in Y_h$.

For the momentum equation, we look for $\boldsymbol{u}_h^n$ in a space of finite elements $X_h \supseteq X_{0,h}$, with $X_h \subset H^1(\Omega,\mathbb{R}^N)$ for C^0 finite elements and $X_h \subset H^2(\Omega,\mathbb{R}^N)$ for

C^1 finite elements. If X_h is a C^0 finite-element space and has a nodal basis, we enforce the boundary condition

$$\boldsymbol{u}_h^{n+1} = \boldsymbol{g}(t_{n+1}) \tag{4.59}$$

at all boundary nodes. Let ∂_τ denote tangential derivatives. If X_h is a C^1 finite-element space, we require

$$\boldsymbol{u}_h^{n+1} = \boldsymbol{g}(t_{n+1}), \qquad \partial_\tau \boldsymbol{u}_h^{n+1} = \partial_\tau \boldsymbol{g}(t_{n+1}) \tag{4.60}$$

for all corresponding boundary degrees of freedom (DOF, i.e., those parameters which uniquely define a function in the space X_h). Once the DOF at the boundary are taken care of, the DOF at interior points of the triangulated domain are determined by solving the same equation as before: (1.19) for the C^0 case and (1.20) for the C^1 case, for all $\boldsymbol{v}_h \in X_{0,h}$. In the C^1 case, when the domain contains an obtuse corner, the space X_h is augmented using corner elements as described in the previous subsection.

4.3.4 Higher-order time integration

Higher-order time integration methods can easily be incorporated. For example, using 2nd order Crank-Nicholson/Adams-Bashforth (CN/AB) time stepping for the momentum equation yields the following semi-discrete scheme:

$$\begin{aligned} &\frac{\boldsymbol{u}^{n+1} - \boldsymbol{u}^n}{\Delta t} + \frac{3}{2}\left(\nabla p^n + \boldsymbol{u}^n \cdot \nabla \boldsymbol{u}^n\right) - \frac{1}{2}\left(\nabla p^{n-1} + \boldsymbol{u}^{n-1} \cdot \nabla \boldsymbol{u}^{n-1}\right) \\ &\qquad = \frac{\nu}{2}\Delta(\boldsymbol{u}^n + \boldsymbol{u}^{n+1}) + \boldsymbol{f}(t_{n+1/2}). \end{aligned} \tag{4.61}$$

The pressure equation remains unchanged. We discretize spatially as before.

One can also use explicit time stepping like Runge-Kutta (RK) for the momentum equation. See [EL2] for a discussion of the advantages of using high-order RK methods when the Reynolds number $\mathrm{Re} = \nu^{-1}$ is large. For completeness, we also write out the semi-discrete explicit RK4 scheme that we have used:

$$\frac{\boldsymbol{u}_1 - \boldsymbol{u}^n}{\Delta t/2} + \boldsymbol{u}^n \cdot \nabla \boldsymbol{u}^n + \nabla p^n = \nu \Delta \boldsymbol{u}^n + \boldsymbol{f}^n, \qquad p_1 = \mathcal{F}(\boldsymbol{u}_1, \boldsymbol{f}^{n+1/2}), \tag{4.62}$$

$$\frac{\boldsymbol{u}_2 - \boldsymbol{u}^n}{\Delta t/2} + \boldsymbol{u}_1 \cdot \nabla \boldsymbol{u}_1 + \nabla p_1 = \nu \Delta \boldsymbol{u}_1 + \boldsymbol{f}^{n+1/2}, \quad p_2 = \mathcal{F}(\boldsymbol{u}_2, \boldsymbol{f}^{n+1/2}), \tag{4.63}$$

$$\frac{\boldsymbol{u}_3 - \boldsymbol{u}^n}{\Delta t} + \boldsymbol{u}_2 \cdot \nabla \boldsymbol{u}_2 + \nabla p_2 = \nu \Delta \boldsymbol{u}_2 + \boldsymbol{f}^{n+1/2}, \quad p_3 = \mathcal{F}(\boldsymbol{u}_3, \boldsymbol{f}^{n+1}), \tag{4.64}$$

$$\frac{\boldsymbol{u}_4 - \boldsymbol{u}^n}{\Delta t} + \boldsymbol{u}_3 \cdot \nabla \boldsymbol{u}_3 + \nabla p_3 = \nu \Delta \boldsymbol{u}_3 + \boldsymbol{f}^{n+1}, \tag{4.65}$$

$$\boldsymbol{u}^{n+1} = -\frac{1}{2}\boldsymbol{u}^n + \frac{1}{6}(2\boldsymbol{u}_1 + 4\boldsymbol{u}_2 + 2\boldsymbol{u}_3 + \boldsymbol{u}_4), \quad p^{n+1} = \mathcal{F}(\boldsymbol{u}^{n+1}, \boldsymbol{f}^{n+1}), \tag{4.66}$$

where $p = \mathcal{F}(\boldsymbol{u}, \boldsymbol{f})$ satisfies

$$\langle \nabla p, \nabla q \rangle = \langle \boldsymbol{f} - \boldsymbol{u} \cdot \nabla \boldsymbol{u}, \nabla q \rangle + \nu \langle \nabla \times \boldsymbol{u}, \boldsymbol{n} \times \nabla q \rangle_\Gamma \qquad \forall q \in H^1(\Omega).$$

4.3.5 How to solve for the pressure

We want to briefly indicate how we solve the pressure equation (1.18), because typically one has to deal with a singular mass matrix $A = \big(\langle \nabla \phi_i, \nabla \phi_j \rangle\big)$, where $\{\phi_i\}_{i=1}^D$ is a basis for the finite-element pressure space Y_h. Here D is the number of degrees of freedom in Y_h. If we write $p_h^n = \sum_i p_i \phi_i$ and

$$b_i = \langle \boldsymbol{f}^n - \boldsymbol{u}_h^n \cdot \nabla \boldsymbol{u}_h^n, \nabla \phi_i \rangle + \nu \langle \nabla \times \boldsymbol{u}_h^n, \boldsymbol{n} \times \nabla \phi_i \rangle_\Gamma, \tag{4.67}$$

the pressure equation (1.18) is equivalent to the system of equations

$$A\boldsymbol{p} = \boldsymbol{b}, \tag{4.68}$$

with $\boldsymbol{p} = (p_i)$ and $\boldsymbol{b} = (b_i)$. If $A\boldsymbol{p} = 0$ for some $\boldsymbol{p} \in \mathbb{R}^D$ then correspondingly $\boldsymbol{p}^T A\boldsymbol{p} = \int_\Omega |\nabla p_h^n|^2 = 0$ and hence p_h^n must be a constant in Ω. Thus A is singular if and only if the constant $1 \in Y_h$, which is typical. A solution of (4.68) always exists, however, since if $1 = \sum_i c_i \phi_i \in Y_h$, then $\boldsymbol{b}$ in (4.67) naturally satisfies the solvability condition $\boldsymbol{c}^T \boldsymbol{b} = 0$.

What we can do to compute a solution is simply remove some single basis element ϕ_j from the set $\{\phi_i\}_{i=1}^D$, such that if $1 = \sum_i c_i \phi_i$ then $c_j \neq 0$. In practice, this usually means deleting a single basis element ϕ_j such that the value p_j corresponds to a nodal value of p_h^n. Then it follows that $1 \notin \hat{Y}_h = \text{span}\{\phi_i : i \neq j\}$. Hence we can solve (4.68) by deleting the jth row and column from matrix A, and the jth row from $\boldsymbol{b}$, solving the resulting $(D-1) \times (D-1)$ (symmetric positive-definite) system, and setting $p_j = 0$ afterward.

4.4 Numerical results

In this section, we report numerical results for both the C^1 and C^0 finite-element schemes. For both kinds of schemes, we perform a spatial accuracy check and stability check for a smooth flow, and computations for two benchmark test problems: driven cavity flow and flow over a backward-facing step. In the benchmark computations, we also compare the results obtained with and without divergence damping. Our numerical results will be shown in four groups of figures:

- Figures 4.3–4.5: accuracy & stability check for C^1 finite elements
- Figures 4.6-4.15: benchmark computations for C^1 finite elements

- Figures 4.16–4.18: accuracy & stability check for C^0 finite elements
- Figures 4.19–4.23: benchmark computations for C^0 finite elements

4.4.1 Test problems and parameters

For the stability and accuracy checks for both C^1 and C^0 schemes, we take the domain to be $[-1,1]\times[-1,1]$ and let the exact solution be

$$u_{\text{ex}}(x,y,t) = \quad g(t)\cos^2(\pi x/2)\sin(\pi y), \tag{4.69}$$

$$v_{\text{ex}}(x,y,t) = -g(t)\sin(\pi x)\cos^2(\pi y/2), \tag{4.70}$$

$$p_{\text{ex}}(x,y,t) = \quad g(t)\cos(\pi x/2)\sin(\pi y/2), \tag{4.71}$$

where $g(t)$ is a given function. The forcing term $\boldsymbol{f}$ is chosen so that (4.69)–(4.71) is a solution of NSE.

The parameters that we use in computations with the above given exact solution are listed in Table 4.1. In the table, Re is the Reynolds number, h is the size of the element (we use uniform meshes in this case), Δt is the size of the time step, and T is the final time we integrated to. P4 means 4th-order Lagrange elements. FVS/FVS means FVS finite elements for both velocity and pressure. BE/FE means Backward Euler for the viscosity term and Forward Euler for pressure and convection terms.

The notation used in the legends of the figures mentioned in Table 4.1 is as follows. Lower-case letters u, v or p stand for the numerical solution. Capital letters U, V or P stand for the interpolants of the exact solution in the finite-element spaces. We also use ω and Ω to denote the numerical and interpolated vorticities.

Fig.	FE space	time stepping	Re	$g(t)$	h	Δt	T
4.3	FVS/FVS	CN/AB	0.5	$\cos(t)$	varying	h^2	2
4.4	FVS/FVS	BE/FE	0.5	$(t-1)$	varying	0.01	2
4.5	FVS/FVS	BE/FE	0.5	$\cos(t)$	1/8	varying	1000
4.16	P1/P1	CN/AB	0.5	$\cos(t)$	varying	h^2	2
4.17	P1/P1	BE/FE	0.5	$\cos(t)$	1/16	varying	1000
4.18	P4/P4	RK4	1000	$(t-1)^4$	varying	0.003	2

Table 4.1: Parameters for computations with exact solutions

Next, we explain the benchmark computations. For the driven cavity flow, we compute the flow in the domain $[0,1] \times [0,1]$ and start from rest, impulsively imposing horizontal velocity $u = 1$ on the top boundary for $t > 0$. Following [BP], we plot the contours of vorticity with values [-5, -4, -3, -2, -1, -0.5, 0, 0.5, 1, 2, 3]. We also follow [KM] to plot the normalized velocity fields in order to visualize flow details near the corner. These plots also show the non-uniform mesh used. We refer to the computational results of [KM, BP] for comparison.

For the backward-facing step, we compute the flow in the domain

$$\Omega = [0, L] \times [-0.5, 0.5] \setminus [0, 0.5] \times [-0.5, 0]$$

with no-slip boundary conditions everywhere except at the inflow boundary $x = 0$ and the outflow boundary $x = L$. We take $L = 8$ when Re=100 and $L = 20$ when Re=600. We use CN/AB time-stepping in every case. We start from rest

and gradually increase the boundary velocity (u, v) to $(12y(1-2y), 0)$ at the inflow boundary and $(-3y^2 + 3/4, 0)$ at the outflow boundary, with no net influx at each time. The time-dependent function we used for gradually increasing velocity is $(1-\cos(\pi t))/2$ on $[0, 1]$. Once the velocity field is obtained, we use the `streamline` function in MATLAB to plot the streamlines. We also show color contour plots of the divergence error when Re=100. We will focus on the region near the corner at $(0.5, 0)$ because the divergence error is small in other places. The colorbar associated with the contour plot indicates the range of the divergence error.

We list below the parameters used in the benchmark computations. In addition to the notations we have explained and used in Table 4.1, λ is the divergence damping coefficient in (4.51) or (4.58). "Corner elements" means we augment X_h using basis functions with jumps in directional derivatives supported near the corner as described in section 4.3.2. Here, h is the side length of the smallest element of the mesh (FVS square or Lagrange triangle).

4.4.2 Numerical results for C^1 FE schemes like (1.18),(1.20)

Accuracy and stability checks for scheme (1.18),(1.20)

Although the square domain we used does not meet the C^3 regularity requirement set forth in the theorems, we find that the scheme still performs well with a smooth solution (4.69)–(4.71). The results are reported in Figure 4.3 and 4.5. The parameters that we used in the computations can be found in Table 4.1.

In Figure 4.3 we plot the errors that result as we vary h. Note that since we

Fig. #	FE spaces	Time stepping	Re	# of elements	h	Δt	λ	T
4.6	FVS/FVS	BE/FE	1000	48×48	0.0086	0.004	0	40
4.7	FVS/FVS	BE/FE	1000	48×48	0.0086	0.004	150	40
4.8	FVS/FVS	BE/FE	1000	64×64	0.0064	0.004	150	40
4.9	FVS/FVS	CN/AB	2000	48×48	0.0086	0.002	0	60
4.10	FVS/FVS	CN/AB	2000	48×48	0.0086	0.002	300	60
4.19	P4/P4	RK4	1000	2×32×32	0.0119	0.0006	0	40
4.20	P4/P4	RK4	2000	2×32×32	0.0119	0.0009	15	60

Table 4.2: Parameters for driven cavity flow computations

use second-order-accurate time stepping and take $\Delta t = h^2$, the error is mainly due to spatial discretization. Errors for u and p in the L^2 and L^∞ norms appear in the left plot, and errors for ∇u, ∇p and the divergence $u_x + v_y$ appear in the right plot. The v component behaves similar to u. If we use randomly distorted grids with $h_{max}/h_{min} \approx 2$, the behavior is similar.

From the results in Figure 4.3, we see that our theoretical error estimates (Theorem 1) do not appear to be sharp—the scheme performs better than the theory suggests. Indeed, the order of accuracy achieved in solving the Navier-Stokes equations is the same as that for the heat equation. For purposes of comparison, in Figure 4.4 we plot errors for the numerical solution at $t = 2$ of a forced heat equation $\partial_t u = \nu \Delta u + f$ with exact solution $u = u_{\text{ex}}$ in (4.69). We compute using

Fig. #	FE spaces	Re	# of ele-ments	h	Δt	λ	T	Corner elements
4.11	FVS/FVS	100	594	0.0301	0.006	0	20	Y
4.13	FVS/FVS	100	594	0.0301	0.006	150	20	N
4.14	FVS/FVS	100	594	0.0301	0.006	150	20	Y
4.15	FVS/FVS	600	1107	0.0307	0.003	150	120	Y
4.21	P4/P4	100	528	0.048	0.003	20	20	N
4.22	P4/P4	100	1188	0.0301	0.003	20	20	N
4.23	P4/P4	600	984	0.0502	0.0025	20	120	N

Table 4.3: Parameters for backward-facing step flow computations. (CN/AB time stepping is used)

the scheme

$$\left\langle \frac{\nabla u_h^{n+1} - \nabla u_h^n}{\Delta t}, \nabla v_h \right\rangle + \nu \langle \Delta u_h^{n+1}, \Delta v_h \rangle = \langle f^{n+1}, \Delta v_h \rangle \quad \forall v_h \in X_{0,h}. \tag{4.72}$$

If we take $g(t) = t - 1$, the error is completely due to spatial discretization. To see this, one just needs to compare with (4.41) and see that the exact solution satisfies

$$\left\langle \frac{\nabla u(t_{n+1}) - \nabla u(t_n)}{\Delta t}, \nabla v \right\rangle + \nu \langle \Delta u(t_{n+1}), \Delta v \rangle = \langle f(t_{n+1}), \Delta v \rangle \quad \forall v \in H_0^1(\Omega).$$

without any truncation error $\boldsymbol{g}^n \Delta t$ like in (4.41).

Figure 4.5 is the stability check. Our numerical tests indicate that the C^1 scheme (1.18)+(1.20) for NSE is unconditionally stable. With a fixed 16×16 grid

and increasing the time step up to $\Delta t = 8$, the solution and its first derivatives remain order $O(1)$ up to time $t = 1000$.

Driven cavity and backward-facing step

In Figures 4.6–4.10, we draw the contour plot of vorticity and normalized velocity field for the driven cavity flow with different Reynolds numbers and divergence damping coefficient λ.

Figure 4.6 shows the results with Re=1000 and no divergence damping ($\lambda = 0$). In Figure 4.7, we show the results with the same Reynolds number but with $\lambda = 150$. Comparing the two, we see that the results are almost the same. Then in Figure 4.8 we do a mesh refinement study (with the same Δt as in Figure 4.7) and see almost no difference comparing with Figure 4.7.

However, when we increase Re to 2000 we see that divergence damping does make a difference. Figure 4.9 shows the normalized velocity field when we do not add the damping. As shown in the plot on the right, if we zoom into the upper left corner, we see that a vortex in the corner is missed. However, Figure 4.10 shows that this vortex is recovered once we add local divergence damping.

Our backward-facing step computations are reported in Figures 4.11 to 4.15. In each figure, we plot the streamlines on the top. On the bottom is also a contour plot of the divergence error when Re=100. The first results, shown in Figure 4.11, are without divergence damping. The flow is totally unphysical, with streamlines emerging from the boundary below the step. This appears to be associated with

divergence error—we have a positive divergence $\nabla \cdot \boldsymbol{u}_h > 0$ in the region below the step. So we add divergence damping for all the remaining cases.

If we only add divergence damping, but stay completely with C^1 elements throughout, which forces the x and y derivatives of velocity at the corner to be zero in elements I, II and III as indicated in Figure 4.2, we get the poor results shown in figure 4.13. The flow contains two large eddies, in disagreement with related computations in other sources, for example [MPT, KM, GDN].

We are able to get better results with the treatment described in section 4.3.2, adding a few basis elements with jumps in x and y derivatives at the corner. With these corner elements, we obtain Figure 4.14 for Re = 100, and Figure 4.15 for Re = 600. For a comparison of our results with experiment and other classical computations, we refer to table 4.4 below.

Looking at the divergence errors in Figure 4.11, 4.13 and 4.14, one might argue that to determine if one result is more reliable than another, one should examine not only the L^∞ norm of the divergence error, but also and probably more importantly, the size of the support of the divergence error.

4.4.3 Numerical results for C^0 FE schemes like (1.18),(1.19)

Accuracy and stability check

Figures 4.16 and 4.17 are accuracy and stability checks for the scheme (1.18),(1.19) with P1 finite elements for both velocity and pressure. Figure 4.18 is the spatial accuracy check when we use explicit RK4 time stepping and P4/P4 finite element

spaces. The parameters used in the computations can be found in Table 4.1.

In Figure 4.16, we plot the errors that result as we vary h. Note that since we use second-order-accurate time stepping and take $\Delta t = h^2$, the error is mainly due to spatial discretization. Errors for u and p in the L^2 and L^∞ norms appear in the left plot, and errors for ∇u, ∇p, divergence $u_x + v_y$ and vorticity appear in the right plot. The v component behaves like u. We have used a first-order Lagrange element, which is the simplest C^0 element for both velocity and pressure. Uniform-mesh results are reported here. If we use randomly distorted grids with $h_{max}/h_{min} \approx 2$, the behavior is similar.

Figure 4.17 is the stability check. Our numerical tests indicate that our C^0 scheme (1.18),(1.19) is unconditionally stable at least in this case with a smooth solution. With a fixed uniform $2 \times 32 \times 32$ mesh and increasing the time step up to $\Delta t = 8$, the solution and its first derivatives remain of order $O(1)$ up to time $t = 1000$.

We believe that this is quite remarkable. Traditionally, using the simplest P1/P1 Lagrange elements in incompressible fluid computations has been impossible, due to the instability associated with the failure of the inf-sup condition for coupled Stokes solvers. But now, in our framework, P1/P1 elements work well, and with a scheme implicit only in velocity, we appear to achieve unconditional stability. (As pointed out to us by Hans Johnston, we no longer have unconditional stability, however, when we use CN/AB time stepping.)

Figure 4.18 shows that we get higher-order spatial accuracy if we use higher-order finite elements. We have taken Δt small enough so that the error is mainly

due to spatial discretization.

Driven cavity and backward-facing step

Figure 4.19 and Figure 4.20 are for driven cavity computations with Re=1000 and 2000. In Figure 4.19, we have not yet used local divergence damping and the results agree extremely well with the results in [BP]. But once Re increases to 2000, we have to add divergence damping in order to capture the upper left vortex in Figure 4.20. To demonstrate the versatility of our scheme, we have chosen to use explicit time stepping, namely explicit RK4, although we can use other methods.

Figure 4.21 is a backward-facing step calculation with Re=100. (We do not show it here, but if we do not add divergence damping in the calculation, we get results like Figure 4.11.) Then we do a mesh refinement study (but with the same Δt) in Figure 4.22 and get essentially the same results as in Figure 4.21. With Re= 600 we obtain Figure 4.23. Comparisons of our results with experiment and other classical computations are given in Table 4.4 below.

Comparison of results for backward-facing step flow

For the purpose of comparing our results for backward-facing step flow with other sources, we have computed ratios of various characteristic lengths to the step height. The results are listed in Table 4.4, together with the experimental data from [ADPS], and a classical computation of Kim and Moin [KM]. In the table, S is the step height, R or X_3 is the reattachment length of the lower eddy, and X_1 and

X_2 are the detachment and reattachment length of the upper eddy. The meaning of S, X_1, X_2 and X_3 are also explicitly indicated in Figures 4.15 and 4.23. When Re=600, the values of X_1/S and X_2/S from [KM] are based on measurement of Figure 10 in their paper. Since the exact position of turning points is hard to tell from their figure, we indicate a possible range of values. In [ADPS], the authors report experiments performed at Re=600 and they measured X_2/S. However, the value of this ratio is not on the curve they finally chose to fit the data. Therefore, we have listed both the value from experiment and the value on the curve.

Following [KM], we have chosen the expansion ratio, which is the ratio of the step height to channel height, to be 1:2. However, the experiments in [ADPS] are based in an expansion ratio 1:1.94. Note that Kim and Moin's computational domain does not include an inlet region and they directly impose the inflow boundary condition at $x = 0.5, y \in [0, 0.5]$ in our coordinates. In contrast, our domain contains an inlet region which has made the problem more physically realistic but the computation more challenging. Indeed, it is the inclusion of this inlet region that forces us to find a way to handle corners with obtuse angles.

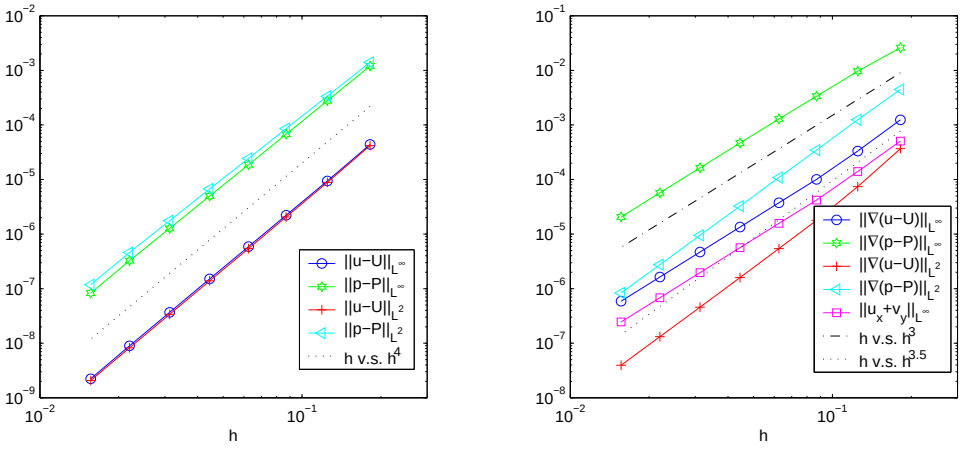

Figure 4.3: Spatial accuracy at $t = 2$ for C^1 scheme with CN/AB time stepping

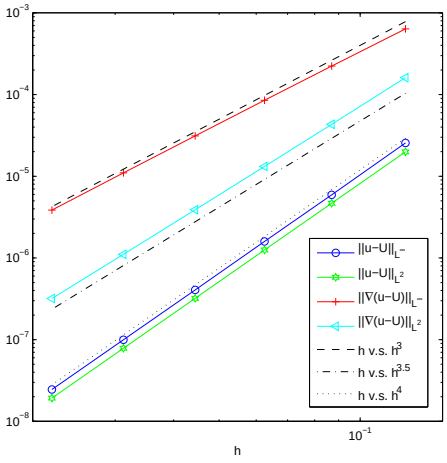

Figure 4.4: Spatial accuracy check for C^1 scheme for heat equation

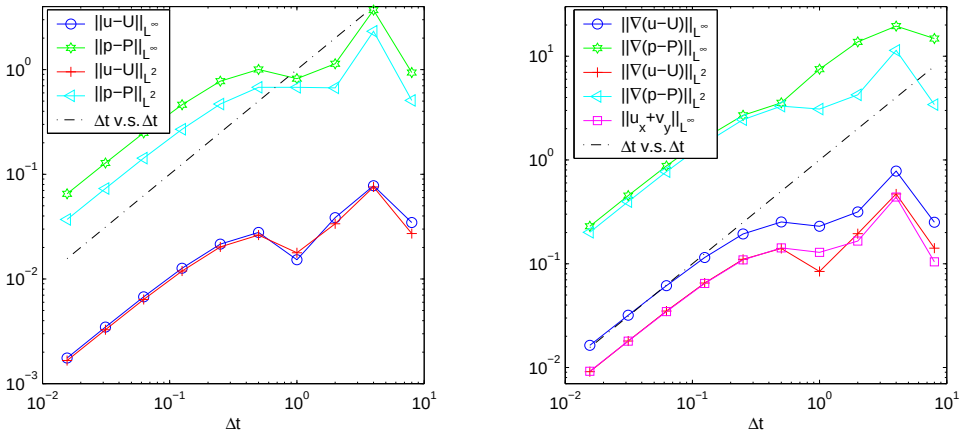

Figure 4.5: Stability check for C^1 scheme (1.18)+(1.20). Integrate until t=1000.

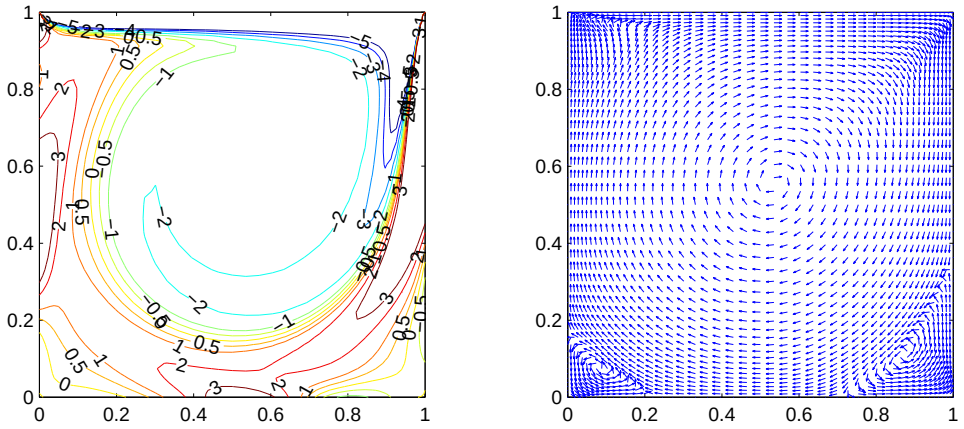

Figure 4.6: Driven cavity. Re=1000. 48×48 FVS elements. $\lambda = 0$.

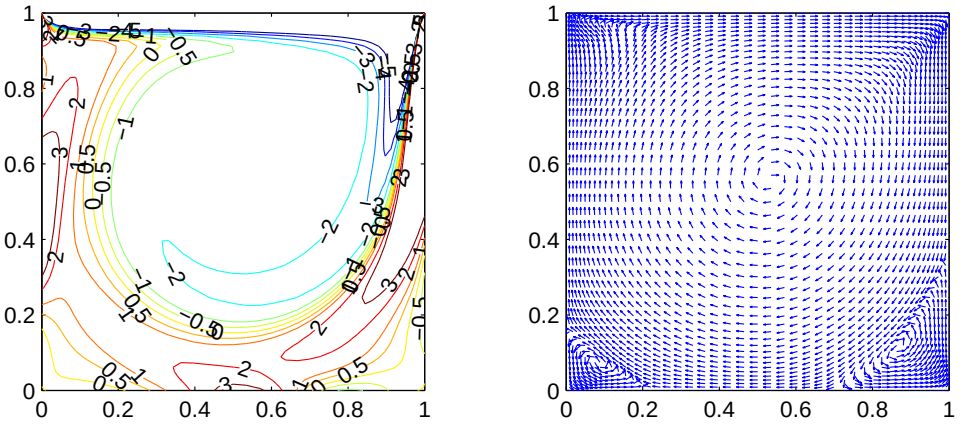

Figure 4.7: Driven cavity. Re=1000. 48×48 FVS elements. $\lambda = 150$.

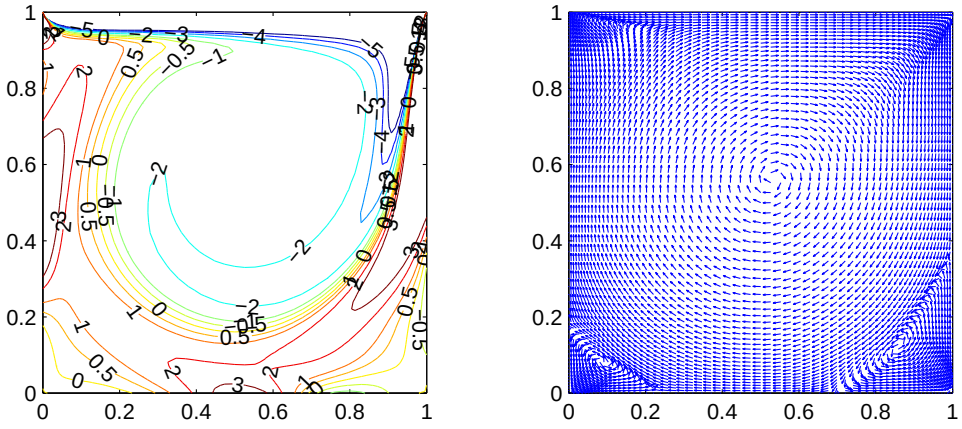

Figure 4.8: Driven cavity. Re=1000. 64×64 FVS elements (mesh refinement study). $\lambda = 150$.

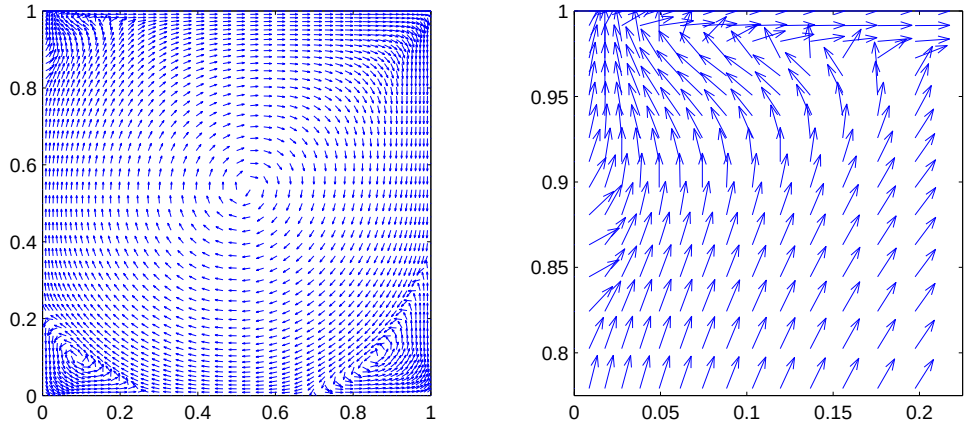

Figure 4.9: Driven cavity. Re=2000. 48×48 FVS elements. $\lambda = 0$.

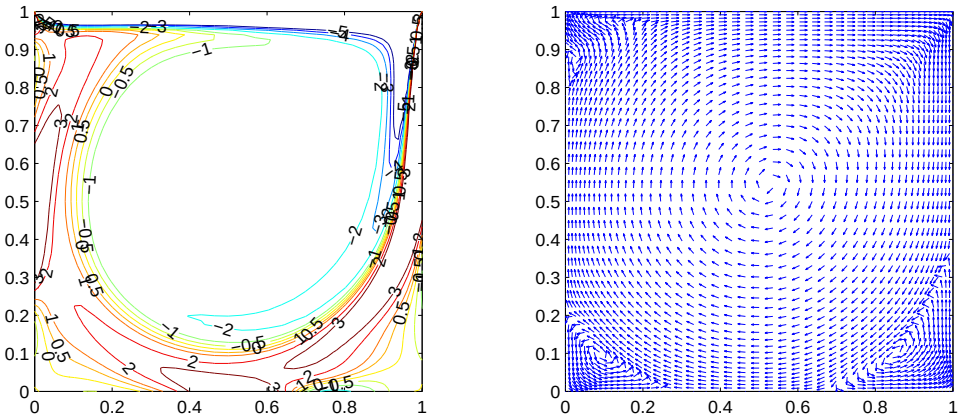

Figure 4.10: Driven cavity. Re=2000. 48×48 FVS elements. $\lambda = 300$

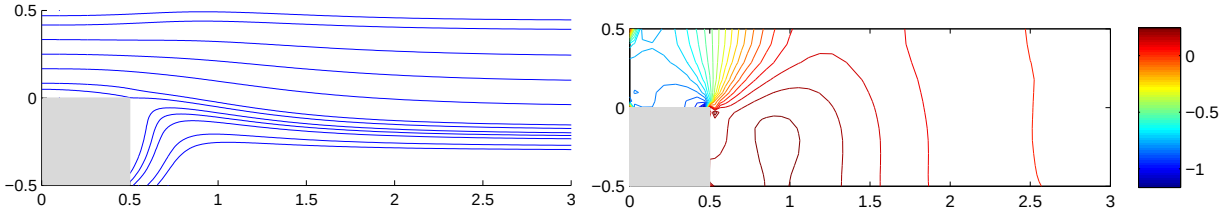

Figure 4.11: Backward facing step. Re=100. 594 FVS elements. $\lambda = 0$.

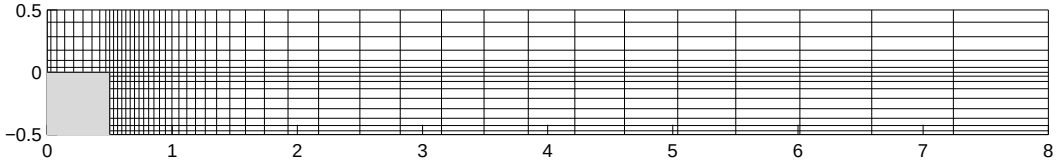

Figure 4.12: Finite element mesh used in backward facing step flow computation when Re=100

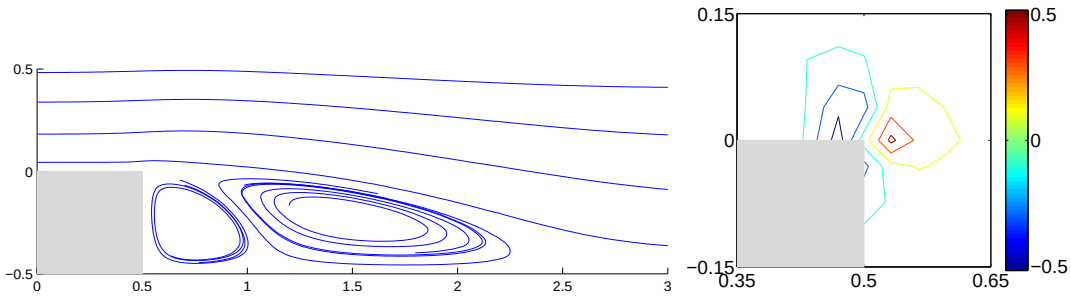

Figure 4.13: Backward-facing step. Re=100. 594 FVS elements, no corner elements. $\lambda = 150$.

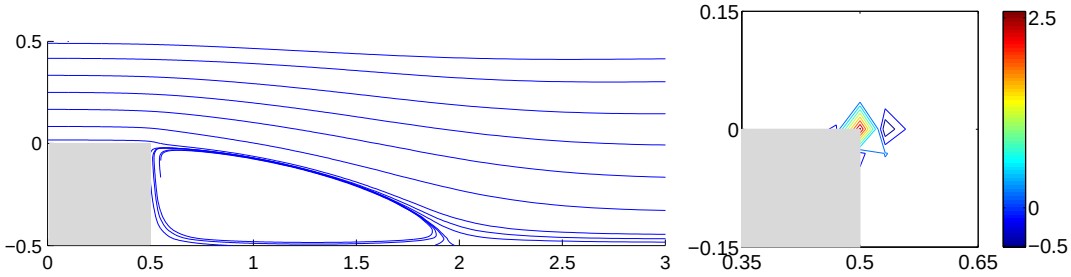

Figure 4.14: Backward-facing step. Re=100. 594 FVS elements + corner elements. $\lambda = 150$.

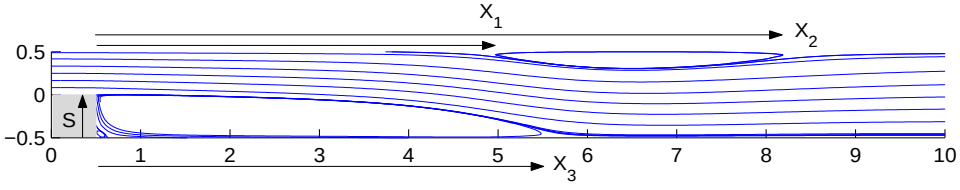

Figure 4.15: Backward-facing step. Re=600. 1107 FVS elements + corner elements. $\lambda = 150$.

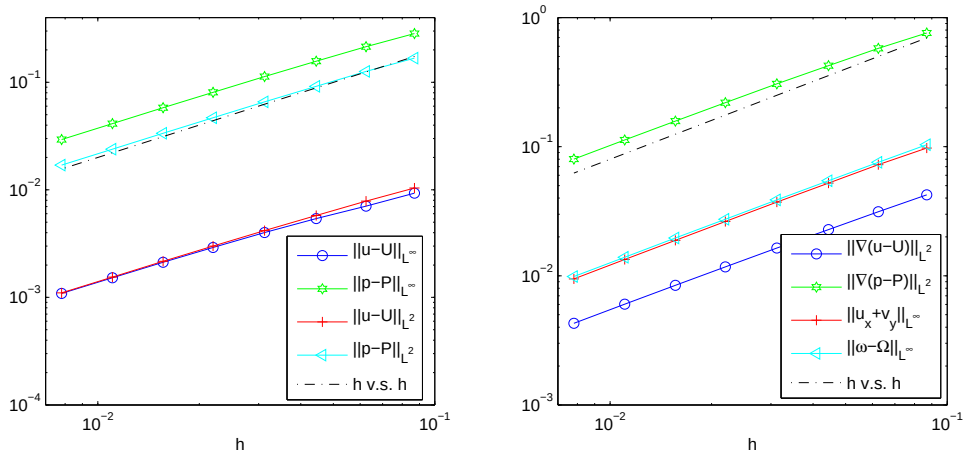

Figure 4.16: Spatial accuracy check at $t = 2$ for C^0 scheme with $P1/P1$ finite element spaces and CN/AB time stepping. $\nu = 2$.

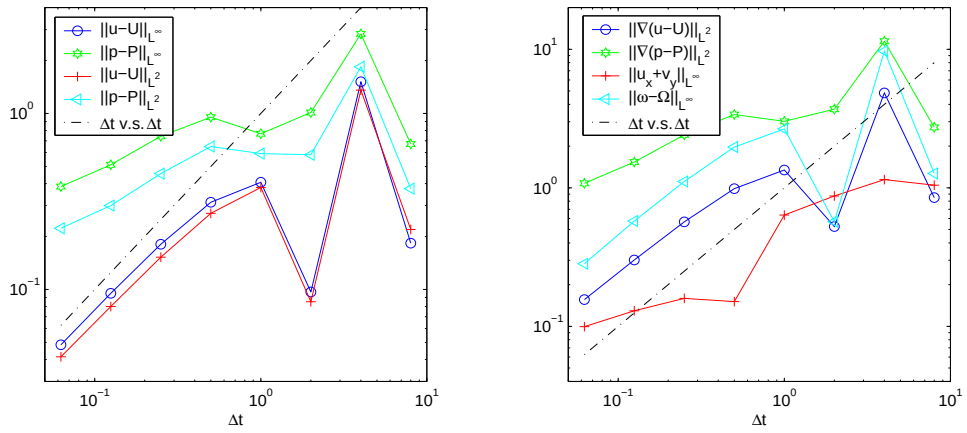

Figure 4.17: Stability check for C^0 scheme (1.18),(1.19) with $P1/P1$ finite element spaces. $\nu = 2$ and integrate until $t = 1000$.

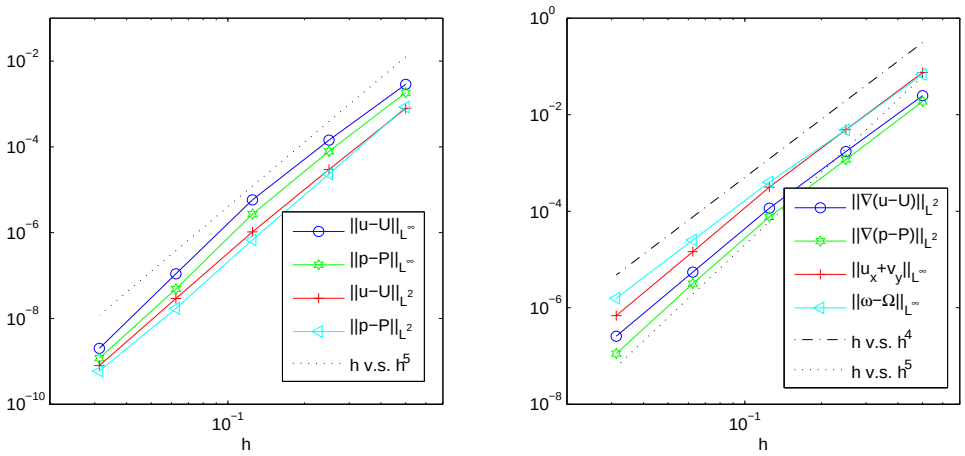

Figure 4.18: Spatial accuracy check at $t = 2$ for $P4/P4$ finite element spaces with RK4 time stepping. $\nu = 0.001$.

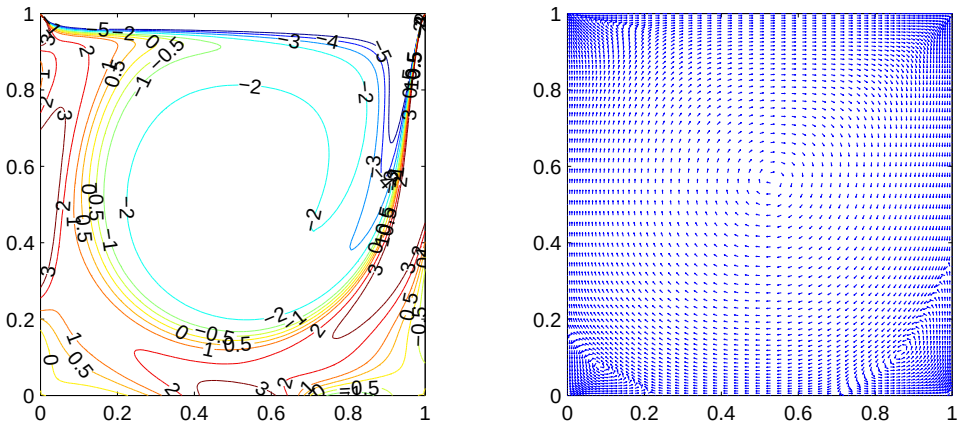

Figure 4.19: Driven cavity. Re=1000. $2 \times 32 \times 32$ P4 elements. $\lambda = 0$.

	R/S
Figure 4.14	2.9
Figure 4.21	2.8
Figure 4.22	2.8
[ADPS]	3
[KM]	3

	X_1/S	X_2/S	X_3/S
Figure 4.15	9	15.4	10
Figure 4.23	8.4	15.6	10
[ADPS]	8.6	[14.5, 16.3]	11.3
[KM]	[8.1,8.7]	[16.5,17.5]	10.7

Table 4.4: Backward-facing step. Left table: Re=100. Right table: Re=600

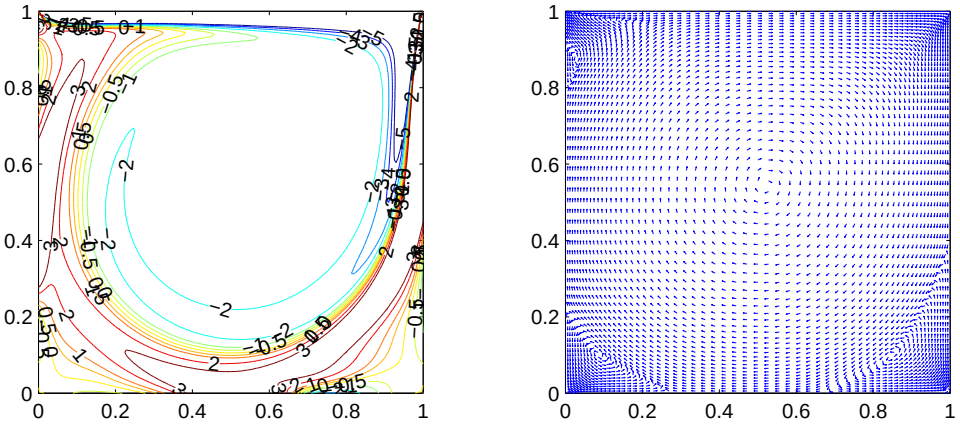

Figure 4.20: Driven cavity. Re=2000. $2 \times 32 \times 32$ P4 elements. $\lambda = 15$.

Chapter 5

Time dependent problems: Part II

As pointed out before, although we have a complete mathematical theory for the C^1 FE scheme (1.18),(1.20), we still want to extend the results to a C^0 FE scheme which is much easier to implement. Moreover, we want to get rid of the C^3

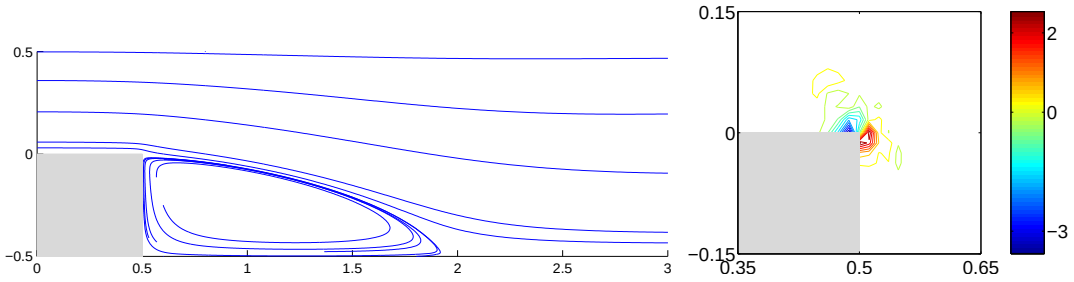

Figure 4.21: Backward-facing step. Re=100. 528 P4 elements. $\lambda = 20$.

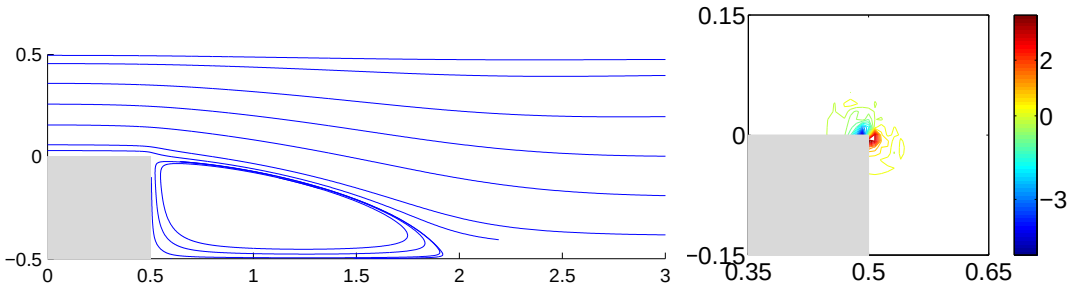

Figure 4.22: Backward-facing step. Re=100. 1188 P4 elements (mesh refinement study). $\lambda = 20$.

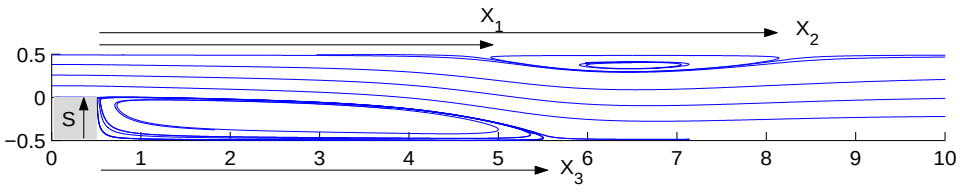

Figure 4.23: Backward-facing step. Re=600. 984 P4 elements. $\lambda = 20$.

boundary condition as well.

In the remain of the thesis, we will see how these two aims can be achieved. The C^0 FE schemes that we proposed for this purpose are the scheme (1.25) and the following variant of it:

$$\begin{aligned}&\left\langle \frac{\boldsymbol{u}_h^{n+1}}{\Delta t}, \boldsymbol{v}_h \right\rangle + \nu\big\langle \nabla \boldsymbol{u}_h^{n+1}, \nabla \boldsymbol{v}_h \big\rangle - \nu\big\langle \nabla \times \boldsymbol{u}_h^{n}, \nabla \times \boldsymbol{v}_h \big\rangle \\ &= \left\langle \mathcal{P}_h \left(\frac{2\boldsymbol{u}_h^n - \boldsymbol{u}_h^{n-1}}{\Delta t} + \boldsymbol{F}^n - \boldsymbol{F}^{n-1} \right), \boldsymbol{v}_h \right\rangle \end{aligned} \tag{5.1}$$

for any $\boldsymbol{v}_h \in X_{0,h}$. Indeed, we have used the tricks of Petersson to add the divergence damping $-\frac{1}{\Delta t}(I - \mathcal{P})\boldsymbol{u}$ to the right-hand side of (1.25) to get (5.1).

We are able to show stability of both (1.25) and (5.1). So far, error estimate are obtained only for (1.25):

Theorem 7 (Stability) *Consider the finite element scheme: (1.25) or (5.1) for the Stokes equations (i.e. $\boldsymbol{F}^n = \boldsymbol{f}^n$). Then, for any $T > 0$ there is a $C > 0$, such that for any $\Delta t > 0$ and $n\Delta t \le T$, we have*

$$\begin{aligned}&\sup_{k\le n}\big(\|(I-\mathcal{P}_h)\boldsymbol{u}_h^k\|^2 + \|\boldsymbol{u}_h^{k+1} - \boldsymbol{u}_h^k\|^2 + \nu\|\nabla\cdot\boldsymbol{u}_h^k\|^2\Delta t\big) \\ &+\nu\sum_{k=0}^{n-1}\|\nabla(\boldsymbol{u}_h^{k+1} - \boldsymbol{u}_h^k)\|^2\Delta t \le C\alpha_0 + C\sum_{k=0}^{n-1}\|\mathcal{P}_h(\boldsymbol{f}^{k+1} - \boldsymbol{f}^k)\|^2\Delta t, \end{aligned} \tag{5.2}$$

where $\alpha_0 = \|(I-\mathcal{P}_h)\boldsymbol{u}_h^0\|^2 + \|\mathcal{P}_h(\boldsymbol{u}_h^1 - \boldsymbol{u}_h^0)\|^2 + \|\nabla\cdot\boldsymbol{u}_h^0\|^2$ for scheme (5.1). Or

$$\begin{aligned}&\sup_{k\le n}\big(\|\boldsymbol{u}_h^{k+1} - \boldsymbol{u}_h^k\|^2 + \nu\|\nabla\cdot\boldsymbol{u}_h^k\|^2\Delta t\big) \\ &+\nu\sum_{k=0}^{n-1}\|\nabla(\boldsymbol{u}_h^{k+1} - \boldsymbol{u}_h^k)\|^2\Delta t \le C\alpha_0 + C\sum_{k=0}^{n-1}\|\mathcal{P}_h(\boldsymbol{f}^{k+1} - \boldsymbol{f}^k)\|^2\Delta t, \end{aligned} \tag{5.3}$$

where $\alpha_0 = \|\mathcal{P}_h(\boldsymbol{u}_h^1 - \boldsymbol{u}_h^0)\|^2 + \|\nabla\cdot\boldsymbol{u}_h^0\|^2$ for scheme (1.25). In both case, we have

$$\sup_{k\le n}\|\nabla\boldsymbol{u}_h^k\| \le \|\nabla\boldsymbol{u}_h^0\| + \left(k\sum_{k=0}^{n-1}\|\nabla(\boldsymbol{u}_h^{k+1} - \boldsymbol{u}_h^k)\|^2\right)^{1/2} \le C. \tag{5.4}$$

Theorem 8 (Error estimates) *Consider the finite element scheme (1.25) for the Stokes equations (i.e.* $\boldsymbol{F}^n = \boldsymbol{f}^n$*). Assume enough regularity of the force* $\boldsymbol{f}$ *and exact solution* $(\boldsymbol{u}, p)$*. Assume that the spaces* $X_{0,h} \subset H_0^1(\Omega, \mathbb{R}^N)$ *and* $Y_h \subset H^1(\Omega)$ *have the following approximation properties:*

$$\inf_{\boldsymbol{v}_h \in X_{0,h}} \|\nabla(\boldsymbol{a} - \boldsymbol{v}_h)\| \le Ch^m \|\boldsymbol{a}\|_{H^{m+1}}, \qquad \inf_{\phi_h \in Y_h} \|\nabla(q - \phi_h)\| \le Ch^{m'} \|q\|_{H^{m'+1}}.$$

Let $\boldsymbol{e}^n = \boldsymbol{u}(t_n) - \boldsymbol{u}_h^n$ *and let* $\alpha_0^2 := \|\mathcal{P}_h(\boldsymbol{e}_h^0 - \boldsymbol{e}_h^{-1})\| + \Delta t \|\nabla \cdot \boldsymbol{e}_h^0\|^2$*. Then we have*

$$\begin{aligned}
&\|\boldsymbol{e}^n - \boldsymbol{e}^{n-1}\|^2 + \Delta t \nu \|\nabla \cdot \boldsymbol{e}^n\|^2 + \nu \sum_{k=1}^{n} \|\nabla(\boldsymbol{e}^k - \boldsymbol{e}^{k-1})\|^2 \Delta t \\
&\qquad\qquad \le C\left(\alpha_0^2 + h^{2m} + h^{2m'} + \Delta t^4\right), \\
&\|\nabla \cdot \boldsymbol{e}^n\| \le C \frac{\alpha_0 + h^m + h^{m'} + \Delta t^2}{\sqrt{\Delta t}}, \\
&\|\nabla \boldsymbol{e}^n\| \le \|\nabla \boldsymbol{e}^0\| + \left(n \sum_{k=0}^{n} \|\nabla(\boldsymbol{e}^k - \boldsymbol{e}^{k-1})\|^2 \right)^{1/2} \le C \frac{\alpha_0 + h^m + h^{m'} + \Delta t^2}{\Delta t}.
\end{aligned}$$

In the following, we will first derive scheme (1.25) and (5.1). After that, we will study the semi-discrete schemes (keeping spatial variable continuous) before we turn to the fully discrete C^0 FE schemes. This chapter ends up with some numerical computations.

5.1 Another reformulation of NSE

Behind scheme (1.25) or (5.1) is another general class of Navier-Stokes solvers. It is indeed motivated by Guermond and Shen's work on projection method [GS2]. To begin with, recall that we have proved in Lemma 2 that the pressure in (1.9) can

be written as $\nabla p = \nu \nabla p_{\mathrm{s}} + (I - \mathcal{P})\boldsymbol{F}$ where

$$\nabla p_{\mathrm{s}}(\boldsymbol{u}) = (I - \mathcal{P})(\Delta \boldsymbol{u} - \nabla \nabla \cdot \boldsymbol{u}) = (I - \mathcal{P})\Delta \boldsymbol{u} - \nabla \nabla \cdot \boldsymbol{u}, \tag{5.5}$$

and $\boldsymbol{F} = \boldsymbol{f} - \boldsymbol{u} \cdot \nabla \boldsymbol{u}$. Substituting (5.5) into (1.9), we can rewrite (1.9) as

$$\partial_t \boldsymbol{u} + \nu \nabla p_{\mathrm{s}}(\boldsymbol{u}) = \nu \Delta \boldsymbol{u} + \mathcal{P}\boldsymbol{F}.$$

Now, we are considering the SE, so we choose $\boldsymbol{F} = \boldsymbol{f}$. From the above equation, we derive

$$\frac{\boldsymbol{u}(t_{n+1}) - \boldsymbol{u}(t_n)}{\Delta t} + \nu \nabla p_{\mathrm{s}}(\boldsymbol{u}(t_n)) = \nu \Delta \boldsymbol{u}(t_{n+1}) + \mathcal{P}\boldsymbol{F}(t_n) + \boldsymbol{g}(t_n)\Delta t. \tag{5.6}$$

Using (5.5) as well as $\Delta \boldsymbol{u} - \nabla \nabla \cdot \boldsymbol{u} = -\nabla \times \nabla \times \boldsymbol{u}$, we get

$$\nabla p_{\mathrm{s}}(\boldsymbol{u}) = -\mathcal{P}\Delta \boldsymbol{u} - \nabla \times \nabla \times \boldsymbol{u}.$$

Substituting this equation into (5.6), we obtain

$$\begin{aligned} &\frac{\boldsymbol{u}(t_{n+1}) - \boldsymbol{u}(t_n)}{\Delta t} - \nu \Delta \boldsymbol{u}(t_{n+1}) - \nu \nabla \times \nabla \times \boldsymbol{u}(t_n) \\ =&\nu \mathcal{P}\Delta \boldsymbol{u}(t_n) + \mathcal{P}\boldsymbol{F}(t_n) + \boldsymbol{g}(t_n)\Delta t. \end{aligned} \tag{5.7}$$

Operating the projection $\mathcal{P}$ on (5.6) with t_{n+1} replaced by t_n, we get

$$\mathcal{P}\left(\frac{\boldsymbol{u}(t_n) - \boldsymbol{u}(t_{n-1})}{\Delta t} - \boldsymbol{F}(t_{n-1}) - \boldsymbol{g}(t_{n-1})\Delta t\right) = \nu \mathcal{P}\Delta \boldsymbol{u}(t_n).$$

Substituting the above equation into (5.7), we see that (5.7) can be written as

$$\begin{aligned} &\frac{\boldsymbol{u}(t_{n+1}) - \boldsymbol{u}(t_n)}{\Delta t} - \nu \Delta \boldsymbol{u}(t_{n+1}) - \nu \nabla \times \nabla \times \boldsymbol{u}(t_n) \\ =&\mathcal{P}\left(\frac{\boldsymbol{u}(t_n) - \boldsymbol{u}(t_{n-1})}{\Delta t} + \boldsymbol{F}(t_n) - \boldsymbol{F}(t_{n-1})\right) + \left(\boldsymbol{g}(t_n) - \mathcal{P}\boldsymbol{g}(t_{n-1})\right)\Delta t. \end{aligned} \tag{5.8}$$

Based on (5.8), we propose the following semi-discrete numerical scheme: Given $\boldsymbol{u}^0$ and $\boldsymbol{u}^1$, find $\boldsymbol{u}^{n+1}$ $(n \geq 1)$ by solving

$$\frac{\boldsymbol{u}^{n+1}-\boldsymbol{u}^n}{\Delta t} - \nu\Delta\boldsymbol{u}^{n+1} - \nu\nabla\times\nabla\times\boldsymbol{u}^n = \mathcal{P}\left(\frac{\boldsymbol{u}^n-\boldsymbol{u}^{n-1}}{\Delta t} + \boldsymbol{F}^n - \boldsymbol{F}^{n-1}\right), \quad (5.9)$$

where $\boldsymbol{F}^n = \boldsymbol{f}^n - \boldsymbol{u}^n\cdot\nabla\boldsymbol{u}^n$ for the NSE and $\boldsymbol{F}^n = \boldsymbol{f}^n$ for the SE. Dotting (5.9) with $\boldsymbol{v} \in H_0^1(\Omega,\mathbb{R}^N)$, we get

$$\begin{aligned}&\Big\langle\frac{\boldsymbol{u}^{n+1}-\boldsymbol{u}^n}{\Delta t},\boldsymbol{v}\Big\rangle + \nu\big\langle\nabla\boldsymbol{u}^{n+1},\nabla\boldsymbol{v}\big\rangle - \nu\big\langle\nabla\times\boldsymbol{u}^n,\nabla\times\boldsymbol{v}\big\rangle\\ =&\Big\langle\mathcal{P}\left(\frac{\boldsymbol{u}^n-\boldsymbol{u}^{n-1}}{\Delta t} + \boldsymbol{F}^n - \boldsymbol{F}^{n-1}\right),\boldsymbol{v}\Big\rangle, \end{aligned} \quad (5.10)$$

which directly leads to the C^0 finite element scheme (1.25).

If instead of (5.6), we start from

$$\frac{\boldsymbol{u}(t_{n+1})-\mathcal{P}\boldsymbol{u}(t_n)}{\Delta t} + \nu\nabla p_{\mathrm{s}}(\boldsymbol{u}(t_n)) = \nu\Delta\boldsymbol{u}(t_{n+1}) + \mathcal{P}\boldsymbol{F}(t_n) + \boldsymbol{g}(t_n)\Delta t, \quad (5.11)$$

then the same procedure leads to the semi-discrete numerical scheme

$$\frac{\boldsymbol{u}^{n+1}}{\Delta t} - \nu\Delta\boldsymbol{u}^{n+1} - \nu\nabla\times\nabla\times\boldsymbol{u}^n = \mathcal{P}\left(\frac{2\boldsymbol{u}^n-\boldsymbol{u}^{n-1}}{\Delta t} + \boldsymbol{F}^n - \boldsymbol{F}^{n-1}\right), \quad (5.12)$$

and hence to the finite element scheme (5.1).

5.1.1 Stability and error estimates of the semi-discrete scheme

Theorem 9 *For SE, scheme (5.9) and (5.12) is unconditionally stable and convergent. For scheme (5.9)*

$$\sup_{k\leq n}\|\nabla\cdot\boldsymbol{u}^k\| + \|\nabla(\boldsymbol{u}(t_k)-\boldsymbol{u}^k)\| \leq C\Delta t.$$

For scheme (5.12)

$$\sup_{k\leq n}\Delta t^{-1/2}\|(I-\mathcal{P})\boldsymbol{u}^k\| + \|\nabla\cdot\boldsymbol{u}^k\| + \Delta t^{1/2}\|\nabla(\boldsymbol{u}(t_k)-\boldsymbol{u}^k)\| \leq C\Delta t$$

Proof: To save place, we only show the error estimates. The stability proof follows the same idea and is easier to get. We first obtain the error estimate of (5.12), and then obtain a refined error estimate of (5.9).

Error estimates of (5.12): Letting $\boldsymbol{e}^n = \boldsymbol{u}(t_n) - \boldsymbol{u}^n$ and subtracting (5.12) from (5.8), we get

$$\frac{\boldsymbol{e}^{n+1} - \mathcal{P}\boldsymbol{e}^n}{\Delta t} - \nu\Delta\boldsymbol{e}^{n+1} - \nu\nabla\times\nabla\times\boldsymbol{e}^n = \mathcal{P}\left(\frac{\boldsymbol{e}^n - \boldsymbol{e}^{n-1}}{\Delta t}\right) + \left(\boldsymbol{g}^n - \mathcal{P}\boldsymbol{g}^{n-1}\right)\Delta t, \quad (5.13)$$

where we have used the fact that $\boldsymbol{u}(t_n) = \mathcal{P}\boldsymbol{u}(t_n)$. We rewrite (5.13) as

$$\begin{aligned}&\frac{(I-\mathcal{P})\boldsymbol{e}^{n+1}}{\Delta t} + \mathcal{P}\left(\frac{\boldsymbol{e}^{n+1} - 2\boldsymbol{e}^n + \boldsymbol{e}^{n-1}}{\Delta t}\right)\\ &\quad + \nu\nabla\times\nabla\times(\boldsymbol{e}^{n+1} - \boldsymbol{e}^n) - \nu\nabla\nabla\cdot\boldsymbol{e}^{n+1} = \left(\boldsymbol{g}^n - \mathcal{P}\boldsymbol{g}^{n-1}\right)\Delta t. \qquad (5.14)\end{aligned}$$

Dotting (5.14) with $2\Delta t(\boldsymbol{e}^{n+1} - \boldsymbol{e}^n)$, we get

$$\begin{aligned}&\|(I-\mathcal{P})\boldsymbol{e}^{n+1}\|^2 - \|(I-\mathcal{P})\boldsymbol{e}^n\|^2 + \|(I-\mathcal{P})(\boldsymbol{e}^{n+1} - \boldsymbol{e}^n)\|^2\\ &\quad + \|\mathcal{P}(\boldsymbol{e}^{n+1} - \boldsymbol{e}^n)\|^2 - \|\mathcal{P}(\boldsymbol{e}^n - \boldsymbol{e}^{n-1})\|^2 + \|\mathcal{P}(\boldsymbol{e}^{n+1} - 2\boldsymbol{e}^n + \boldsymbol{e}^{n-1})\|^2\\ &\quad + 2\Delta t\nu\|\nabla\times(\boldsymbol{e}^{n+1} - \boldsymbol{e}^n)\|^2\\ &\quad + \Delta t\nu\left(\|\nabla\cdot\boldsymbol{e}^{n+1}\|^2 - \|\nabla\cdot\boldsymbol{e}^n\|^2 + \|\nabla\cdot(\boldsymbol{e}^{n+1} - \boldsymbol{e}^n)\|^2\right) \qquad (5.15)\\ =&2\Delta t^2\left\langle\mathcal{P}(\boldsymbol{g}^n - \boldsymbol{g}^{n-1}), \boldsymbol{e}^{n+1} - \boldsymbol{e}^n\right\rangle + 2\Delta t^2\left\langle(I-\mathcal{P})\boldsymbol{g}^n, \boldsymbol{e}^{n+1} - \boldsymbol{e}^n\right\rangle\\ =&I + II.\end{aligned}$$

Now, we try to estimate the two terms on the right-hand side using $\left\langle\mathcal{P}\boldsymbol{a}, \boldsymbol{b}\right\rangle = \left\langle\mathcal{P}\boldsymbol{a}, \mathcal{P}\boldsymbol{b}\right\rangle$ and $\left\langle(I-\mathcal{P})\boldsymbol{a}, \boldsymbol{b}\right\rangle = \left\langle(I-\mathcal{P})\boldsymbol{a}, (I-\mathcal{P})\boldsymbol{b}\right\rangle$:

$$|I| \le \Delta t\|\mathcal{P}(\boldsymbol{e}^{n+1} - \boldsymbol{e}^n)\|^2 + C\Delta t^5,$$

$$|II| \le \|(I-\mathcal{P})(\boldsymbol{e}^{n+1}-\boldsymbol{e}^n)\|^2 + C\Delta t^4.$$

Letting

$$L_n = \|(I-\mathcal{P})\boldsymbol{e}^n\|^2 + \|\mathcal{P}(\boldsymbol{e}^n-\boldsymbol{e}^{n-1})\|^2 + \Delta t\nu\|\nabla\cdot\boldsymbol{e}^n\|^2,$$

we have

$$L_{n+1} - L_n + \Delta t\nu\|\nabla(\boldsymbol{e}^{n+1}-\boldsymbol{e}^n)\|^2 \le L_{n+1}\Delta t + C\Delta t^4.$$

By the discrete Gronwall inequality, we have

$$L_n + \nu\sum_{k=0}^{n}\|\nabla(\boldsymbol{e}^k-\boldsymbol{e}^{k-1})\|^2\Delta t \le C\left(L_0+\Delta t^3\right).$$

If we choose $L_0 = C\Delta t^3$, then

$$\sup_{k\le n}\Delta t^{-1/2}\|(I-\mathcal{P})\boldsymbol{e}^k\| + \|\nabla\cdot\boldsymbol{e}^k\| \le C\Delta t,$$
$$\sup_{k\le n}\|\nabla\boldsymbol{e}^k\| \le \|\nabla\boldsymbol{e}^0\| + \left(n\sum_{k=0}^{n}\|\nabla(\boldsymbol{e}^k-\boldsymbol{e}^{k-1})\|^2\right)^{1/2} \le C\Delta t^{1/2}.$$

Error estimates of (5.9): It turns out that if we directly compare $\boldsymbol{u}_h^n$ with $\boldsymbol{u}(t_n)$ from (5.8), we are not able to prove full accuracy in time. Instead, we shall construct a bounded function $\boldsymbol{v}$ and compare $\boldsymbol{u}^n$ with $\boldsymbol{u}(t_n)+\Delta t\boldsymbol{v}(t_n)$. Taylor expanding the SE at time $t^{n+1/2}$, we see that

$$\begin{aligned}&\frac{\boldsymbol{u}(t_{n+1})-\boldsymbol{u}(t_n)}{\Delta t} + \nabla p_{\mathrm{S}}\left(\boldsymbol{u}(t_n)+\frac{\Delta t}{2}\partial_t\boldsymbol{u}(t_n)\right)\\ =&\Delta\left(\boldsymbol{u}(t_{n+1})-\frac{\Delta t}{2}\partial_t\boldsymbol{u}(t_{n+1})\right) + \mathcal{P}\left(\boldsymbol{f}(t_n)+\frac{\Delta t}{2}\partial_t\boldsymbol{f}(t_n)\right) + O(\Delta t^2).\end{aligned}$$

So, let $\boldsymbol{v}(t)$ be the solution of

$$\partial_t\boldsymbol{v} + \nabla p_{\mathrm{S}}(\boldsymbol{v}) = \Delta\boldsymbol{v} + \frac{1}{2}\partial_t\left(\nabla p_{\mathrm{S}}(\boldsymbol{u}) + \Delta\boldsymbol{u} - \mathcal{P}\boldsymbol{f}(t)\right), \qquad \boldsymbol{v}|_\Gamma = 0.$$

We have the regularity of $\boldsymbol{v}$ from the paper [LLP]. (Indeed, $(\Delta - \nabla p_{\mathrm{s}})(\boldsymbol{v})$ is a sectorial operator and has bounded imaginary power. A proof of this will appear in a separate paper.) Then, letting $\tilde{\boldsymbol{u}} = \boldsymbol{u} + \Delta t \boldsymbol{v}$, we have

$$\frac{\tilde{\boldsymbol{u}}(t_{n+1}) - \tilde{\boldsymbol{u}}(t_n)}{\Delta t} + \nu \nabla p_{\mathrm{s}}(\tilde{\boldsymbol{u}}(t_n)) = \nu \Delta \tilde{\boldsymbol{u}}(t_{n+1}) + \mathcal{P}\boldsymbol{f}(t_n) + \boldsymbol{g}(t_n)\Delta t^2. \tag{5.16}$$

Starting from (5.16) instead of (5.6) and repeating the steps we carried out in the beginning of section 5.1, we can derive

$$\begin{aligned} &\frac{\tilde{\boldsymbol{u}}(t_{n+1}) - \tilde{\boldsymbol{u}}(t_n)}{\Delta t} - \nu \Delta \tilde{\boldsymbol{u}}(t_{n+1}) - \nu \nabla \times \nabla \times \tilde{\boldsymbol{u}}(t_n) \qquad (5.17) \\ =&\mathcal{P}\left(\frac{\tilde{\boldsymbol{u}}(t_n) - \tilde{\boldsymbol{u}}(t_{n-1})}{\Delta t} + \boldsymbol{f}(t_n) - \boldsymbol{f}(t_{n-1}) \right) + \left(\boldsymbol{g}(t_n) - \mathcal{P}\boldsymbol{g}(t_{n-1})\right) \Delta t^2. \end{aligned}$$

Let $\boldsymbol{e}^n = \tilde{\boldsymbol{u}}(t_n) - \boldsymbol{u}^n$ and subtract (5.9) from (5.17) to get

$$\frac{\boldsymbol{e}^{n+1} - \boldsymbol{e}^n}{\Delta t} + \nu \nabla \times \nabla \times (\boldsymbol{e}^{n+1} - \boldsymbol{e}^n) - \nu \nabla \nabla \cdot \boldsymbol{e}^{n+1} = \mathcal{P}\left(\frac{\boldsymbol{e}^n - \boldsymbol{e}^{n-1}}{\Delta t} \right) + \left(\boldsymbol{g}^n - \mathcal{P}\boldsymbol{g}^{n-1}\right) \Delta t^2. \tag{5.18}$$

Dotting (5.18) with $2\Delta t(\boldsymbol{e}^{n+1} - \boldsymbol{e}^n)$, we get

$$\begin{aligned} &2\|\boldsymbol{e}^{n+1} - \boldsymbol{e}^n\|^2 + 2\Delta t \nu \|\nabla \times (\boldsymbol{e}^{n+1} - \boldsymbol{e}^n)\|^2 \\ &\qquad + \Delta t \nu \left(\|\nabla \cdot \boldsymbol{e}^{n+1}\|^2 - \|\nabla \cdot \boldsymbol{e}^n\|^2 + \|\nabla \cdot (\boldsymbol{e}^{n+1} - \boldsymbol{e}^n)\|^2 \right) \\ =&2\left\langle \mathcal{P}(\boldsymbol{e}^n - \boldsymbol{e}^{n-1}), \boldsymbol{e}^{n+1} - \boldsymbol{e}^n \right\rangle + 2\Delta t^3 \left\langle \mathcal{P}(\boldsymbol{g}^n - \boldsymbol{g}^{n-1}), \boldsymbol{e}^{n+1} - \boldsymbol{e}^n \right\rangle \\ &\qquad + 2\Delta t^3 \left\langle (I - \mathcal{P})\boldsymbol{g}^n, \boldsymbol{e}^{n+1} - \boldsymbol{e}^n \right\rangle \\ =&I + II + III. \end{aligned}$$

Now, we try to estimate the three terms on the right-hand side using $\left\langle \mathcal{P}\boldsymbol{a}, \boldsymbol{b} \right\rangle = \left\langle \mathcal{P}\boldsymbol{a}, \mathcal{P}\boldsymbol{b} \right\rangle$ and $\left\langle (I - \mathcal{P})\boldsymbol{a}, \boldsymbol{b} \right\rangle = \left\langle (I - \mathcal{P})\boldsymbol{a}, (I - \mathcal{P})\boldsymbol{b} \right\rangle$:

$$|I| \le \|\mathcal{P}(\boldsymbol{e}^{n+1} - \boldsymbol{e}^n)\|^2 + \|\mathcal{P}(\boldsymbol{e}^n - \boldsymbol{e}^{n-1})\|^2,$$

$$|II| \le \|\mathcal{P}(\boldsymbol{e}^{n+1} - \boldsymbol{e}^n)\|^2 \Delta t + C\Delta t^7,$$

$$|III| \le \|(I - \mathcal{P})(\boldsymbol{e}^{n+1} - \boldsymbol{e}^n)\|^2 + C\Delta t^6.$$

Letting

$$L_n = \|\boldsymbol{e}^n - \boldsymbol{e}^{n-1}\|^2 + \Delta t \|\nabla \cdot \boldsymbol{e}^n\|^2,$$

we have

$$L_{n+1} - L_n + \Delta t \nu \|\nabla(\boldsymbol{e}^{n+1} - \boldsymbol{e}^n)\|^2 \le L_{n+1}\Delta t + C\Delta t^6.$$

By the discrete Gronwall inequality, we have

$$L_n + \Delta t \nu \sum_{k=0}^{n} \|\nabla(\boldsymbol{e}^k - \boldsymbol{e}^{k-1})\|^2 \le C\left(L_0 + \Delta t^5\right).$$

Indeed, $L_0 = \|\mathcal{P}(\boldsymbol{e}^0 - \boldsymbol{e}^{-1})\|^2 + \Delta t \|\nabla \cdot \boldsymbol{e}^0\|^2$. If we choose $L_0 = C\Delta t^4$, we have

$$\sup_{k \le n} \|\nabla \cdot \boldsymbol{e}^k\| \le C\Delta t^{3/2},$$

$$\|\nabla \boldsymbol{e}^n\| \le \|\nabla \boldsymbol{e}^0\| + \left(n \sum_{k=0}^{n} \|\nabla(\boldsymbol{e}^k - \boldsymbol{e}^{k-1})\|^2 \right)^{1/2} \le C\Delta t.$$

5.1.2 How large we can take for coefficient of the divergence damping?

Consider the backward Euler scheme with the divergence damping due to Petersson:

$$\frac{\boldsymbol{u}^{n+1} - \boldsymbol{u}^n}{\Delta t} + \nabla p^n = \nu \Delta \boldsymbol{u}^{n+1} + \mathcal{P}\boldsymbol{f}^n - \lambda(I - \mathcal{P})\boldsymbol{u}^n, \tag{5.19}$$

$$\nabla p^n = (I - \mathcal{P})\Delta \boldsymbol{u}^n - \nabla \nabla \cdot \boldsymbol{u}^n. \tag{5.20}$$

We want to study how large λ can be taken. Using the techniques in the beginning of this section, we can rewritten (5.19) and (5.20) as

$$\frac{\boldsymbol{u}^{n+1}-\boldsymbol{u}^n}{\Delta t}-\mathcal{P}\frac{\boldsymbol{u}^n-\boldsymbol{u}^{n-1}}{\Delta t}+\nu\nabla\times\nabla\times(\boldsymbol{u}^{n+1}-\boldsymbol{u}^n)-\nu\nabla\nabla\cdot\boldsymbol{u}^{n+1}$$
$$+\lambda(I-\mathcal{P})\boldsymbol{u}^n=\mathcal{P}(\boldsymbol{f}^n-\boldsymbol{f}^{n-1}). \tag{5.21}$$

Note that

$$\begin{aligned}&\big\langle\nabla\times\nabla\times(\boldsymbol{u}^{n+1}-\boldsymbol{u}^n)-\nabla\nabla\cdot\boldsymbol{u}^{n+1},\boldsymbol{u}^{n+1}-\boldsymbol{u}^n\big\rangle\\ =&\|\nabla\times(\boldsymbol{u}^{n+1}-\boldsymbol{u}^n)\|^2+\frac{1}{2}\big(\|\nabla\cdot\boldsymbol{u}^{n+1}\|^2-\|\nabla\cdot\boldsymbol{u}^n\|^2+\|\nabla\cdot(\boldsymbol{u}^{n+1}-\boldsymbol{u}^n)\|^2\big)\end{aligned} \tag{5.22}$$

and

$$\begin{aligned}&\frac{1}{\Delta t}\|\boldsymbol{u}^{n+1}-\boldsymbol{u}^n\|^2-\frac{1}{\Delta t}\big\langle\mathcal{P}(\boldsymbol{u}^n-\boldsymbol{u}^{n-1}),\boldsymbol{u}^{n+1}-\boldsymbol{u}^n\big\rangle\\ &\quad+\lambda\big\langle(I-\mathcal{P})\boldsymbol{u}^n,(I-\mathcal{P})(\boldsymbol{u}^{n+1}-\boldsymbol{u}^n)\big\rangle\\ \geq&\frac{1}{\Delta t}\|(I-\mathcal{P})(\boldsymbol{u}^{n+1}-\boldsymbol{u}^n)\|^2+\frac{1}{2\Delta t}\left(\|\mathcal{P}(\boldsymbol{u}^{n+1}-\boldsymbol{u}^n)\|^2-\|\mathcal{P}(\boldsymbol{u}^n-\boldsymbol{u}^{n-1})\|^2\right)\\ &\quad+\frac{\lambda}{2}\left(\|(I-\mathcal{P})\boldsymbol{u}^{n+1}\|^2-\|(I-\mathcal{P})\boldsymbol{u}^n\|^2-\|(I-\mathcal{P})(\boldsymbol{u}^{n+1}-\boldsymbol{u}^n)\|^2\right).\end{aligned}$$

Hence, if we dot (5.21) with $\boldsymbol{u}^{n+1}-\boldsymbol{u}^n$ and do the same energy estimate as in Theorem 9, we get

Theorem 10 *Consider the semi-discrete scheme (5.19) and (5.20). It is stable as long as*

$$\lambda\leq\frac{2}{\Delta t}.$$

Moreover, when $\lambda=O(\frac{1}{\Delta t})$, we have

$$\sup_{k\leq n}\Delta t^{-1/2}\|(I-\mathcal{P})\boldsymbol{u}^k\|+\|\nabla\cdot\boldsymbol{u}^k\|+\Delta t^{1/2}\|\nabla(\boldsymbol{u}(t_k)-\boldsymbol{u}^k)\|\leq C\Delta t,$$

and when $\lambda = O(1)$, we can directly use the pressure estimate from Theorem 2 to derive

$$\sup_{k\le n} \|\nabla(\boldsymbol{u}(t_k) - \boldsymbol{u}^k)\| + \|\Delta(\boldsymbol{u}(t_k) - \boldsymbol{u}^k)\| \le C\Delta t.$$

5.2 C^0 finite element schemes (1.25) and (5.1)

Now, we are ready to study the fully discrete scheme. We will first prove the stability and then the error estimates.

5.2.1 Proof of Theorem 7

We only show the proof of scheme (5.1) since the proof of (1.25) is similar (or see the proof of Theorem 8). Using

$$\left\langle \nabla \boldsymbol{u}_h^{n+1}, \nabla \boldsymbol{v}_h \right\rangle = \left\langle \nabla \times \boldsymbol{u}_h^{n+1}, \nabla \times \boldsymbol{v}_h \right\rangle + \left\langle \nabla \cdot \boldsymbol{u}_h^{n+1}, \nabla \cdot \boldsymbol{v}_h \right\rangle, \tag{5.23}$$

we can rewrite the FE scheme (5.1) as

$$\begin{aligned} &\left\langle \frac{(I - \mathcal{P}_h)\boldsymbol{u}_h^{n+1}}{\Delta t}, \boldsymbol{v}_h \right\rangle + \left\langle \mathcal{P}_h \left(\frac{\boldsymbol{u}_h^{n+1} - 2\boldsymbol{u}_h^n + \boldsymbol{u}_h^{n-1}}{\Delta t} \right), \boldsymbol{v}_h \right\rangle + \nu \left\langle \nabla \cdot \boldsymbol{u}_h^{n+1}, \nabla \cdot \boldsymbol{v}_h \right\rangle \\ &\quad + \nu \left\langle \nabla \times (\boldsymbol{u}_h^{n+1} - \boldsymbol{u}_h^n), \nabla \times \boldsymbol{v}_h \right\rangle = \left\langle \mathcal{P}_h \left(\boldsymbol{f}^n - \boldsymbol{f}^{n-1} \right), \boldsymbol{v}_h \right\rangle, \end{aligned} \tag{5.24}$$

Taking $\boldsymbol{v}_h = 2\Delta t(\boldsymbol{u}_h^{n+1} - \boldsymbol{u}_h^n)$ and using Lemma 3, we get

$$\begin{aligned}
&\|(I-\mathcal{P}_h)\boldsymbol{u}_h^{n+1}\|^2 - \|(I-\mathcal{P}_h)\boldsymbol{u}_h^n\|^2 + \|(I-\mathcal{P}_h)(\boldsymbol{u}_h^{n+1}-\boldsymbol{u}_h^n)\|^2 \\
&\quad + \|\mathcal{P}_h(\boldsymbol{u}_h^{n+1}-\boldsymbol{u}_h^n)\|^2 - \|\mathcal{P}_h(\boldsymbol{u}_h^{n}-\boldsymbol{u}_h^{n-1})\|^2 + \|\mathcal{P}_h(\boldsymbol{u}_h^{n+1}-2\boldsymbol{u}_h^n+\boldsymbol{u}_h^{n-1})\|^2 \\
&\quad + \Delta t\nu\left(\|\nabla\cdot\boldsymbol{u}_h^{n+1}\|^2 - \|\nabla\cdot\boldsymbol{u}_h^n\|^2 + \|\nabla\cdot(\boldsymbol{u}_h^{n+1}-\boldsymbol{u}_h^n)\|^2\right) \\
&\quad + 2\Delta t\nu\|\nabla\times(\boldsymbol{u}_h^{n+1}-\boldsymbol{u}_h^n)\|^2 \\
\le& 2\Delta t\|\mathcal{P}_h(\boldsymbol{f}^n-\boldsymbol{f}^{n-1})\|\|\mathcal{P}_h(\boldsymbol{u}_h^{n+1}-\boldsymbol{u}_h^n)\| \\
\le& \Delta t\|\mathcal{P}_h(\boldsymbol{u}_h^{n+1}-\boldsymbol{u}_h^n)\|^2 + \Delta t\|\mathcal{P}_h(\boldsymbol{f}^n-\boldsymbol{f}^{n-1})\|^2.
\end{aligned}$$

Note that

$$\|(I-\mathcal{P}_h)(\boldsymbol{u}_h^{n+1}-\boldsymbol{u}_h^n)\|^2 + \|\mathcal{P}_h(\boldsymbol{u}_h^{n+1}-\boldsymbol{u}_h^n)\|^2 = \|\boldsymbol{u}_h^{n+1}-\boldsymbol{u}_h^n\|^2$$

$$\|\nabla\cdot(\boldsymbol{u}_h^{n+1}-\boldsymbol{u}_h^n)\|^2 + \|\nabla\times(\boldsymbol{u}_h^{n+1}-\boldsymbol{u}_h^n)\|^2 = \|\nabla(\boldsymbol{u}_h^{n+1}-\boldsymbol{u}_h^n)\|^2.$$

Using the Gronwall inequality, we get (5.2).

5.2.2 Proof of Theorem 8

As in the second part of the proof of Theorem 9, we first have to construct $\boldsymbol{v}$ and get (5.17). Dotting (5.17) with $\boldsymbol{v}_h$, we get

$$\begin{aligned}
&\left\langle \frac{\tilde{\boldsymbol{u}}(t_{n+1})-\tilde{\boldsymbol{u}}(t_n)}{\Delta t}, \boldsymbol{v}_h\right\rangle + \nu\left\langle \nabla\left(\tilde{\boldsymbol{u}}(t_{n+1})-\tilde{\boldsymbol{u}}(t_n)\right), \nabla\boldsymbol{v}_h\right\rangle + \nu\left\langle \nabla\cdot\tilde{\boldsymbol{u}}(t_n), \nabla\cdot\boldsymbol{v}_h\right\rangle \\
=&\Delta t^2\left\langle \boldsymbol{g}^n - \mathcal{P}\boldsymbol{g}^{n-1}, \boldsymbol{v}_h\right\rangle + \left\langle \mathcal{P}\left(\frac{\tilde{\boldsymbol{u}}(t_n)-\tilde{\boldsymbol{u}}(t_{n-1})}{\Delta t} + \boldsymbol{f}^n - \boldsymbol{f}^{n-1}\right), \boldsymbol{v}_h\right\rangle. \qquad (5.25)
\end{aligned}$$

Denote the H^1 projection of $\tilde{\boldsymbol{u}}(t_n)$ by $\tilde{\boldsymbol{u}}_h^n := \boldsymbol{\Pi}_h\tilde{\boldsymbol{u}}(t_n) \in X_{0,h}$ which is defined as

$$\left\langle \nabla(\tilde{\boldsymbol{u}}(t_n)-\tilde{\boldsymbol{u}}_h^n), \nabla\boldsymbol{v}_h\right\rangle = 0 \qquad \forall \boldsymbol{v}_h \in X_{0,h}.$$

We have

$$\|\tilde{\boldsymbol{u}}(t_n) - \tilde{\boldsymbol{u}}_h^n\| \le Ch^{m+1}, \qquad \|\nabla(\tilde{\boldsymbol{u}}(t_n) - \tilde{\boldsymbol{u}}_h^n)\| \le Ch^m.$$

Using the H^1 projection, from (5.25), we obtain

$$\begin{aligned}
&\left\langle \frac{\tilde{\boldsymbol{u}}_h^{n+1} - \tilde{\boldsymbol{u}}_h^n}{\Delta t}, \boldsymbol{v}_h \right\rangle + \nu\big\langle \nabla(\tilde{\boldsymbol{u}}_h^{n+1} - \tilde{\boldsymbol{u}}_h^n), \nabla \boldsymbol{v}_h \big\rangle + \nu\big\langle \nabla \cdot \tilde{\boldsymbol{u}}_h^n, \nabla \cdot \boldsymbol{v}_h \big\rangle \\
&- \left\langle \mathcal{P}_h \left(\frac{\tilde{\boldsymbol{u}}_h^n - \tilde{\boldsymbol{u}}_h^{n-1}}{\Delta t} + \boldsymbol{f}^n - \boldsymbol{f}^{n-1} \right), \boldsymbol{v}_h \right\rangle \\
=&\nu\big\langle \nabla \cdot (\tilde{\boldsymbol{u}}_h^n - \tilde{\boldsymbol{u}}(t_n)), \nabla \cdot \boldsymbol{v}_h \big\rangle - \left\langle \frac{(I - \boldsymbol{\Pi}_h)(\tilde{\boldsymbol{u}}(t_{n+1}) - \tilde{\boldsymbol{u}}(t_n))}{\Delta t}, \boldsymbol{v}_h \right\rangle \\
&+ \left\langle \frac{(\mathcal{P} - \mathcal{P}_h\boldsymbol{\Pi}_h)(\tilde{\boldsymbol{u}}(t_n) - \tilde{\boldsymbol{u}}(t_{n-1}))}{\Delta t}, \boldsymbol{v}_h \right\rangle \\
&+ \big\langle (\mathcal{P} - \mathcal{P}_h)(\boldsymbol{f}^n - \boldsymbol{f}^{n-1}), \boldsymbol{v}_h \big\rangle + \Delta t^2 \big\langle \boldsymbol{g}^n - \mathcal{P}\boldsymbol{g}^{n-1}, \boldsymbol{v}_h \big\rangle \\
=:& \big\langle \nabla \cdot (\boldsymbol{\Pi}_h - I)\tilde{\boldsymbol{u}}(t_n), \nabla \cdot \boldsymbol{v}_h \big\rangle + \big\langle R_n, \boldsymbol{v}_h \big\rangle,
\end{aligned} \tag{5.26}$$

where we have denote the sum of the terms on the right-hand side except the first one by $\langle R_n, \boldsymbol{v}_h \rangle$. We will first estimate $\langle R_n, \boldsymbol{v}_h \rangle$. For this reason, we need to estimate $(\mathcal{P} - \mathcal{P}_h)\boldsymbol{a}$. But note that $\mathcal{P}\boldsymbol{a} = \boldsymbol{a} - \nabla q$ and $\mathcal{P}_h\boldsymbol{a} = \boldsymbol{a} - \nabla q_h$, where

$$\big\langle \nabla q_h, \nabla \phi_h \big\rangle = \big\langle a, \nabla \phi_h \big\rangle = \big\langle \nabla q, \nabla \phi_h \big\rangle.$$

So, we can get

$$|(\mathcal{P} - \mathcal{P}_h)\boldsymbol{a}| = \|\nabla(q - q_h)\| \le \inf_{\phi_h \in Y_h} \|\nabla(q - \phi_h)\| \le Ch^{m'}.$$

Thus,

$$\big|\big\langle R_n, \boldsymbol{v}_h \big\rangle\big| \le C(h^{m+1} + h^{m'} + \Delta t^2)\|\boldsymbol{v}_h\|. \tag{5.27}$$

Defining $\boldsymbol{e}_h^n = \tilde{\boldsymbol{u}}_h^n - \boldsymbol{u}_h^n$, and subtracting (1.25) from (5.26), we get

$$\begin{aligned}
&\left\langle \frac{\boldsymbol{e}_h^{n+1} - \boldsymbol{e}_h^n}{\Delta t}, \boldsymbol{v}_h \right\rangle + \nu\big\langle \nabla \times (\boldsymbol{e}_h^{n+1} - \boldsymbol{e}_h^n), \nabla \times \boldsymbol{v}_h \big\rangle + \nu\big\langle \nabla \cdot \boldsymbol{e}_h^{n+1}, \nabla \cdot \boldsymbol{v}_h \big\rangle \\
&- \big\langle \mathcal{P}_h \frac{\boldsymbol{e}_h^n - \boldsymbol{e}_h^{n-1}}{\Delta t}, \boldsymbol{v}_h \big\rangle = \big\langle \nabla \cdot (\boldsymbol{\Pi}_h - I)\tilde{\boldsymbol{u}}(t_n), \nabla \cdot \boldsymbol{v}_h \big\rangle + \big\langle R_n, \boldsymbol{v}_h \big\rangle.
\end{aligned} \tag{5.28}$$

Now, letting $\boldsymbol{v}_h = 2\Delta t(\boldsymbol{e}_h^{n+1} - \boldsymbol{e}_h^n)$ in (5.28) and using the Cauchy-Schwarz inequality on $\left\langle \mathcal{P}_h \frac{\boldsymbol{e}_h^n - \boldsymbol{e}_h^{n-1}}{\Delta t}, \boldsymbol{v}_h \right\rangle = \left\langle \mathcal{P}_h \frac{\boldsymbol{e}_h^n - \boldsymbol{e}_h^{n-1}}{\Delta t}, \mathcal{P}_h \boldsymbol{v}_h \right\rangle$, we obtain

$$\begin{aligned}
&2\|\boldsymbol{e}_h^{n+1} - \boldsymbol{e}_h^n\|^2 + 2\Delta t\nu \|\nabla \times (\boldsymbol{e}_h^{n+1} - \boldsymbol{e}_h^n)\|^2 \\
&\quad + \Delta t\nu \left(\|\nabla \cdot \boldsymbol{e}_h^{n+1}\|^2 - \|\nabla \cdot \boldsymbol{e}_h^n\|^2 + \|\nabla \cdot (\boldsymbol{e}_h^{n+1} - \boldsymbol{e}_h^n)\|^2 \right) \\
\leq &\|\mathcal{P}_h(\boldsymbol{e}_h^n - \boldsymbol{e}_h^{n-1})\|^2 + \|\mathcal{P}_h(\boldsymbol{e}_h^{n+1} - \boldsymbol{e}_h^n)\|^2 + Ch^m \|\nabla \cdot (\boldsymbol{e}_h^{n+1} - \boldsymbol{e}_h^n)\| \Delta t \\
&\quad + C(h^{m+1} + h^{m'} + \Delta t^2)\Delta t \|\boldsymbol{e}_h^{n+1} - \boldsymbol{e}_h^n\|.
\end{aligned}$$

Using the Cauchy-Schwarz inequality, we get

$$\begin{aligned}
&\|\boldsymbol{e}_h^{n+1} - \boldsymbol{e}_h^n\|^2 + \frac{1}{2}\Delta t\nu \|\nabla(\boldsymbol{e}_h^{n+1} - \boldsymbol{e}_h^n)\|^2 + \Delta t\nu \left(\|\nabla \cdot \boldsymbol{e}_h^{n+1}\|^2 - \|\nabla \cdot \boldsymbol{e}_h^n\|^2 \right) \\
\leq &\|\mathcal{P}_h(\boldsymbol{e}_h^n - \boldsymbol{e}_h^{n-1})\|^2 + \|\boldsymbol{e}_h^{n+1} - \boldsymbol{e}_h^n\|^2 \Delta t + C(h^{2m} + h^{2m'} + \Delta t^4)\Delta t.
\end{aligned}$$

By the Gronwall inequality, we have

$$\begin{aligned}
&\|\boldsymbol{e}_h^n - \boldsymbol{e}_h^{n-1}\|^2 + \Delta t\nu \|\nabla \cdot \boldsymbol{e}_h^n\|^2 + \frac{1}{2}\Delta t\nu \sum_{k=1}^{n} \|\nabla(\boldsymbol{e}_h^k - \boldsymbol{e}_h^{k-1})\|^2 \\
\leq &C \left(\|\mathcal{P}_h(\boldsymbol{e}_h^0 - \boldsymbol{e}_h^{-1})\|^2 + \Delta t \|\nabla \cdot \boldsymbol{e}_h^0\|^2 + h^{2m} + h^{2m'} + \Delta t^4 \right).
\end{aligned}$$

From it, we derive the desired error estimates. □

5.3 Numerics of FE schemes (1.25) and (5.1)

We first do the computation with the given exact solution (4.69)–(4.71) on domain $[-1, 1] \times [-1, 1]$. We always use P3/P3 finite elements and take $\nu = 2$. Our aim is to check accuracy as well as demonstrate the unconditional stability.

Then we apply scheme (1.25) to the driven cavity flow on domain $[0, 1] \times [0, 1]$. For both $Re = 1000$ and $Re = 2000$, the parameters used for the computations are

the same: We use third order Lagrange element for both velocity and pressure. The mesh is of size $2 \times 50 \times 50$ and the smallest triangle has length 0.0075. We choose $\Delta t = 0.002$.

We exhibit the contour plot of the vorticity as well as the normalized velocity fields. Note that we need both $\boldsymbol{u}^0$ and $\boldsymbol{u}^1$ to start our iteration. $\boldsymbol{u}^0$ are set equal to $(1, 0)$ on the top boundary and $(0, 0)$ otherwise. $\boldsymbol{u}^1$ are computed from (1.18),(1.19). Then we iterate with (1.25). Unfortunately, the vorticity contain unphysical oscillations. We have found that if we apply (1.18),(1.19) on the final results from (1.25) and iterate them a few times, the oscillations are gone.

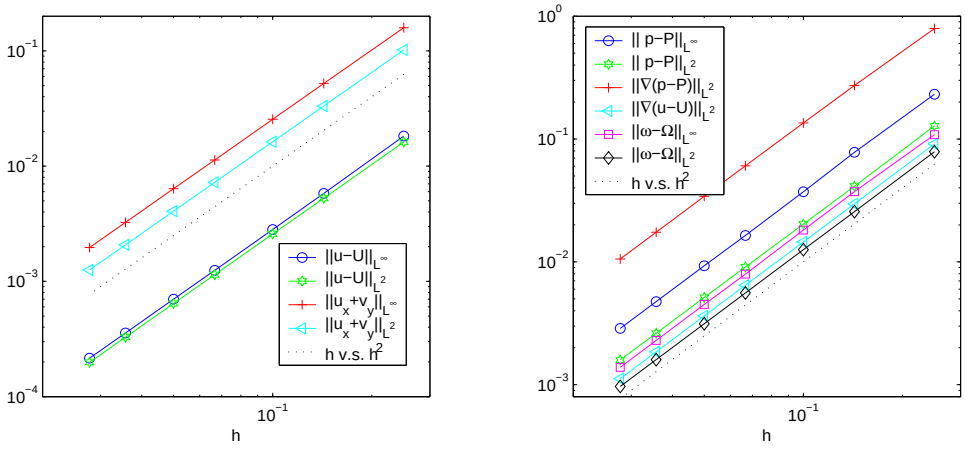

Figure 5.1: Scheme (1.25). $\Delta t = h^2$. $g(t) = 2t - 1/2$. $T = 0.5$

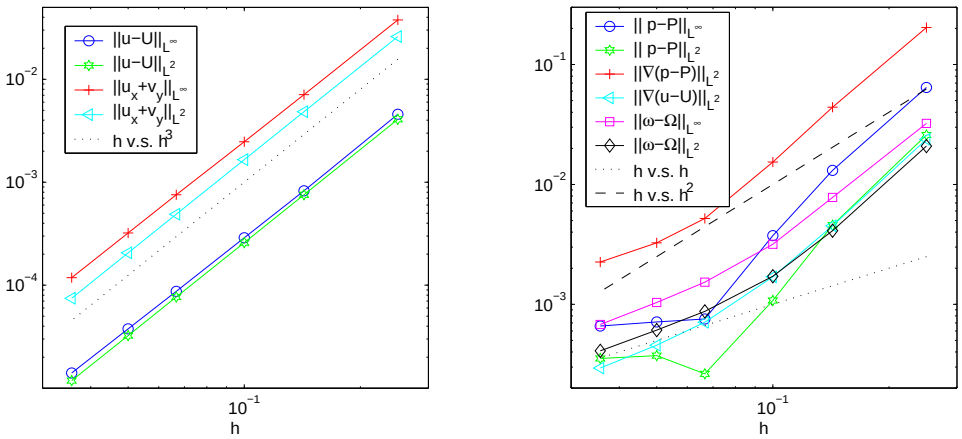

Figure 5.2: Scheme (1.25). $\Delta t = h^3$. $g(t) = 2t - 1/2$. $T = 0.5$

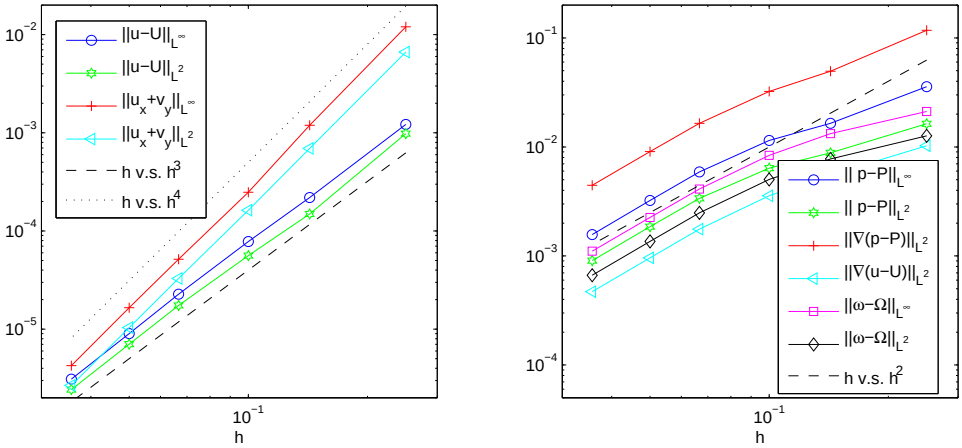

Figure 5.3: Scheme (1.25). $\Delta t = h^4$. $g(t) = 2t - 1/2$. $T = 0.1$

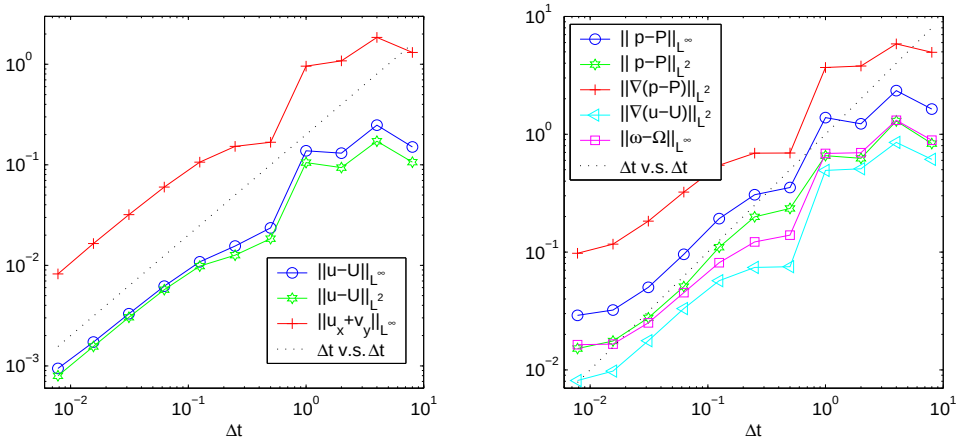

Figure 5.4: Stability check of scheme (1.25). Fixed grid with $h = 2/16$. $g(t) = \cos(t)$. $t = 1000$.

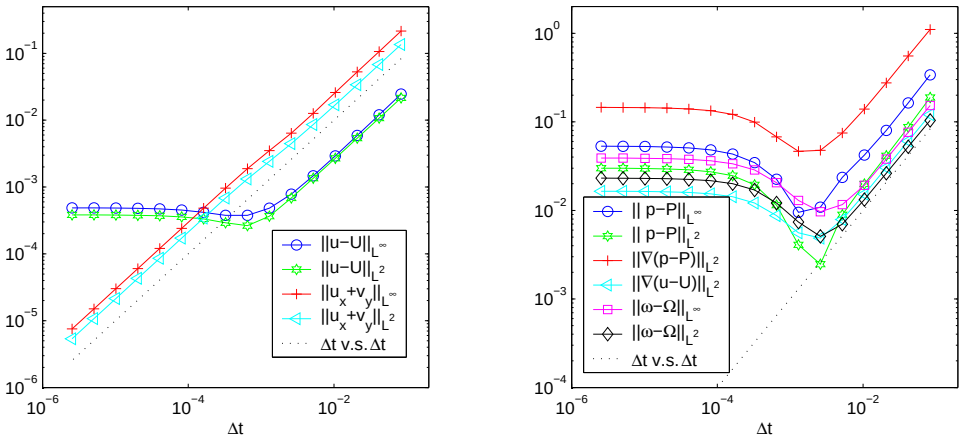

Figure 5.5: Scheme (1.25). Fixed grid with $h = 2/12$. $g(t) = 2t - 1/2$. $T = 0.5$

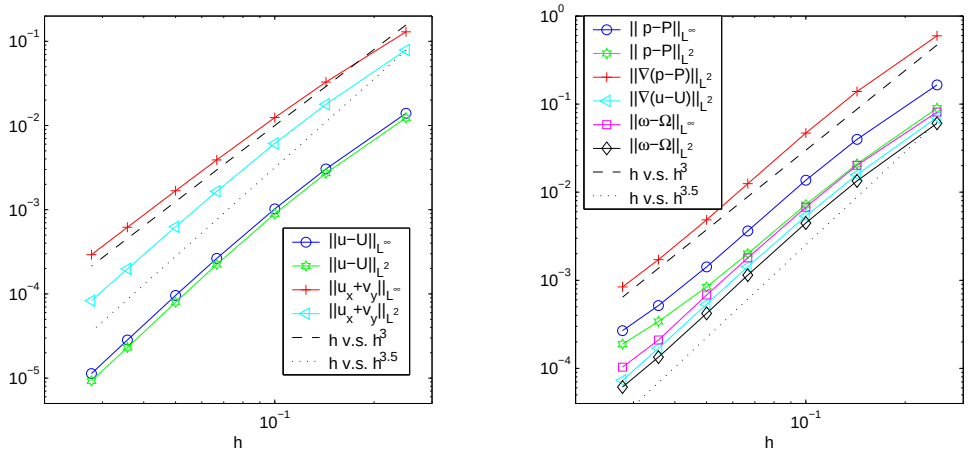

Figure 5.6: Scheme (5.1). $\Delta t = h^2$. $g(t) = 2t - 1/2$. $T = 0.5$

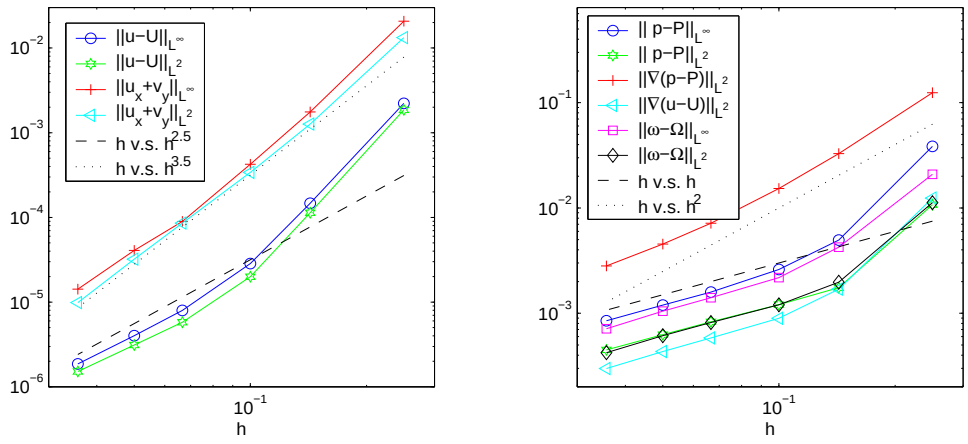

Figure 5.7: Scheme (5.1). $\Delta t = h^3$. $g(t) = 2t - 1/2$. $T = 0.5$

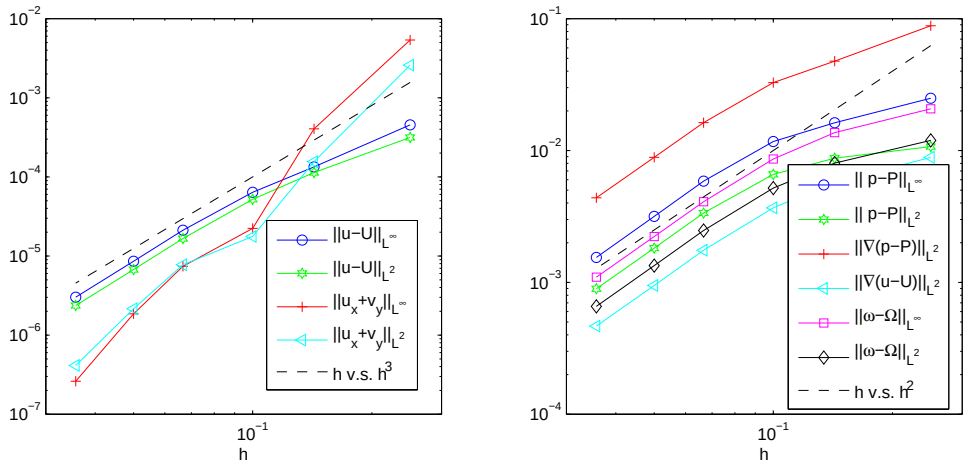

Figure 5.8: Scheme (5.1). $\Delta t = h^4$. $g(t) = 2t - 1/2$. $T = 0.1$

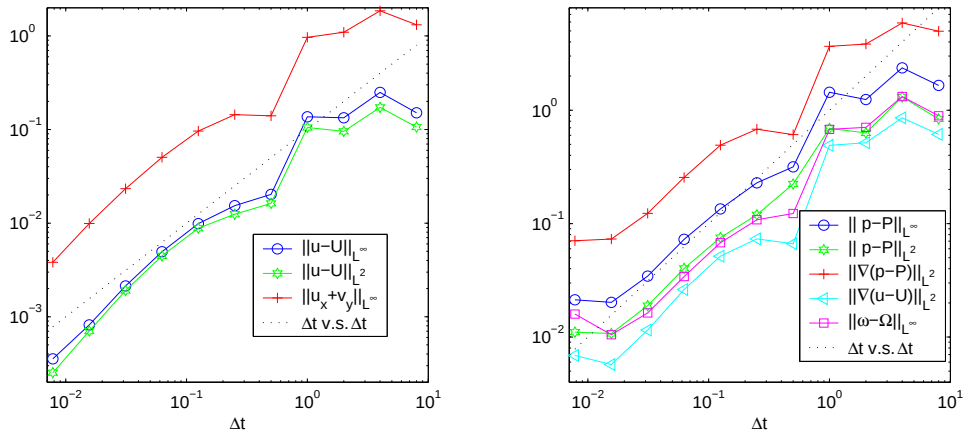

Figure 5.9: Stability check of scheme (5.1). Fixed grid with $h = 2/16$. $g(t) = \cos(t)$. $t = 1000$.

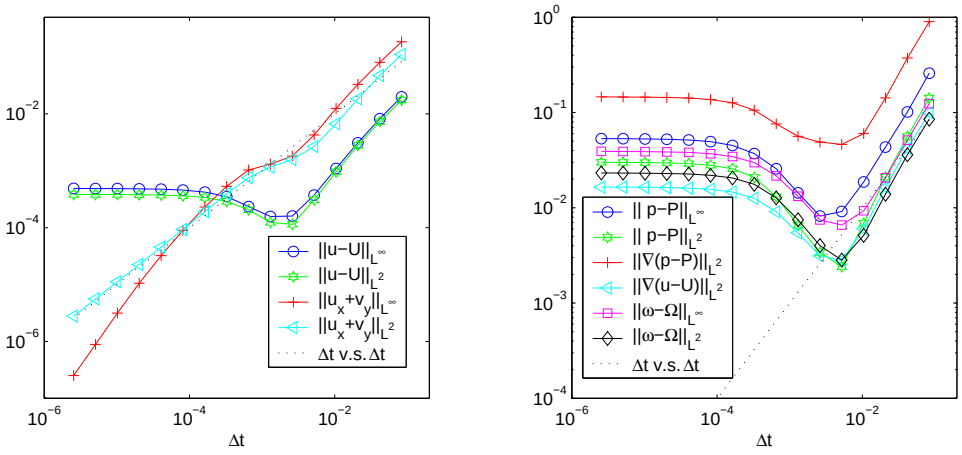

Figure 5.10: Scheme (1.25). Fixed grid with $h = 2/12$. $g(t) = 2t - 1/2$. $T = 0.5$

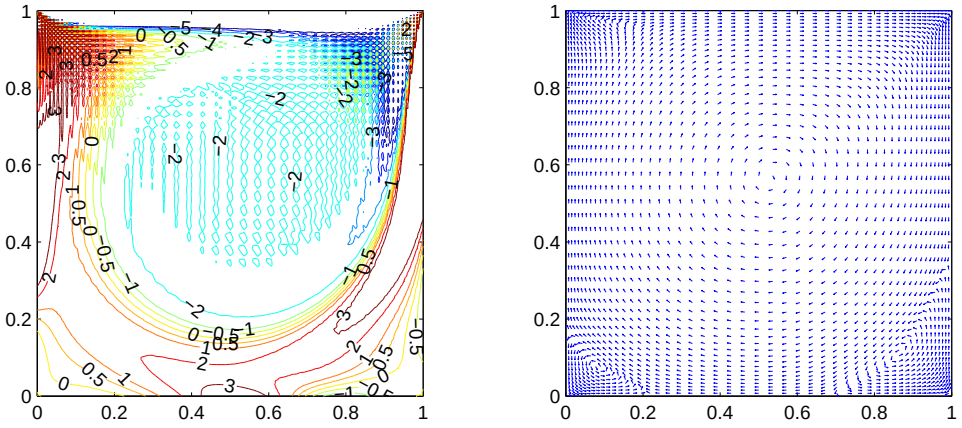

Figure 5.11: Driven cavity with $Re = 1000$. Scheme (1.25). Integrate to $t = 40$

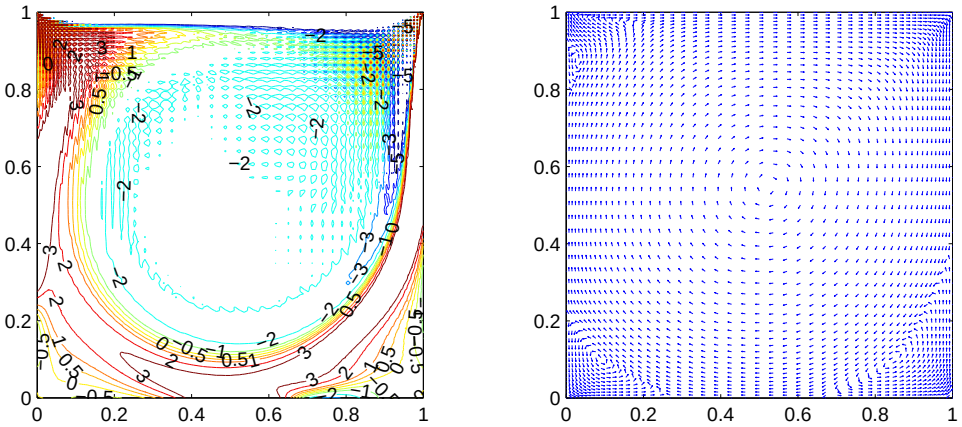

Figure 5.12: Driven cavity with $Re = 2000$. Scheme (1.25). Integrate to $t = 60$

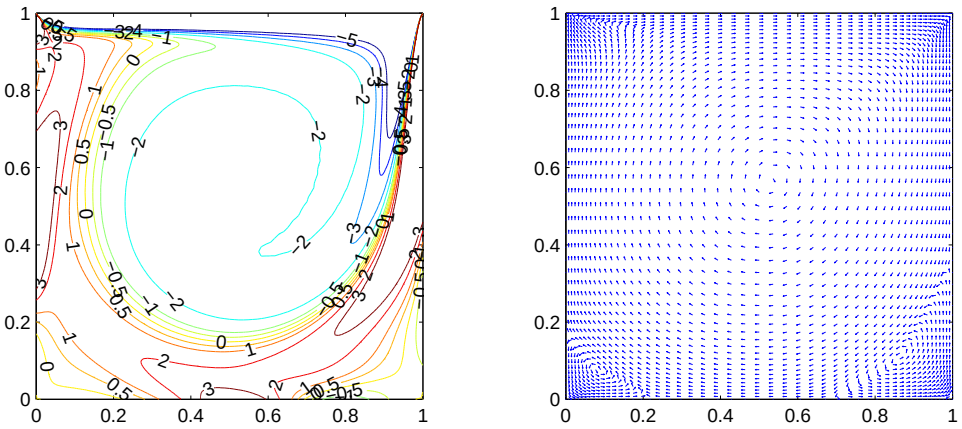

Figure 5.13: Driven cavity with $Re = 1000$. Start from the data of Figure 5.11 and use (1.18),(1.19) to do 50 iterations.

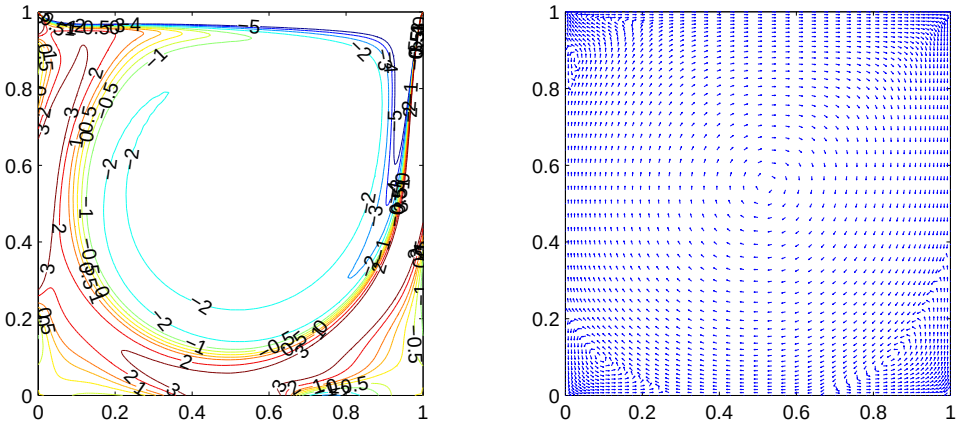

Figure 5.14: Driven cavity with $Re = 2000$. Start from the data of Figure 5.12 and use (1.18),(1.19) to do 100 iterations.

Chapter 6

Conclusions

A class of Navier-Stokes solvers based on a new pressure Poisson equation formulation of incompressible NSE has been studied. They enjoy the following good properties:

- efficient (Decoupling the update of $\boldsymbol{u}$ and p. Explicit treatment of p and $\boldsymbol{u}\cdot\nabla\boldsymbol{u}$)
- high order accurate (In contrast to Projection methods)
- first order time stepping can be unconditional stable if Γ is smooth.
- If use finite element, then we do not need inf-sup compatibility condition.

We mainly studied finite element schemes in this thesis, which covers both steady-state as well as time-dependent problems. The schemes as well as the theorem associated with them are listed below:

- steady-state Stokes equations

  C^1 FE scheme solving $(\boldsymbol{u}, p)$ together: (scheme (3.19)+(3.20). Theorem 4)

  C^1 iterative FE solver: (scheme (3.29)+(3.30). Theorem 5)

- time-dependent NSE

  C^0 FE scheme (1.19)+(1.18): (no theorem for the fully discrete case)

C^1 FE scheme (1.20)+(1.18): (Theorem 6 and 1)

C^0 FE scheme (1.25): (Theorem 7 and 8)

Besides the fully discrete schemes listed above, we have also obtained some results for the semi-discrete schemes. Those results are stated in Theorem 3 (steady-state Stokes) and Theorem 9 ((5.9) and (5.12) for time dependent SE).

Associated numeric computations have demonstrated the accuracy and good stability properties of these schemes.

Appendix A

Projection methods

The aim of this appendix is to compare the method that we have studied with the projection methods that exist in the literature. As a result, we have obtain a clean classification of all the projection methods, both first order and second order, together with this new method [JL] and the gauge method [EL].

A.1 First order projection methods

Proposition 1 *We can classify all the 1st order projection methods using the following table:*

Remark: To consider NSE instead of Stokes systems, we simply need to change $\mathcal{P}\boldsymbol{f}^n$ in the table to

$$\mathcal{P}(-\boldsymbol{u}^n\nabla\boldsymbol{u}^n+\boldsymbol{f}^n).$$

A.1.1 Chorin [Ch]; Temam [Te]

In [Ch] and [Te], it is presented as

$$\frac{\boldsymbol{u}^{n+1}-\mathcal{P}(\boldsymbol{u}^n)}{\Delta t}=\Delta\boldsymbol{u}^{n+1}+\mathcal{P}\boldsymbol{f}^n,\qquad \boldsymbol{u}^{n+1}|_\Gamma=0 \tag{A.1}$$

$$\nabla p^{n+1}=\frac{(I-\mathcal{P})\boldsymbol{u}^{n+1}}{\Delta t} \tag{A.2}$$

Author	1st order scheme
[Ch];[Te]	$\frac{\boldsymbol{u}^{n+1}-\mathcal{P}\boldsymbol{u}^n}{\Delta t} = \Delta \boldsymbol{u}^{n+1} + \mathcal{P}\boldsymbol{f}^n$ or $\frac{\boldsymbol{u}^{n+1}-\boldsymbol{u}^n}{\Delta t} + \nabla p_{\mathrm{s}}(\boldsymbol{u}^n) + \nabla\nabla\cdot\boldsymbol{u}^n = \Delta \boldsymbol{u}^{n+1} + \mathcal{P}\boldsymbol{f}^n$
[vK];[BCG]	$\frac{\boldsymbol{u}^{n+1}-\mathcal{P}\boldsymbol{u}^n}{\Delta t} + \nabla p_{\mathrm{s}}(\boldsymbol{u}^n) + \nabla\nabla\cdot\boldsymbol{u}^n = \Delta \boldsymbol{u}^{n+1} + \mathcal{P}\boldsymbol{f}^n$
[OID];[TMV];[KM]; [Pe];[BCM];[GS2]	$\frac{\boldsymbol{u}^{n+1}-\mathcal{P}\boldsymbol{u}^n}{\Delta t} + \nabla p_{\mathrm{s}}(\boldsymbol{u}^n) = \Delta \boldsymbol{u}^{n+1} + \mathcal{P}\boldsymbol{f}^n$
[JL]; [EL]; [GS1]	$\frac{\boldsymbol{u}^{n+1}-\boldsymbol{u}^n}{\Delta t} + \nabla p_{\mathrm{s}}(\boldsymbol{u}^n) = \Delta \boldsymbol{u}^{n+1} + \mathcal{P}\boldsymbol{f}^n$

Taking $\mathcal{P} - I$ on both sides of (A.1) and change $n+1$ to n , we get

$$\frac{(\mathcal{P}-I)\boldsymbol{u}^n}{\Delta t} + (I-\mathcal{P})\Delta \boldsymbol{u}^n = 0 \tag{A.3}$$

Add (A.3) to (A.1), we get

$$\frac{\boldsymbol{u}^{n+1}-\boldsymbol{u}^n}{\Delta t} + \nabla q^n = \Delta \boldsymbol{u}^{n+1} + \mathcal{P}\boldsymbol{f}^n. \tag{A.4}$$

where

$$\nabla q^n = (I-\mathcal{P})\Delta \boldsymbol{u}^n = \nabla p_{\mathrm{s}}(\boldsymbol{u}^n) + \nabla\nabla\cdot\boldsymbol{u}^n.$$

A.1.2 van Kan [vK]; Bell, Colella and Glaz [BCG]

$$\frac{\boldsymbol{u}^{n+1}-\mathcal{P}\boldsymbol{u}^n}{\Delta t} + \nabla p^n = \Delta \boldsymbol{u}^{n+1} + \mathcal{P}\boldsymbol{f}^n, \qquad \boldsymbol{u}^{n+1}|_\Gamma = 0, \tag{A.5}$$

$$\nabla(p^{n+1}-p^n) = (I-\mathcal{P})\frac{\boldsymbol{u}^{n+1}}{\Delta t}, \tag{A.6}$$

Plugging $\nabla p^n = \nabla p^{n+1} - (I-\mathcal{P})\frac{\boldsymbol{u}^{n+1}}{\Delta t}$ into the first equation and taking $(I-\mathcal{P})$ on both sides, we see that

$$\nabla p^{n+1} = (I-\mathcal{P})\Delta \boldsymbol{u}^{n+1}. \tag{A.7}$$

A.1.3 Orszag, Israeli and Deville [OID]; Timmermans, Minev and Van De Vosse [TMV]; Kim and Moin [KM]; Petersson [Pe]; Brown, Cortez and Minion [BCM]; Guermond and Shen [GS2]

All of them can be characterized as

$$\frac{\boldsymbol{u}^{n+1} - \mathcal{P}\boldsymbol{u}^n}{\Delta t} + \nabla p_{\mathrm{s}}(\boldsymbol{u}^n) = \Delta \boldsymbol{u}^{n+1} + \mathcal{P}\boldsymbol{f}^n \tag{A.8}$$

[OID]

In [OID], it is called accurate boundary condition for pressure and is presented as

$$\begin{aligned} \frac{\boldsymbol{u}^{n+1} - \boldsymbol{u}^{*,n}}{\Delta t} = \frac{1}{2}\Delta(\boldsymbol{u}^{n+1} + \boldsymbol{u}^{*,n}) + \mathcal{P}\boldsymbol{f}^n, \qquad \boldsymbol{u}^{n+1}|_\Gamma = 0 \\ \nabla p^{n+1/2} = \nabla p_{\mathrm{s}}(\boldsymbol{u}^{n+1}) + \frac{(I-\mathcal{P})\boldsymbol{u}^{n+1}}{\Delta t}, \\ \boldsymbol{u}^{*,n+1} = \boldsymbol{u}^{n+1} - \Delta t \nabla p^{n+1/2} \end{aligned}$$

Its first order form can be written as

$$\frac{\boldsymbol{u}^{n+1} - (\boldsymbol{u}^n - \Delta t \nabla p_{\mathrm{s}}(\boldsymbol{u}^n) - (I-\mathcal{P})\boldsymbol{u}^n)}{\Delta t} = \Delta \boldsymbol{u}^{n+1} + \mathcal{P}\boldsymbol{f}^n, \qquad \boldsymbol{u}^{n+1}|_\Gamma = 0. \tag{A.9}$$

[TMV]

In [TMV], it is called pressure increment formulation and is presented as

$$\frac{\boldsymbol{u}^{n+1}-\mathcal{P}\boldsymbol{u}^n}{\Delta t}+\nabla p^n=\Delta\boldsymbol{u}^{n+1}+\mathcal{P}\boldsymbol{f}^n,\qquad \boldsymbol{u}^{n+1}|_\Gamma=0, \tag{A.10}$$

$$\mathcal{P}\boldsymbol{u}^{n+1}=\boldsymbol{u}^{n+1}-\Delta t\nabla\phi^{n+1}, \tag{A.11}$$

$$p^{n+1}=p^n-\nabla\cdot\boldsymbol{u}^{n+1}+\phi^{n+1}. \tag{A.12}$$

Plug $p^n=p^{n+1}+\nabla\cdot\boldsymbol{u}^{n+1}-\phi^{n+1}$ into (A.10) and using (A.11), we get

$$\frac{\mathcal{P}\boldsymbol{u}^{n+1}-\mathcal{P}\boldsymbol{u}^n}{\Delta t}+\nabla p^{n+1}=-\nabla\times\nabla\times\boldsymbol{u}^{n+1}+\mathcal{P}\boldsymbol{f}^n.$$

Then, taking $I-\mathcal{P}$ on both side of the equation, we get

$$\nabla p^{n+1}=\nabla p_{\mathrm{S}}(\boldsymbol{u}^{n+1}). \tag{A.13}$$

[KM]

In [KM], it is called accurate boundary condition for intermediate velocity field and is presented as

$$\frac{\boldsymbol{u}^{n+1}-\mathcal{P}\boldsymbol{u}^n}{\Delta t}=\frac{1}{2}\Delta(\boldsymbol{u}^{n+1}+\mathcal{P}\boldsymbol{u}^n)+\mathcal{P}\boldsymbol{f}^{n+1/2},\qquad \boldsymbol{u}^{n+1}|_\Gamma=\Delta t\nabla\phi^n|_\Gamma,$$

$$\nabla\phi^{n+1}=\frac{(I-\mathcal{P})\boldsymbol{u}^{n+1}}{\Delta t},$$

$$p^{n+1/2}=\phi^{n+1}-\frac{1}{2}\Delta t\Delta\phi^{n+1}.$$

Its first order form can be written as:

$$\frac{\boldsymbol{u}^{n+1}-\mathcal{P}\boldsymbol{u}^n}{\Delta t}=\Delta\boldsymbol{u}^{n+1}+\mathcal{P}\boldsymbol{f}^n,\qquad \boldsymbol{u}^{n+1}|_\Gamma=(I-\mathcal{P})\boldsymbol{u}^n|_\Gamma. \tag{A.14}$$

Let $\boldsymbol{v}^{n+1} = \boldsymbol{u}^{n+1} - (I - \mathcal{P})\boldsymbol{u}^n$, then $\mathcal{P}\boldsymbol{u}^n = \mathcal{P}\boldsymbol{v}^n$ and

$$\frac{\boldsymbol{v}^{n+1} - \mathcal{P}\boldsymbol{v}^n}{\Delta t} + \nabla p^n = \Delta \boldsymbol{v}^{n+1} + \mathcal{P}\boldsymbol{f}^n, \qquad \boldsymbol{v}^{n+1}|_\Gamma = 0. \tag{A.15}$$

where

$$\nabla p^n = \frac{(I - \mathcal{P})\boldsymbol{u}^n}{\Delta t} - \Delta(I - \mathcal{P})\boldsymbol{u}^n = \frac{\boldsymbol{u}^n}{\Delta t} - \Delta \boldsymbol{u}^n - \frac{\mathcal{P}\boldsymbol{u}^n}{\Delta t} + \Delta \mathcal{P}\boldsymbol{u}^n$$

Taking $(I - \mathcal{P})$ on both sides of the equation and using $\frac{\boldsymbol{u}^n}{\Delta t} - \Delta \boldsymbol{u}^n = \frac{\mathcal{P}\boldsymbol{u}^{n-1}}{\Delta t}$, we get

$$\begin{aligned} \nabla p^n =& (I - \mathcal{P})\Delta \mathcal{P}\boldsymbol{u}^n = (I - \mathcal{P})\Delta \mathcal{P}\boldsymbol{v}^n = -(I - \mathcal{P})\nabla \times \nabla \times \mathcal{P}\boldsymbol{v}^n \\ =& -(I - \mathcal{P})\nabla \times \nabla \times \boldsymbol{v}^n = \nabla p_{\mathrm{s}}(\boldsymbol{v}^n). \end{aligned} \tag{A.16}$$

This fact that Kim and Moin's scheme can be transformed into Timmermans, Minev and Van De Vosse's scheme has been observed in [GMS].

[Pe]

In [Pe], it is represented as

$$\frac{\boldsymbol{u}^{n+1} - \boldsymbol{u}^n}{\Delta t} + \lambda(I - \mathcal{P})\boldsymbol{u}^n + \nabla p_{\mathrm{s}}(\boldsymbol{u}^n) = \Delta \boldsymbol{u}^{n+1} + \mathcal{P}\boldsymbol{f}^n, \qquad \boldsymbol{u}^{n+1}|_\Gamma = 0.$$

If choose $\lambda = 1/\Delta t$, it can be written as (A.8).

A.1.4 Johnston and Liu [JL], E and Liu [EL], Guermond and Shen [GS1]

$$\frac{\boldsymbol{u}^{n+1} - \boldsymbol{u}^n}{\Delta t} + \nabla p_{\mathrm{s}}(\boldsymbol{u}^n) = \Delta \boldsymbol{u}^{n+1} + \mathcal{P}\boldsymbol{f}^n, \qquad \boldsymbol{u}^{n+1}|_\Gamma = 0. \tag{A.17}$$

A.2 Second order projection methods

Proposition 2 *We can rewrite all the 2nd order projection methods in the following table:*

From it we can see that all of them are consistent 2nd order methods.

A.2.1 van Kan [vK]; Bell, Colella and Glaz [BCG]

$$\frac{\boldsymbol{u}^{n+1}-\mathcal{P}\boldsymbol{u}^n}{\Delta t}+\nabla p^n=\frac{1}{2}\Delta(\boldsymbol{u}^{n+1}+\mathcal{P}\boldsymbol{u}^n)+\mathcal{P}\boldsymbol{f}^{n+1/2},\qquad \boldsymbol{u}^{n+1}|_\Gamma=0, \tag{A.18}$$

$$\nabla(p^{n+1}-p^n)=(I-\mathcal{P})\frac{\boldsymbol{u}^{n+1}}{\Delta t}. \tag{A.19}$$

Plugging $\nabla p^n=\nabla p^{n+1}-(I-\mathcal{P})\frac{\boldsymbol{u}^{n+1}}{\Delta t}$ into the first equation and taking $(I-\mathcal{P})$ on both sides, and using the fact that

$$\Delta\mathcal{P}\boldsymbol{u}^n=-\nabla\times\nabla\times\boldsymbol{u}^n,$$

we see that

$$\nabla p^{n+1}=\frac{1}{2}\left((I-\mathcal{P})\Delta\boldsymbol{u}^{n+1}+\nabla p_{\mathrm{s}}(\boldsymbol{u}^n)\right)=\frac{1}{2}\nabla p_{\mathrm{s}}(\boldsymbol{u}^{n+1}+\boldsymbol{u}^n)+\frac{1}{2}\nabla\nabla\cdot\boldsymbol{u}^{n+1}. \tag{A.20}$$

To see the consistency of the scheme, we do the following: Take $\mathcal{P}-I$ on both sides of (A.18) and change $n+1$ to n, we get

$$\frac{(\mathcal{P}-I)\boldsymbol{u}^n}{\Delta t}-\nabla p^{n-1}+\frac{1}{2}(I-\mathcal{P})\Delta(\boldsymbol{u}^n+\mathcal{P}\boldsymbol{u}^{n-1})=0.$$

Add it to (A.18), we get

$$\frac{\boldsymbol{u}^{n+1}-\boldsymbol{u}^n}{\Delta t}+\nabla q=\frac{1}{2}\Delta(\boldsymbol{u}^{n+1}+\boldsymbol{u}^n)$$

Author	2nd order scheme
[vK];[BCG]	$\frac{\boldsymbol{u}^{n+1}-\mathcal{P}\boldsymbol{u}^n}{\Delta t}+\nabla p^n=\frac{1}{2}\Delta(\boldsymbol{u}^{n+1}+\mathcal{P}\boldsymbol{u}^n)+\mathcal{P}\boldsymbol{f}^{n+1/2}$ where $\nabla p^n=\frac{1}{2}\nabla p_{\mathrm{S}}(\boldsymbol{u}^n+\boldsymbol{u}^{n-1})+\frac{1}{2}\nabla\nabla\cdot\boldsymbol{u}^n$ or $\frac{\boldsymbol{u}^{n+1}-\boldsymbol{u}^n}{\Delta t}+\nabla q^{n+1/2}=\frac{1}{2}\Delta(\boldsymbol{u}^{n+1}+\boldsymbol{u}^n)+\mathcal{P}\boldsymbol{f}^{n+1/2}$ where $\nabla q^{n+1/2}=\nabla p_{\mathrm{S}}(\boldsymbol{u}^n+\frac{1}{2}\boldsymbol{u}^{n-1}-\frac{1}{2}\boldsymbol{u}^{n-2})+\frac{1}{2}\nabla\nabla\cdot(3\boldsymbol{u}^n-\boldsymbol{u}^{n-1})$
[OID]	$\frac{\boldsymbol{u}^{n+1}-\mathcal{P}\boldsymbol{u}^n}{\Delta t}+\nabla p_{\mathrm{S}}(\boldsymbol{u}^n)=\frac{1}{2}\Delta(\boldsymbol{u}^{n+1}+\mathcal{P}\boldsymbol{u}^n)+\mathcal{P}\boldsymbol{f}^{n+1/2}$ or $\frac{\boldsymbol{u}^{n+1}-\boldsymbol{u}^n}{\Delta t}+\nabla q^{n+1/2}=\frac{1}{2}\Delta(\boldsymbol{u}^{n+1}+\boldsymbol{u}^n)+\mathcal{P}\boldsymbol{f}^{n+1/2}$ where $\nabla q^{n+1/2}=\frac{1}{2}\nabla p_{\mathrm{S}}(3\boldsymbol{u}^n-\boldsymbol{u}^{n-1})+\nabla\nabla\cdot\boldsymbol{u}^n$
[TMV]	$\frac{3\boldsymbol{u}^{n+1}-4\mathcal{P}\boldsymbol{u}^n+\mathcal{P}\boldsymbol{u}^{n-1}}{2\Delta t}+\nabla p_{\mathrm{S}}(\boldsymbol{u}^n)=\Delta\boldsymbol{u}^{n+1}+\mathcal{P}\boldsymbol{f}^{n+1}$ or $\frac{3\boldsymbol{u}^{n+1}-4\boldsymbol{u}^n+\boldsymbol{u}^{n-1}}{2\Delta t}+\nabla q^{n+1}=\Delta\boldsymbol{u}^{n+1}+\mathcal{P}\boldsymbol{f}^{n+1}$ where $\nabla q^{n+1}=\frac{1}{3}\nabla p_{\mathrm{S}}(7\boldsymbol{u}^n-5\boldsymbol{u}^{n-1}+\boldsymbol{u}^{n-2})+\frac{1}{3}\nabla\nabla\cdot(4\boldsymbol{u}^n-\boldsymbol{u}^{n-1})$
[KM]	$\frac{\boldsymbol{v}^{n+1}-\mathcal{P}\boldsymbol{v}^n}{\Delta t}+\frac{1}{2}\nabla p_{\mathrm{S}}(\boldsymbol{v}^n+\boldsymbol{v}^{n-1})=\frac{1}{2}\Delta(\boldsymbol{v}^{n+1}+\mathcal{P}\boldsymbol{v}^n)+\mathcal{P}\boldsymbol{f}^{n+1/2}$ or $\frac{\boldsymbol{v}^{n+1}-\boldsymbol{v}^n}{\Delta t}+\nabla q^{n+1/2}=\frac{1}{2}\Delta(\boldsymbol{v}^{n+1}+\boldsymbol{v}^n)+\mathcal{P}\boldsymbol{f}^{n+1/2}$ where $\nabla q^{n+1/2}=\nabla p_{\mathrm{S}}\left(\boldsymbol{v}^n+\frac{1}{2}\boldsymbol{v}^{n-1}-\frac{1}{2}\boldsymbol{v}^{n-2}\right)+\nabla\nabla\cdot\boldsymbol{v}^n$
[JL]; [EL]; [GS1]	$\frac{\boldsymbol{u}^{n+1}-\boldsymbol{u}^n}{\Delta t}+\frac{1}{2}\nabla p_{\mathrm{S}}(3\boldsymbol{u}^n-\boldsymbol{u}^{n-1})=\frac{1}{2}\Delta(\boldsymbol{u}^{n+1}+\boldsymbol{u}^n)+\mathcal{P}\boldsymbol{f}^{n+1/2}$

where

$$\nabla q = \nabla p^n - \nabla p^{n-1} + \frac{1}{2}(I-\mathcal{P})\Delta(\boldsymbol{u}^n + \mathcal{P}\boldsymbol{u}^{n-1}) + \frac{1}{2}\Delta(I-\mathcal{P})\boldsymbol{u}^n$$

Plugging in (A.20), after some calculation, we get

$$\nabla q = \nabla p_{\mathrm{S}}(\boldsymbol{u}^n + \frac{1}{2}\boldsymbol{u}^{n-1} - \frac{1}{2}\boldsymbol{u}^{n-2}) + \frac{1}{2}\nabla\nabla\cdot(3\boldsymbol{u}^n - \boldsymbol{u}^{n-1}) \tag{A.21}$$

which are second order accurate at time level $t^{n+1/2}$. Note that we have used

$$(I-\mathcal{P})\Delta\mathcal{P}\boldsymbol{u} = \nabla p_{\mathrm{S}}(\boldsymbol{u}), \qquad \Delta(I-\mathcal{P})\boldsymbol{u} = \nabla\nabla\cdot\boldsymbol{u}$$

A.2.2 Orszag, Israeli and Deville [OID]; Timmermans, Minev and Van De Vosse [TMV]; Kim and Moin [KM]; Petersson [Pe]; Brown, Cortez and Minion [BCM]; Guermond and Shen [GS2] [OID]

In [OID], it is called accurate boundary condition for pressure and can be rewritten as

$$\frac{\boldsymbol{u}^{n+1} - (\boldsymbol{u}^n - \Delta t\nabla p_{\mathrm{S}}(\boldsymbol{u}^n) - (I-\mathcal{P})\boldsymbol{u}^n)}{\Delta t} = \frac{1}{2}\Delta(\boldsymbol{u}^{n+1} + \mathcal{P}\boldsymbol{u}^n) + \mathcal{P}\boldsymbol{f}^{n+1/2}, \tag{A.22}$$
$$\boldsymbol{u}^{n+1}|_\Gamma = 0.$$

Note that in the process of rewriting, we have used the fact that $\Delta\nabla p_{\mathrm{S}}(\boldsymbol{u}^n) = 0$. To see the consistency of the scheme, we do the following: Take $\mathcal{P} - I$ on both sides of (A.22) and change $n+1$ to n, we get

$$\frac{(\mathcal{P}-I)\boldsymbol{u}^n}{\Delta t} - \nabla p_{\mathrm{S}}(\boldsymbol{u}^{n-1}) + \frac{1}{2}(I-\mathcal{P})\Delta(\boldsymbol{u}^n + \mathcal{P}\boldsymbol{u}^{n-1}) = 0.$$

Add it with (A.22), we see that (A.22) can be rewritten as

$$\frac{\boldsymbol{u}^{n+1}-\boldsymbol{u}^n}{\Delta t}+\nabla q=\frac{1}{2}\Delta(\boldsymbol{u}^{n+1}+\boldsymbol{u}^n)+\mathcal{P}\boldsymbol{f}^{n+1/2}$$

where

$$\nabla q=\nabla p_{\mathrm{S}}(\boldsymbol{u}^n-\boldsymbol{u}^{n-1})+\frac{1}{2}(I-\mathcal{P})\Delta(\boldsymbol{u}^n+\mathcal{P}\boldsymbol{u}^{n-1})+\frac{1}{2}\Delta(I-\mathcal{P})\boldsymbol{u}^n$$

After some calculation, we get

$$\nabla q=\frac{1}{2}\nabla p_{\mathrm{S}}(3\boldsymbol{u}^n-\boldsymbol{u}^{n-1})+\nabla\nabla\cdot\boldsymbol{u}^n \tag{A.23}$$

Without $\nabla\nabla\cdot\boldsymbol{u}^n$, it is 2nd order accurate at $t^{n+1/2}$. Since the original NSE satisfies $\nabla\cdot\boldsymbol{u}=0$, the truncation error is $O(\Delta t^2)$.

[TMV]

In [TMV], it is called pressure increment formulation and is presented as

$$\frac{3\boldsymbol{u}^{n+1}-4\mathcal{P}\boldsymbol{u}^n+\mathcal{P}\boldsymbol{u}^{n-1}}{2\Delta t}+\nabla p^n=\Delta\boldsymbol{u}^{n+1}+\mathcal{P}\boldsymbol{f}^{n+1}\qquad \boldsymbol{u}^{n+1}|_\Gamma=0, \tag{A.24}$$

$$\mathcal{P}\boldsymbol{u}^{n+1}=\boldsymbol{u}^{n+1}-\frac{2\Delta t}{3}\nabla\phi^{n+1}, \tag{A.25}$$

$$p^{n+1}=p^n-\nabla\cdot\boldsymbol{u}^{n+1}+\phi^{n+1}. \tag{A.26}$$

Plug $p^n=p^{n+1}+\nabla\cdot\boldsymbol{u}^{n+1}-\phi^{n+1}$ into (A.24) and using (A.25), we get

$$\frac{3\mathcal{P}\boldsymbol{u}^{n+1}-4\mathcal{P}\boldsymbol{u}^n+\mathcal{P}\boldsymbol{u}^{n-1}}{2\Delta t}+\nabla p^{n+1}=-\nabla\times\nabla\times\boldsymbol{u}^{n+1}+\mathcal{P}\boldsymbol{f}^{n+1}.$$

Then, taking $I-\mathcal{P}$ on both side of the equation, we get

$$\nabla p^{n+1}=\nabla p_{\mathrm{S}}(\boldsymbol{u}^{n+1}). \tag{A.27}$$

To see the consistency of this 2nd order scheme, rewrite it as

$$\frac{3\boldsymbol{u}^{n+1}-4\boldsymbol{u}^{n}+\boldsymbol{u}^{n-1}}{2\Delta t}+\frac{4(I-\mathcal{P})\boldsymbol{u}^{n}-(I-\mathcal{P})\boldsymbol{u}^{n-1}}{2\Delta t}+\nabla p_{\mathrm{S}}(\boldsymbol{u}^{n})=\Delta\boldsymbol{u}^{n+1}+\mathcal{P}\boldsymbol{f}^{n+1}.$$

Take $(I-\mathcal{P})$ on both sides of (A.24) and change $n+1$ to n, we get

$$\frac{(I-\mathcal{P})\boldsymbol{u}^{n}}{2\Delta t}=\frac{1}{3}\left(-\nabla p_{\mathrm{S}}(\boldsymbol{u}^{n-1})+(I-\mathcal{P})\Delta\boldsymbol{u}^{n}\right)=\frac{1}{3}\nabla p_{\mathrm{S}}(\boldsymbol{u}^{n}-\boldsymbol{u}^{n-1})+\frac{1}{3}\nabla\nabla\cdot\boldsymbol{u}^{n}.$$

Plug in, and after some computation, we get

$$\frac{3\boldsymbol{u}^{n+1}-4\boldsymbol{u}^{n}+\boldsymbol{u}^{n-1}}{2\Delta t}+\nabla q=\Delta\boldsymbol{u}^{n+1}$$

where

$$\nabla q=\frac{1}{3}\nabla p_{\mathrm{S}}\left(7\boldsymbol{u}^{n}-5\boldsymbol{u}^{n-1}+\boldsymbol{u}^{n-2}\right)+\frac{1}{3}(I-\mathcal{P})\nabla\nabla\cdot(4\boldsymbol{u}^{n}-\boldsymbol{u}^{n-1})$$

Without $\frac{1}{3}(I-\mathcal{P})\nabla\nabla\cdot(4\boldsymbol{u}^{n}-\boldsymbol{u}^{n-1})$, it is 2nd order accurate at t^{n+1}. Since the original NSE satisfies $\nabla\cdot\boldsymbol{u}=0$, the truncation error is $O(\Delta t^{2})$.

[KM]

In [KM], it is called accurate boundary condition for intermediate velocity field and can be rewritten as

$$\frac{\boldsymbol{u}^{n+1}-\mathcal{P}\boldsymbol{u}^{n}}{\Delta t}=\frac{1}{2}\Delta(\boldsymbol{u}^{n+1}+\mathcal{P}\boldsymbol{u}^{n})+\mathcal{P}\boldsymbol{f}^{n+1/2},\qquad\boldsymbol{u}^{n+1}|_{\Gamma}=(I-\mathcal{P})\boldsymbol{u}^{n}|_{\Gamma}.\quad\text{(A.28)}$$

Let $\boldsymbol{v}^{n+1}=\boldsymbol{u}^{n+1}-(I-\mathcal{P})\boldsymbol{u}^{n}$, then $\mathcal{P}\boldsymbol{u}^{n}=\mathcal{P}\boldsymbol{v}^{n}$ and

$$\frac{\boldsymbol{v}^{n+1}-\mathcal{P}\boldsymbol{v}^{n}}{\Delta t}+\nabla p^{n}=\frac{1}{2}\Delta(\boldsymbol{v}^{n+1}+\mathcal{P}\boldsymbol{v}^{n})+\mathcal{P}\boldsymbol{f}^{n+1/2},\qquad\boldsymbol{v}^{n+1}|_{\Gamma}=0.\qquad\text{(A.29)}$$

where

$$\nabla p^{n}=\frac{(I-\mathcal{P})\boldsymbol{u}^{n}}{\Delta t}-\frac{1}{2}\Delta(I-\mathcal{P})\boldsymbol{u}^{n}=\frac{\boldsymbol{u}^{n}}{\Delta t}-\frac{1}{2}\Delta\boldsymbol{u}^{n}-\frac{\mathcal{P}\boldsymbol{u}^{n}}{\Delta t}+\frac{1}{2}\Delta\mathcal{P}\boldsymbol{u}^{n}$$

Taking $(I-\mathcal{P})$ on both sides of the equation and using $\frac{\boldsymbol{u}^n}{\Delta t}-\frac{1}{2}\Delta\boldsymbol{u}^n=\frac{\mathcal{P}\boldsymbol{u}^{n-1}}{\Delta t}+\frac{1}{2}\Delta\mathcal{P}\boldsymbol{u}^{n-1}$, we get

$$\begin{aligned}\nabla p^n =&\frac{1}{2}(I-\mathcal{P})\Delta\mathcal{P}(\boldsymbol{u}^n+\boldsymbol{u}^{n-1})=\frac{1}{2}(I-\mathcal{P})\Delta\mathcal{P}(\boldsymbol{v}^n+\boldsymbol{v}^{n-1})\\ =&\frac{1}{2}\nabla p_{\mathrm{s}}(\boldsymbol{v}^n+\boldsymbol{v}^{n-1}).\end{aligned}\tag{A.30}$$

To see the consistency of the scheme, take $\mathcal{P}-I$ on both sides of (A.29) and change $n+1$ to n, we get

$$\frac{(\mathcal{P}-I)\boldsymbol{v}^n}{\Delta t}-\nabla p^{n-1}+\frac{1}{2}(I-\mathcal{P})\Delta(\boldsymbol{v}^n+\mathcal{P}\boldsymbol{v}^{n-1})=0$$

Add it to (A.29), we get

$$\frac{\boldsymbol{v}^{n+1}-\boldsymbol{v}^n}{\Delta t}+\nabla q=\frac{1}{2}\Delta(\boldsymbol{v}^{n+1}+\boldsymbol{v}^n)$$

where

$$\nabla q=\nabla p^n-\nabla p^{n-1}+\frac{1}{2}(I-\mathcal{P})\Delta(\boldsymbol{v}^n+\mathcal{P}\boldsymbol{v}^{n-1})+\frac{1}{2}\Delta(I-\mathcal{P})\boldsymbol{v}^n$$

Plugging in (A.30), after some calculation, we get

$$\nabla q=\nabla p_{\mathrm{s}}\left(\boldsymbol{v}^n+\frac{1}{2}\boldsymbol{v}^{n-1}-\frac{1}{2}\boldsymbol{v}^{n-2}\right)+\nabla\nabla\cdot\boldsymbol{v}^n.\tag{A.31}$$

Without $\nabla\nabla\cdot\boldsymbol{v}^n$, it is 2nd order accurate at $t^{n+1/2}$. Since the original NSE satisfies $\nabla\cdot\boldsymbol{u}=0$, the truncation error is $O(\Delta t^2)$.

A.2.3 Johnston and Liu [JL], E and Liu [EL], Guermond and Shen [GS1]

$$\frac{\boldsymbol{u}^{n+1}-\boldsymbol{u}^{n}}{\Delta t}+\frac{3}{2}\nabla p_{\mathrm{s}}(\boldsymbol{u}^{n})-\frac{1}{2}\nabla p_{\mathrm{s}}(\boldsymbol{u}^{n-1})=\frac{1}{2}\Delta(\boldsymbol{u}^{n+1}+\boldsymbol{u}^{n}),\qquad \boldsymbol{u}^{n+1}|_{\Gamma}=0. \tag{A.32}$$

Proposition 3 *The actual computed pressure used in Chorin&Temam and all the 2nd order projection method are listed in Table 3:*

As one can see, some method can achieve better approximation of pressure by choosing the way in Table 2 to compute pressure at the appropriate time level.

Author	pressure practically computed	order of accuracy when using exact velocity
[Ch];[Te]	$\nabla p^n = \nabla p_{\rm S}(\boldsymbol{u}^n) + \nabla\nabla\cdot\boldsymbol{u}^n$	1
[vK];[BCG]	$\nabla p^n = \frac{1}{2}\nabla p_{\rm S}(\boldsymbol{u}^n + \boldsymbol{u}^{n-1}) + \frac{1}{2}\nabla\nabla\cdot\boldsymbol{u}^n$	1 but 2nd order at $n-1/2$
[OID]	$\nabla p^{n+1/2} = \nabla p_{\rm S}(\boldsymbol{u}^{n+1}) + \frac{(I-\mathcal{P})\boldsymbol{u}^{n+1}}{\Delta t}$ $= \frac{1}{2}\nabla p_{\rm S}(3\boldsymbol{u}^{n+1} - \boldsymbol{u}^n)$ $+\frac{1}{2}\nabla\nabla\cdot\boldsymbol{u}^{n+1}$	1 but 2nd order at $n+3/2$
[TMV]	$\nabla p^n = \nabla p_{\rm S}(\boldsymbol{u}^n)$	2
[KM]	$\nabla p^{n+1/2} = \frac{(I-\mathcal{P})\boldsymbol{u}^n}{\Delta t} - \frac{1}{2}\nabla\cdot\boldsymbol{u}^n$ $= \frac{1}{2}\nabla p_{\rm S}(\boldsymbol{v}^{n+1} + \boldsymbol{v}^n)$	2
[JL]; [EL]; [GS1]	$\nabla p^n = \nabla p_{\rm S}(\boldsymbol{u}^n)$	2

Author	equation of ϕ^n
[Ch];[Te];[KM]	$\frac{\phi^{n+1}}{\Delta t} - \Delta\phi^{n+1} - p_{\rm S}^{n+1} = 0$
[vK];[BCG]	$\frac{\phi^{n+1}}{\Delta t} - \Delta(\phi^{n+1} - \phi^n) - (p_{\rm S}^{n+1} - p_{\rm S}^n) = 0$
[OID]; [TMV]	$\frac{\phi^{n+1}}{\Delta t} - \Delta\phi^{n+1} - (p_{\rm S}^{n+1} - p_{\rm S}^n) = 0$
[JL]; [EL]	$\frac{\phi^{n+1}-\phi^n}{\Delta t} - \Delta\phi^{n+1} - (p_{\rm S}^{n+1} - p_{\rm S}^n) = 0$

A.3 Analysis of projection methods

Proposition 4 *Consider all the first order projection methods with Dirichlet boundary condition. For any of them, $\mathcal{P}\boldsymbol{u}^n$ satisfies*

$$\frac{\mathcal{P}\boldsymbol{u}^{n+1} - \mathcal{P}\boldsymbol{u}^n}{\Delta t} + \nabla p_s(\mathcal{P}\boldsymbol{u}^{n+1}) = \Delta\mathcal{P}\boldsymbol{u}^{n+1} + \mathcal{P}\boldsymbol{f}^n. \tag{A.33}$$

The equation satisfied by $\nabla\phi^n = \boldsymbol{u}^n - \mathcal{P}\boldsymbol{u}^n$ are listed in Table 4

A.3.1 Chorin [Ch]; Temam [Te]

Consider

$$\frac{\boldsymbol{u}^{n+1} - \mathcal{P}\boldsymbol{u}^n}{\Delta t} = \Delta\boldsymbol{u}^{n+1} + \mathcal{P}\boldsymbol{f}^n, \qquad \boldsymbol{u}^{n+1}|_\Gamma = \boldsymbol{g} \tag{A.34}$$

Recall $\nabla p_{\rm S}(\boldsymbol{u}) = (\Delta\mathcal{P} - \mathcal{P}\Delta)\boldsymbol{u}$, we have

$$\Delta\boldsymbol{u} = \Delta\mathcal{P}\boldsymbol{u} + \Delta(I - \mathcal{P})\boldsymbol{u} = \nabla p_{\rm S}(\boldsymbol{u}) + \mathcal{P}\Delta\boldsymbol{u} + \Delta(I - \mathcal{P})\boldsymbol{u}. \tag{A.35}$$

So, (A.34) can be rewritten as

$$\mathcal{P}\frac{\boldsymbol{u}^{n+1} - \boldsymbol{u}^n}{\Delta t} + \frac{(I - \mathcal{P})\boldsymbol{u}^{n+1}}{\Delta t} = \nabla p_{\rm S}(\boldsymbol{u}^{n+1}) + \mathcal{P}\Delta\boldsymbol{u}^{n+1} + \Delta(I - \mathcal{P})\boldsymbol{u}^{n+1} + \mathcal{P}\boldsymbol{f}^n.$$

$$\mathcal{P}\left(\frac{\boldsymbol{u}^{n+1}-\boldsymbol{u}^n}{\Delta t}-\Delta\boldsymbol{u}^{n+1}-\boldsymbol{f}^n\right)+\frac{(I-\mathcal{P})\boldsymbol{u}^{n+1}}{\Delta t}-\nabla p_{\mathrm{S}}(\boldsymbol{u}^{n+1})-\Delta(I-\mathcal{P})\boldsymbol{u}^{n+1}=0$$

Since it is of the form $\mathcal{P}\boldsymbol{a}+\nabla\phi=0$, we must have

$$\mathcal{P}\left(\frac{\boldsymbol{u}^{n+1}-\boldsymbol{u}^n}{\Delta t}-\Delta\boldsymbol{u}^{n+1}-\boldsymbol{f}^n\right)=0 \tag{A.36}$$

and

$$\frac{(I-\mathcal{P})\boldsymbol{u}^{n+1}}{\Delta t}-\Delta(I-\mathcal{P})\boldsymbol{u}^{n+1}-\nabla p_{\mathrm{S}}(\boldsymbol{u}^{n+1})=0. \tag{A.37}$$

We can rewrite (A.36) as

$$\frac{\mathcal{P}\boldsymbol{u}^{n+1}-\mathcal{P}\boldsymbol{u}^n}{\Delta t}+\nabla p_{\mathrm{S}}(\mathcal{P}\boldsymbol{u}^{n+1})=\Delta\mathcal{P}\boldsymbol{u}^{n+1}+\mathcal{P}\boldsymbol{f}^n \tag{A.38}$$

where we have used $\nabla p_{\mathrm{S}}(\boldsymbol{u})=\nabla p_{\mathrm{S}}(\mathcal{P}\boldsymbol{u})$. Let

$$\boldsymbol{u}=\mathcal{P}\boldsymbol{u}+\nabla\phi \tag{A.39}$$

Then, (A.37) can be written as

$$\frac{\phi^{n+1}}{\Delta t}-\Delta\phi^{n+1}-p_{\mathrm{S}}^{n+1}=0 \tag{A.40}$$

which is a gauge formulation. But it is not the ψ used in

$$\boldsymbol{u}=\boldsymbol{a}+\nabla\psi.$$

Indeed, $\phi^{n+1}=-\psi^{n+1}+\psi^n$. This can also be seen from the later section on [JL], where we have the difference of pressure as forcing term:

$$\frac{\phi^{n+1}-\phi^n}{\Delta t}-\Delta\phi^{n+1}-(p_{\mathrm{S}}^{n+1}-p_{\mathrm{S}}^n)=0.$$

Back to (A.39). Note that the size of ϕ tells us two things. First

$$\mathcal{P}\boldsymbol{u}|_\Gamma=\boldsymbol{u}-\nabla\phi|_\Gamma$$

Second

$$\nabla\cdot\boldsymbol{u}=\Delta\phi.$$

boundary condition of $\mathcal{P}\boldsymbol{u}$ and comparison with Kim&Moin's scheme

For many of the projection methods, when used in practice, it is $\mathcal{P}\boldsymbol{u}^n$ that is used as the computed velocity. We have seen that for all the projection methods, $\mathcal{P}\boldsymbol{u}^n$ satisfies the right equation (A.38). But boundary condition of $\mathcal{P}\boldsymbol{u}^n$ in different method has different form and is coming from different ϕ^n.

In Chorin and Temam, the boundary condition of $\mathcal{P}\boldsymbol{u}^n$ is

$$\mathcal{P}\boldsymbol{u}^n|_\Gamma = \boldsymbol{u}^n - (I-\mathcal{P})\boldsymbol{u}^n = \boldsymbol{g}^n - \nabla\phi^n. \tag{A.41}$$

The inconsistent error is $-\nabla\phi^n$.

Recall that the first order scheme of Kim&Moin ([KM]) can be written as

$$\frac{\boldsymbol{u}^{n+1}-\mathcal{P}\boldsymbol{u}^n}{\Delta t} = \Delta\boldsymbol{u}^{n+1} + \mathcal{P}\boldsymbol{f}^n, \qquad \boldsymbol{u}^{n+1}|_\Gamma = \boldsymbol{g}^{n+1} + (I-\mathcal{P})\boldsymbol{u}^n$$

We will get the same equation of $\mathcal{P}\boldsymbol{u}$ and ϕ as in Chorin and Temam. But on Γ,

$$\mathcal{P}\boldsymbol{u}^n|_\Gamma = \boldsymbol{u}^n - (I-\mathcal{P})\boldsymbol{u}^n = \boldsymbol{g}^n + (I-\mathcal{P})(\boldsymbol{u}^{n-1}-\boldsymbol{u}^n) = \boldsymbol{g}^n - \nabla(\phi^n - \phi^{n-1}). \tag{A.42}$$

Since both Kim&Moin and Chorin and Temam have the same equation for ϕ, the inconsistent term on the boundary in Kim& Moin is smaller.

Kim&Moin and pressure increment formulation of Timmermans&etc.

Recall the ϕ equation in Kim&Moin is

$$\frac{\phi^{n+1}}{\Delta t} - \Delta\phi^{n+1} - p_{\mathrm{s}}^{n+1} = 0 \tag{A.43}$$

and on boundary

$$\mathcal{P}\boldsymbol{u}^n|_\Gamma = \boldsymbol{g}^n - \nabla(\phi^n - \phi^{n-1})$$

Now, let

$$\psi^n = \phi^n - \phi^{n-1}$$

Then (A.43) becomes

$$\frac{\psi^{n+1}}{\Delta t} - \Delta\psi^{n+1} - (p_{\rm S}^{n+1} - p_{\rm S}^n) = 0 \tag{A.44}$$

and

$$\mathcal{P}\boldsymbol{u}^n|_\Gamma = \boldsymbol{g}^n - \nabla\psi^n$$

Claim that the $\boldsymbol{u}$ defined by

$$\boldsymbol{u}^n = \mathcal{P}\boldsymbol{u}^n + \nabla\psi^n.$$

satisfies the Timmermans&etc scheme. This can be seen by adding up (A.38) and the gradient of (A.44), we get

$$\frac{\boldsymbol{u}^{n+1} - \mathcal{P}\boldsymbol{u}^n}{\Delta t} + \nabla p_{\rm S}^n = \Delta\boldsymbol{u}^{n+1} + \mathcal{P}\boldsymbol{f}^n,$$

where we have used the fact that $\nabla p_{\rm S}(\boldsymbol{u}) = \nabla p_{\rm S}(\mathcal{P}\boldsymbol{u})$ implies that the $p_{\rm S}$ computed from $\mathcal{P}\boldsymbol{u} + \nabla\phi$ and $\mathcal{P}\boldsymbol{u} + \nabla\psi$ are the same.

A.3.2 van Kan [vK]; Bell, Colella and Glaz [BCG]

$$\frac{\boldsymbol{u}^{n+1} - \mathcal{P}\boldsymbol{u}^n}{\Delta t} + \nabla p_{\rm S}(\boldsymbol{u}^n) + \nabla\nabla\cdot\boldsymbol{u}^n = \Delta\boldsymbol{u}^{n+1} + \mathcal{P}\boldsymbol{f}^n, \qquad \boldsymbol{u}^{n+1}|_\Gamma = \boldsymbol{g}$$

It can be rewritten as

$$\begin{aligned}&\mathcal{P}\frac{\boldsymbol{u}^{n+1} - \boldsymbol{u}^n}{\Delta t} + \frac{(I-\mathcal{P})\boldsymbol{u}^{n+1}}{\Delta t} + \nabla p_{\rm S}(\boldsymbol{u}^n) + \nabla\nabla\cdot\boldsymbol{u}^n \\ &= \mathcal{P}\Delta\boldsymbol{u}^{n+1} + \nabla p_{\rm S}(\boldsymbol{u}^{n+1}) + \Delta(I-\mathcal{P})\boldsymbol{u}^{n+1} + \mathcal{P}\boldsymbol{f}^n.\end{aligned}$$

Again, we can break it into two equations:

$$\mathcal{P}\frac{\boldsymbol{u}^{n+1}-\boldsymbol{u}^n}{\Delta t}=\mathcal{P}\Delta\boldsymbol{u}^{n+1}+\mathcal{P}\boldsymbol{f}^n$$

which is (A.38), and

$$\frac{(I-\mathcal{P})\boldsymbol{u}^{n+1}}{\Delta t}+\nabla(p_{\mathrm{S}}^n-p_{\mathrm{S}}^{n+1})+\nabla\nabla\cdot\boldsymbol{u}^n-\Delta(I-\mathcal{P})\boldsymbol{u}^{n+1}=0$$

Plug in $\nabla\phi=(I-\mathcal{P})\boldsymbol{u}$, we get

$$\frac{\phi^{n+1}}{\Delta t}-\Delta(\phi^{n+1}-\phi^n)-(p_{\mathrm{S}}^{n+1}-p_{\mathrm{S}}^n)=0 \tag{A.45}$$

A.3.3 Orszag, Israeli and Deville [OID]; Timmermans, Minev and Van De Vosse [TMV]

$$\frac{\boldsymbol{u}^{n+1}-\mathcal{P}\boldsymbol{u}^n}{\Delta t}+\nabla p_{\mathrm{S}}(\boldsymbol{u}^n)=\Delta\boldsymbol{u}^{n+1}+\mathcal{P}\boldsymbol{f}^n,\qquad \boldsymbol{u}^{n+1}|_{\Gamma}=\boldsymbol{g}$$

It can be rewritten as

$$\begin{aligned}&\mathcal{P}\frac{\boldsymbol{u}^{n+1}-\boldsymbol{u}^n}{\Delta t}+\frac{(I-\mathcal{P})\boldsymbol{u}^{n+1}}{\Delta t}+\nabla p_{\mathrm{S}}(\boldsymbol{u}^n)\\ =\ &\mathcal{P}\Delta\boldsymbol{u}^{n+1}+\nabla p_{\mathrm{S}}(\boldsymbol{u}^{n+1})+\Delta(I-\mathcal{P})\boldsymbol{u}^{n+1}+\mathcal{P}\boldsymbol{f}^n.\end{aligned}$$

Again, we can break it into two equations:

$$\mathcal{P}\frac{\boldsymbol{u}^{n+1}-\boldsymbol{u}^n}{\Delta t}=\mathcal{P}\Delta\boldsymbol{u}^{n+1}+\mathcal{P}\boldsymbol{f}^n$$

which is (A.38), and

$$\frac{(I-\mathcal{P})\boldsymbol{u}^{n+1}}{\Delta t}+\nabla(p_{\mathrm{S}}^n-p_{\mathrm{S}}^{n+1})-\Delta(I-\mathcal{P})\boldsymbol{u}^{n+1}=0$$

Plug in $\nabla\phi = (I - \mathcal{P})\boldsymbol{u}$, we get

$$\frac{\phi^{n+1}}{\Delta t} - \Delta\phi^{n+1} - (p_{\mathrm{S}}^{n+1} - p_{\mathrm{S}}^{n}) = 0 \tag{A.46}$$

A.3.4 Johnston and Liu [JL], E and Liu [EL], Guermond and Shen [GS1]

$$\frac{\boldsymbol{u}^{n+1} - \boldsymbol{u}^{n}}{\Delta t} + \nabla p_{\mathrm{S}}(\boldsymbol{u}^{n}) = \Delta\boldsymbol{u}^{n+1} + \mathcal{P}\boldsymbol{f}^{n}, \qquad \boldsymbol{u}^{n+1}|_{\Gamma} = \boldsymbol{g}$$

It can be rewritten as

$$\begin{aligned} &\mathcal{P}\frac{\boldsymbol{u}^{n+1} - \boldsymbol{u}^{n}}{\Delta t} + (I - \mathcal{P})\frac{\boldsymbol{u}^{n+1} - \boldsymbol{u}^{n}}{\Delta t} + \nabla p_{\mathrm{S}}(\boldsymbol{u}^{n}) \\ &= \mathcal{P}\Delta\boldsymbol{u}^{n+1} + \nabla p_{\mathrm{S}}(\boldsymbol{u}^{n+1}) + \Delta(I - \mathcal{P})\boldsymbol{u}^{n+1} + \mathcal{P}\boldsymbol{f}^{n}. \end{aligned}$$

Again, we can break it into two equations:

$$\mathcal{P}\frac{\boldsymbol{u}^{n+1} - \boldsymbol{u}^{n}}{\Delta t} = \mathcal{P}\Delta\boldsymbol{u}^{n+1} + \mathcal{P}\boldsymbol{f}^{n}$$

which is (A.38), and

$$(I - \mathcal{P})\frac{\boldsymbol{u}^{n+1} - \boldsymbol{u}^{n}}{\Delta t} + \nabla(p_{\mathrm{S}}^{n} - p_{\mathrm{S}}^{n+1}) - \Delta(I - \mathcal{P})\boldsymbol{u}^{n+1} = 0$$

Plug in $\nabla\phi = (I - \mathcal{P})\boldsymbol{u}$, we get

$$\frac{\phi^{n+1} - \phi^{n}}{\Delta t} - \Delta\phi^{n+1} - (p_{\mathrm{S}}^{n+1} - p_{\mathrm{S}}^{n}) = 0 \tag{A.47}$$

A.4 Normal modes analysis

On the PDE level, we have

$$\partial_t\boldsymbol{u} + \nabla p_{\mathrm{S}}(\boldsymbol{u}) = \Delta\boldsymbol{u}, \qquad \boldsymbol{u}|_{\Gamma} = 0 \tag{A.48}$$

Assume $\boldsymbol{u}(t) = e^{\sigma t}\boldsymbol{u}$, we get

$$\sigma \boldsymbol{u} + \nabla p_{\mathrm{s}}(\boldsymbol{u}) = \Delta \boldsymbol{u}.$$

Assume the domain is $[-1, 1] \times [0, 2\pi]$ and assume periodic boundary condition in y variable. Define the Fourier coefficient

$$\hat{\boldsymbol{u}}(x, k) = \frac{1}{2\pi} \int_0^{2\pi} \boldsymbol{u}(x, y) e^{-iky} dy.$$

From now on, we will work on the Fourier coefficients and will drop $\hat{}$ for simplicity of notation. Then we know

$$(\Delta_k - \sigma)u = \nabla_k p, \qquad \boldsymbol{u}(\pm 1) = 0,$$

$$\Delta_k p = 0, \qquad \partial_x p(\pm 1) = -ik\partial_x v.$$

By linearity, without loss of generality, we will take the anti-symmetric part of p only

$$p = \sinh kx.$$

Let

$$\mu^2 = -k^2 - \sigma$$

Then

$$(\partial_x^2 + \mu^2)u = k \cosh kx, \qquad u(\pm 1) = 0,$$

$$(\partial_x^2 + \mu^2)v = ik \sinh kx, \qquad v(\pm 1) = 0.$$

We get

$$u(x) = A\left(\frac{\cos \mu x}{\cos \mu} - \frac{\cosh kx}{\cosh k}\right), \qquad A = -\frac{k \cosh k}{k^2 + \mu^2} \tag{A.49}$$

$$v(x) = B\left(\frac{\sin \mu x}{\sin \mu} - \frac{\sinh kx}{\sinh k}\right), \qquad B = -i\frac{k \sinh k}{k^2 + \mu^2} \tag{A.50}$$

We compute

$$\partial_x p + ik\partial_x v = k\cosh kx + \frac{k^2 \sinh k}{k^2+\mu^2}\left(\frac{\mu\cos\mu x}{\sin\mu} - \frac{k\cosh kx}{\sinh k}\right)$$

The satisfaction of boundary condition $\partial_x p = -ik\partial_x v$ at $x = \pm 1$ leads to

$$k\coth k + \frac{k^2}{k^2+\mu^2}\left(\mu\cot\mu - k\coth k\right) = 0$$

which can be simplified to be

$$\mu\tan\mu + k\tanh k = 0 \tag{A.51}$$

which indeed leads to $\partial_x u + ikv = 0$.

A.4.1 normal modes analysis of 1st order numerical scheme

We decompose $\boldsymbol{u} = \mathcal{P}\boldsymbol{u} + \nabla\phi$. For any of the scheme above, $\mathcal{P}\boldsymbol{u}$ satisfies (A.38) which is

$$\frac{\mathcal{P}\boldsymbol{u}^{n+1} - \mathcal{P}\boldsymbol{u}^n}{\Delta t} + \nabla p_{\rm s}(\mathcal{P}\boldsymbol{u}^{n+1}) = \Delta\mathcal{P}\boldsymbol{u}^{n+1}$$

Let $\mathcal{P}\boldsymbol{u}^n = \kappa^n\mathcal{P}\boldsymbol{u}$ and $\mathcal{P}\boldsymbol{u} = \boldsymbol{u}^* = (u^*, v^*)$. Then,

$$\left(\Delta_k - \frac{1-\frac{1}{\kappa}}{\Delta t}\right)u^* = \partial_x p_{\rm s}$$

We will take the anti-symmetric part of $p_{\rm s}$ only

$$p_{\rm s} = \sinh kx.$$

Let

$$\tilde{\mu}^2 = -k^2 - \frac{\kappa - 1}{\kappa\Delta t} \tag{A.52}$$

Then

$$(\partial_x^2 + \tilde{\mu}^2)u^* = k\cosh kx, \qquad u^*(\pm 1) = 0$$

We get

$$u^*(x) = A\left(\frac{\cos\tilde{\mu}x}{\cos\tilde{\mu}} - \frac{\cosh kx}{\cosh k}\right), \qquad A = -\frac{k\cosh k}{k^2+\tilde{\mu}^2} \tag{A.53}$$

From $\partial_x u^* + ikv^* = 0$, we get

$$v^*(x) = iB\left(\frac{\tilde{\mu}}{k}\frac{\sin\tilde{\mu}x}{\cos\tilde{\mu}} + \frac{\sinh kx}{\cosh k}\right), \qquad B = \frac{k\cosh k}{k^2+\tilde{\mu}^2} \tag{A.54}$$

Note that from (A.52), we get

$$\kappa = \frac{1}{1+\Delta t(\tilde{\mu}^2+k^2)} \tag{A.55}$$

To continue, we will need to work on the equation of ϕ for different scheme. Once get ϕ, we can get $\boldsymbol{u} = \boldsymbol{u}^* + \nabla\phi$ and also the pressure p by the formula of pressure in Table 1 (see also Table 3). A equation corresponds to (A.51) will be obtained from enforcing the $v(\pm 1) = 0$ boundary condition. Then the size of boundary layer in both $\boldsymbol{u}$ and p will be analyzed.

The results are summarized in the following proposition

Proposition 5 *Consider the normal modes analysis of all the first order projection methods. With $\lambda^2 = k^2 + 1/\Delta t$, [Ch] and [Te] satisfy*

$$\tilde{\mu}\tan\tilde{\mu} + k\tanh k - \Delta t k^2(k^2+\tilde{\mu}^2)\left(\frac{\tanh\lambda}{\lambda} - \frac{\tanh k}{k}\right) = 0. \tag{A.56}$$

With $\lambda^2 = k^2 + 1/\Delta t$, [KM], [OID] and [TMV] satisfy

$$\tilde{\mu}\tan\tilde{\mu} + k\tanh k + \Delta t^2 k^2(k^2+\tilde{\mu}^2)^2\left(\frac{\tanh\lambda}{\lambda} - \frac{\tanh k}{k}\right) = 0. \tag{A.57}$$

Author	size of boundary layer in $\boldsymbol{u}$			size of boundary layer in p		
	L^∞	L^2	H^1	L^∞	L^2	H^1
[Ch];[Te];	Δt	$\Delta t^{5/4}$	$\Delta t^{3/4}$	$\Delta t^{1/2}$	$\Delta t^{3/4}$	$\Delta t^{1/4}$
[KM]	Δt	$\Delta t^{5/4}$	$\Delta t^{3/4}$	no boundary layer		
[vK];[BCG]	Δt^2	$\Delta t^{5/2}$	$\Delta t^{3/2}$	Δt	$\Delta t^{3/2}$	$\Delta t^{1/2}$
[OID]	Δt^2	$\Delta t^{9/4}$	$\Delta t^{7/4}$	$\Delta t^{3/2}$	$\Delta t^{7/4}$	$\Delta t^{5/4}$
[TMV]	Δt^2	$\Delta t^{9/4}$	$\Delta t^{7/4}$	no boundary layer		
[JL]; [EL]; [GS1]	no boundary layer			no boundary layer		

With $\lambda^2 = k^2 + \frac{\kappa}{(\kappa-1)\Delta t} = k^2 - \frac{1}{\Delta t^2(\tilde{\mu}^2+k^2)}$, [vK] and [BCG] satisfy (A.57). Moreover, we have the following table, (please note that many methods wisely choose $\mathcal{P}\boldsymbol{u}$ as computed velocity, then there is no velocity boundary layer as we have seen from the equation of $\boldsymbol{u}^*$.)

Remark: (If $\frac{\kappa-1}{\kappa} \in \mathbb{R}$, then $0 < \kappa < 1$) Note that when $\frac{\kappa-1}{\kappa} \in \mathbb{R}$, $\tilde{\mu}$ defined by (A.52) can be either real number or pure imaginary number. When $\tilde{\mu} \in \mathbb{R}$, by (A.55), $0 < \kappa < 1$. When $\tilde{\mu}$ is purely imaginary, we claim $|\tilde{\mu}|^2 \leq k^2$, so we would still have $0 < \kappa < 1$. To prove the claim, use negative argument and assume $|\tilde{\mu}| > |k|$. Let $\tilde{\mu} = i\bar{\mu}$, then

$$\tilde{\mu}\tan\tilde{\mu} = -\bar{\mu}\tanh\bar{\mu}, \qquad k^2 + \tilde{\mu}^2 = k^2 - \bar{\mu}^2.$$

Under the assumption $|\bar{\mu}| > |k|$, we always have $|\lambda| > |k|$. Note two things

$$x\tanh x \uparrow \text{ when } x > 0, x \uparrow, \qquad \tanh x/x \downarrow \text{ when } x > 0, x \uparrow$$

Using these facts and $|\bar{\mu}| > |k|$, $|\lambda| > |k|$, one can verify that the left hand side of both (A.56) and (A.57) are negative and thus contradict.

Remark: Assume $\tilde{\mu} = i\bar{\mu}$ with $\bar{\mu} \in \mathbb{R}$, one can compute that

$$\begin{aligned}&\left\langle -\Delta\mathcal{P}\boldsymbol{u}, \mathcal{P}\boldsymbol{u}\right\rangle = \left\langle -\Delta_k u^*, u^*\right\rangle + \left\langle -\Delta_k v^*, v^*\right\rangle \\ =&B^2\left(\frac{(k^2-\bar{\mu}^2)^2}{k^2}\left(1/\cosh^2\bar{\mu} + \tanh\bar{\mu}/\bar{\mu}\right) - 2\frac{k^2-\bar{\mu}^2}{k^2}\left(k\tanh k - \bar{\mu}\tanh\bar{\mu}\right)\right)\end{aligned} \tag{A.58}$$

Since $\bar{\mu} \in \mathbb{R}$, the first term on the right hand side is positive. We want to show that the second term is also positive.

For [Ch] and [Te], plug in (A.56), the second term of (A.58) becomes

$$-2\Delta t(k^2-\bar{\mu}^2)^2\left(\frac{\tanh\lambda}{\lambda} - \frac{\tanh k}{k}\right)$$

which is positive because $|\lambda| > |k|$. Therefore, $\left\langle -\Delta\mathcal{P}\boldsymbol{u}, \mathcal{P}\boldsymbol{u}\right\rangle > 0$ which implies $|\kappa| \leq 1$.

For the other first order scheme, plug (A.57) into (A.58), the second term of (A.58) becomes

$$2\Delta t^2(k^2-\bar{\mu}^2)^3\left(\frac{\tanh\lambda}{\lambda} - \frac{\tanh k}{k}\right) \tag{A.59}$$

If $|\bar{\mu}| > |k|$, we first have $|\lambda| > |k|$, therefore (A.59) is positive. So $\left\langle -\Delta\mathcal{P}\boldsymbol{u}, \mathcal{P}\boldsymbol{u}\right\rangle > 0$, which implies $|\kappa| \leq 1$. If $|\bar{\mu}| \leq |k|$, we get $|\kappa| < 1$ directly from (A.55). So we conclude $|\kappa| \leq 1$.

Remark: For general $\tilde{\mu} = a + bi$, we have

$$\left\langle -\Delta\mathcal{P}\boldsymbol{u}, \overline{\mathcal{P}\boldsymbol{u}}\right\rangle = |B|^2\frac{\tilde{\mu}^2+k^2}{|\cos\tilde{\mu}|^2}\left(\frac{\sin 2a}{2a}\frac{k^2-|\tilde{\mu}|^2}{k^2} + \frac{\sinh 2b}{2b}\frac{k^2+|\tilde{\mu}|^2}{k^2} - \frac{2}{k}|\cos\tilde{\mu}|^2\right)$$

Chorin [Ch]; Temam [Te]

Recall the ϕ equation (A.40), which under our consideration can be written as

$$(\Delta_k - \frac{1}{\Delta t})\phi = -\sinh kx, \qquad \partial_x\phi(\pm 1) = 0 \tag{A.60}$$

Let

$$\lambda^2 = k^2 + \frac{1}{\Delta t} \tag{A.61}$$

Then, the solution satisfying the boundary condition should be of the form

$$\phi = C\left(\frac{\sinh \lambda x}{\lambda \cosh \lambda} - \frac{\sinh kx}{k \cosh k}\right).$$

Once plug it into (A.60), we see that $\Delta_k - \frac{1}{\Delta t}$ kills the λ modes and Δ_k kills the k modes. So,

$$-\frac{1}{\Delta t}C\left(-\frac{\sinh kx}{k\cosh k}\right) = -\sinh kx.$$

So,

$$C = -\Delta t k \cosh k.$$

Then,

$$u = u^* + \partial_x\phi = A\left(\frac{\cos \tilde{\mu}x}{\cos \tilde{\mu}} - \frac{\cosh kx}{\cosh k}\right) + C\left(\frac{\cosh \lambda x}{\cosh \lambda} - \frac{\cosh kx}{\cosh k}\right) \tag{A.62}$$

$$v = v^* + ik\phi = iB\left(\frac{\tilde{\mu}}{k}\frac{\sin \tilde{\mu}x}{\cos \tilde{\mu}} + \frac{\sinh kx}{\cosh k}\right) + iC\left(\frac{k}{\lambda}\frac{\sinh \lambda x}{\cosh \lambda} - \frac{\sinh kx}{\cosh k}\right) \tag{A.63}$$

$$p = p_{\mathrm{s}} + \Delta_k\phi = \sinh kx + C\frac{1}{\Delta t}\frac{1}{\lambda}\frac{\sinh \lambda x}{\cosh \lambda} \tag{A.64}$$

From $v(\pm 1) = 0$, we get

$$\tilde{\mu}\tan \tilde{\mu} + k\tanh k - \Delta t k(k^2 + \tilde{\mu}^2)\left(\frac{k}{\lambda}\tanh \lambda - \tanh k\right) = 0 \tag{A.65}$$

Given Δt, for any k, on each interval $((j-1/2)\pi, (j+1/2)\pi)$, there is a $\tilde{\mu}$ satisfies (A.65) and

$$\tilde{\mu} = \mu + O(\Delta t)$$

Then, from (A.55),

$$\kappa = e^{\sigma \Delta t} + O(\Delta t^2).$$

λ mode is the boundary layer mode. Since $\lambda \geq 1/\sqrt{\Delta t}$, we see that for fixed k, the L^∞ norm of boundary layer mode is $O(\Delta t)$ in $\boldsymbol{u}$ and $O(\Delta t^{1/2})$ in p. Note that

$$\int_{-1}^{1} \left(\frac{\cosh \lambda x}{\cosh \lambda} \right)^2 dx = \frac{1 + \frac{\sinh 2\lambda}{2\lambda}}{\cosh^2 \lambda} = O\left(\frac{1}{\lambda} \right) \tag{A.66}$$

which is $O(\sqrt{\Delta t})$ in this case. Similar result for $\int_{-1}^{1} \left(\frac{\sinh \lambda x}{\cosh \lambda} \right)^2 dx$. The L^2 norm of boundary layer mode is $O(\Delta t^{5/4})$ in $\boldsymbol{u}$ and $O(\Delta t^{3/4})$ in p. The H^1 norm of boundary layer mode is $O(\Delta t^{3/4})$ in $\boldsymbol{u}$ and $O(\Delta t^{1/4})$ in p

Kim and Moin [KM]

For Kim and Moin, from

$$\boldsymbol{u}^{n+1}|_\Gamma = (I - \mathcal{P})\boldsymbol{u}^n = \nabla \phi^n,$$

we get

$$\partial_n \phi^n|_\Gamma = \boldsymbol{n} \cdot \boldsymbol{u}^{n+1}.$$

But we also have

$$\boldsymbol{n} \cdot (\boldsymbol{u}^{n+1} - \boldsymbol{u}^n)|_\Gamma = -\boldsymbol{n} \cdot \mathcal{P}\boldsymbol{u}^n = 0.$$

So, for normal modes analysis, the boundary condition of ϕ is $\partial_x \phi(\pm 1) = 0$.

Comparing with Chorin and Temam, we have the same equation of $\boldsymbol{u}^*$ and ϕ and moreover the same boundary condition. So, we have the same $\boldsymbol{u}^*$ and ϕ and hence same $\boldsymbol{u}$.

Now note that we no longer have $v|_\Gamma = 0$, instead, we get

$$v^{n+1}|_\Gamma = v^n - v^{*,n}.$$

So, $(\kappa - 1)v(\pm 1) = -v^*(\pm 1)$. Plug in the equation of v and v^*, we get

$$\tilde{\mu}\tan\tilde{\mu} + k\tanh k + \Delta t^2(\tilde{\mu}^2 + k^2)^2 k\left(\frac{k}{\lambda}\tanh\lambda - \tanh k\right) = 0 \tag{A.67}$$

So,

$$\tilde{\mu} = \mu + O(\Delta t^2).$$

The pressure used in [KM] is

$$p^n = \frac{\phi^n}{\Delta t} - \Delta\phi^n.$$

Note that $\frac{1}{\Delta t} - \Delta_k$ exactly kills the λ modes, which is the boundary layer, therefore there is no pressure boundary layer. Indeed, we get

$$p = \frac{1}{\Delta t}C\left(-\frac{\sinh kx}{k\cosh k}\right) = \sinh kx.$$

van Kan [vK]; Bell, Colella and Glaz [BCG]

Recall the ϕ equation (A.45), which under our consideration can be written as

$$(\Delta_k - \frac{\kappa}{(\kappa-1)\Delta t})\phi = -\sinh kx, \qquad \partial_x\phi(\pm 1) = 0 \tag{A.68}$$

Let

$$\lambda^2 = k^2 + \frac{\kappa}{(\kappa-1)\Delta t} \tag{A.69}$$

Then, the solution satisfying the boundary condition should be of the form

$$\phi = C\left(\frac{\sinh\lambda x}{\lambda\cosh\lambda} - \frac{\sinh kx}{k\cosh k}\right).$$

Once plug it into (A.68), we see that $\Delta_k - \frac{\kappa}{(\kappa-1)\Delta t}$ kills the λ modes and Δ_k kills the k modes. So,

$$-\frac{\kappa}{(\kappa-1)\Delta t}C\left(-\frac{\sinh kx}{k\cosh k}\right) = -\sinh kx.$$

So,

$$C = -\frac{(\kappa-1)\Delta t}{\kappa}k\cosh k.$$

From (A.52), we know

$$\frac{\kappa-1}{\kappa} = -\Delta t(\tilde{\mu}^2 + k^2). \tag{A.70}$$

So,

$$C = \Delta t^2(\tilde{\mu}^2 + k^2)k\cosh k.$$

Then,

$$u = u^* + \partial_x\phi = A\left(\frac{\cos\tilde{\mu}x}{\cos\tilde{\mu}} - \frac{\cosh kx}{\cosh k}\right) + C\left(\frac{\cosh\lambda x}{\cosh\lambda} - \frac{\cosh kx}{\cosh k}\right) \tag{A.71}$$

$$v = v^* + ik\phi = iB\left(\frac{\tilde{\mu}}{k}\frac{\sin\tilde{\mu}x}{\cos\tilde{\mu}} + \frac{\sinh kx}{\cosh k}\right) + iC\left(\frac{k}{\lambda}\frac{\sinh\lambda x}{\cosh\lambda} - \frac{\sinh kx}{\cosh k}\right) \tag{A.72}$$

$$\begin{aligned} p &= p_{\mathrm{s}} + \Delta_k\phi = \sinh kx + C\frac{\kappa}{(\kappa-1)\Delta t}\frac{1}{\lambda}\frac{\sinh\lambda x}{\cosh\lambda} \\ &= \sinh kx - k\cosh k\frac{1}{\lambda}\frac{\sinh\lambda x}{\cosh\lambda} \end{aligned} \tag{A.73}$$

From $v(\pm 1) = 0$, we get

$$\tilde{\mu}\tan\tilde{\mu} + k\tanh k + \Delta t^2(\tilde{\mu}^2 + k^2)^2 k\left(\frac{k}{\lambda}\tanh\lambda - \tanh k\right) = 0 \tag{A.74}$$

Given Δt, for any k, on each interval $((j-1/2)\pi, (j+1/2)\pi)$, there is a $\tilde{\mu}$ satisfies (A.74), and

$$\tilde{\mu} = \mu + O(\Delta t^2).$$

Then, from (A.55),

$$\kappa = e^{\sigma \Delta t} + O(\Delta t^2).$$

λ mode is the boundary layer mode. Since $C = O(\Delta t^2)$ and $\lambda = O(1/\Delta t)$, we see that for fixed k, the L^∞ norm of the boundary layer mode is $O(\Delta t^2)$ in $\boldsymbol{u}$ and $O(\Delta t)$ in p. Using (A.66), which is of size $O(\Delta t)$ now, we get that the L^2 norm of the boundary layer mode is $O(\Delta t^{5/2})$ in $\boldsymbol{u}$ and $O(\Delta t^{3/2})$ in p. The H^1 norm of the boundary layer mode is $O(\Delta t^{3/2})$ in $\boldsymbol{u}$ and $O(\Delta t^{1/2})$ in p.

Orszag, Israeli and Deville [OID]; Timmermans, Minev and Van De Vosse [TMV]

Recall the ϕ equation (A.46), which under our consideration can be written as

$$(\Delta_k - \frac{1}{\Delta t})\phi = -\left(1 - \frac{1}{\kappa}\right) \sinh kx, \qquad \partial_x \phi(\pm 1) = 0 \tag{A.75}$$

Let

$$\lambda^2 = k^2 + \frac{1}{\Delta t} \tag{A.76}$$

Then, the solution satisfying the boundary condition should be of the form

$$\phi = C\left(\frac{\sinh \lambda x}{\lambda \cosh \lambda} - \frac{\sinh kx}{k \cosh k}\right).$$

Once plug it into (A.75), we see that $\Delta_k - \frac{1}{\Delta t}$ kill the λ modes and Δ_k kills the k modes. So,

$$-\frac{1}{\Delta t} C \left(-\frac{\sinh kx}{k \cosh k} \right) = -\left(1 - \frac{1}{\kappa} \right) \sinh kx.$$

So,

$$C = -\Delta t \left(1 - \frac{1}{\kappa} \right) k \cosh k.$$

From (A.55), we know

$$1 - \frac{1}{\kappa} = -\Delta t (\tilde{\mu}^2 + k^2). \tag{A.77}$$

So,

$$C = \Delta t^2 (\tilde{\mu}^2 + k^2) k \cosh k.$$

Then,

$$u = u^* + \partial_x \phi = A \left(\frac{\cos \tilde{\mu} x}{\cos \tilde{\mu}} - \frac{\cosh kx}{\cosh k} \right) + C \left(\frac{\cosh \lambda x}{\cosh \lambda} - \frac{\cosh kx}{\cosh k} \right) \tag{A.78}$$

$$v = v^* + ik\phi = iB \left(\frac{\tilde{\mu}}{k} \frac{\sin \tilde{\mu} x}{\cos \tilde{\mu}} + \frac{\sinh kx}{\cosh k} \right) + iC \left(\frac{k}{\lambda} \frac{\sinh \lambda x}{\cosh \lambda} - \frac{\sinh kx}{\cosh k} \right) \tag{A.79}$$

In [OID], $p^{n+1/2} = \nabla p_{\mathrm{S}} (2\boldsymbol{u}^{n+1} - \boldsymbol{u}^n) + \nabla \nabla \cdot \boldsymbol{u}^{n+1}$ is used as pressure. So

$$\begin{aligned} p &= \left(2\kappa^{1/2} - \frac{1}{\kappa^{1/2}} \right) p_{\mathrm{S}} + \kappa^{1/2} \Delta_k \phi = \left(2\kappa^{1/2} - \frac{1}{\kappa^{1/2}} \right) \sinh kx + \kappa^{1/2} C \frac{1}{\Delta t} \frac{1}{\lambda} \frac{\sinh \lambda x}{\cosh \lambda} \\ &= \left(2\kappa^{1/2} - \frac{1}{\kappa^{1/2}} \right) \sinh kx - \kappa^{1/2} \Delta t (\tilde{\mu}^2 + k^2) k \cosh k \frac{1}{\lambda} \frac{\sinh \lambda x}{\cosh \lambda} \end{aligned} \tag{A.80}$$

In [TMV], $p^n = \nabla p_{\mathrm{S}} (\boldsymbol{u}^n)$ is used, so

$$p = \sinh kx \tag{A.81}$$

From $v(\pm 1) = 0$, we get

$$\tilde{\mu} \tan \tilde{\mu} + k \tanh k + \Delta t^2 (\tilde{\mu}^2 + k^2)^2 k \left(\frac{k}{\lambda} \tanh \lambda - \tanh k \right) = 0 \tag{A.82}$$

Given Δt, for any k, on each interval $((j-1/2)\pi, (j+1/2)\pi)$, there is a $\tilde{\mu}$ satisfies (A.82), and

$$\tilde{\mu} = \mu + O(\Delta t^2).$$

Then, from (A.55),

$$\kappa = e^{\sigma \Delta t} + O(\Delta t^2).$$

λ mode is the boundary layer mode. Since $C = O(\Delta t^2)$ and $\lambda \geq 1/\sqrt{\Delta t}$, we see that for fixed k, the L^∞ norm of the boundary layer mode is $O(\Delta t^2)$ in $\boldsymbol{u}$ and $O(\Delta t^{3/2})$ in p used by [OID]. There is no pressure boundary layer in [TMV].

Using (A.66), which is of size $O(\Delta t^{1/2})$ now, we get that the L^2 norm of the boundary layer mode is $O(\Delta t^{9/4})$ in $\boldsymbol{u}$ and $O(\Delta t^{7/4})$ in p of [OID]. The H^1 norm of the boundary layer mode is $O(\Delta t^{7/4})$ in $\boldsymbol{u}$ and $O(\Delta t^{5/4})$ in p of [OID].

Johnston and Liu [JL], E and Liu [EL]

From the ϕ equation (A.47), we get

$$\left(\Delta_k - \frac{1 - \frac{1}{\kappa}}{\Delta t}\right)\phi = -\left(1 - \frac{1}{\kappa}\right)\sinh kx.$$

Notice that this time

$$\lambda^2 = k^2 + \frac{\kappa - 1}{\kappa \Delta t} = -\tilde{\mu}^2$$

So, the λ modes is actually $\tilde{\mu}$ mode and it is not boundary layer mode.

BIBLIOGRAPHY

[ADPS] B. F. Armaly, F. Durst, J. C. F. Pereira and B. Schönung, Experimental and theoretical investigation of backward-facing step flow, J. Fluid Mech. 127 (1983) 473-496.

[BBGS] T. Barth, P. Bochev, M. Gunzburger and J. Shadid, A taxonomy of consistently stabilized finite element methods for the Stokes problem, SIAM J. Sci. Comput. 25 (2004) 1585–1607.

[BCG] J. B. Bell, P. Colella and H. Glaz, A second-order projection method for the incompressible Navier-Stokes equations, J. Comp. Phys. 101 (1992) 334–348

[BCM] D. L. Brown, R. Cortez and M. L. Minion, Accurate projection methods for the incompressible Navier-Stokes equations, J. Comp. Phys. 168 (2001) 464–499.

[BP] O. Botella and R. Peyret, Benchmark spectral results on the lid-driven cavity flow, Comput. & Fluids, 27 (1998) 421–433.

[Ch] A. J. Chorin, Numerical solution of the Navier-Stokes equations, Math. Comp., 22 (1968) 745–762

[Ci] P. G. Ciarlet, *the Finite Element Method for Elliptic Problems*, North Holland, Amsterdam, 1977.

[EL] W. E and J.-G. Liu, Gauge method for viscous incompressible flows, Commun. Math. Sci. 1(2) (2003) 317–332.

[EL2] W. E and J.-G. Liu, Vorticity boundary condition and related issues for finite difference schemes, J. Comput. Phys. 124 (1996) 368–382.

[FV] B. Fraeijis de Veubeke, A conforming finite element for plate bending, Internat. J. Solids and Structures, 4 (1968), 95–108.

[GDN] M. Griebel, T. Dornseifer and T. Neunhoeffer, *Numerical simulation in fluid dynamics: a practical introduction*, SIAM, Philadelphia, 1998.

[GMS] J. L. Guermond, P. Minev and J. Shen, An overview of projection methods for incompressible flows, Comput. Methods Appl. Mech. Eng., to appear.

[GS1] J. L. Guermond and J. Shen, A new class of truly consistent splitting schemes for incompressible flows, J. Comp. Phys. 192 (2003) 262–276

[GS2] J. L. Guermond and J. Shen, Velocity-correction projection methods for incompressible flows, SIAM J. Numer. Anal. 41 (1) (2003) 112–134

[HP] W. D. Henshaw and N. A. Petersson, A split-step scheme for the incompressible Navier-Stokes equations, in *Numerical simulations of incompressible flows (Half Moon Bay, CA, 2001)*, 108–125, World Sci. Publishing, River Edge, NJ, 2003.

[JL] H. Johnston and J.-G. Liu, Accurate, stable and efficient Navier-Stokes solvers based on explicit treatment of the pressure term, J. Comp. Phys. 199 (1) (2004) 221–259.

[KM] J. Kim and P. Moin, Application of a fractional-step method to incompressible Navier-Stokes equations. J. Comp. Phys. 59 (1985) 308–323.

[LS] M. J. Lai and L. L. Schumaker, On the approximation power of splines on triangulated quadrangulations, SIAM J. Num. Anal., 36 (1999) 143–159.

[LLP] J.-G. Liu, J. Liu and R. Pego, Stability and convergence of efficient Navier-Stokes solvers via a commutator estimate, accepted by Comm. Pure Appl. Math.

[MPT] K. Morgan, J. Periaux and F. Thomasset (Editors), *Analysis of laminar flow over a backward-facing step: a GAMM-workshop*, Friedr Vieweg & Sohn, Braunschweig/Wiesbaden, Germany, 1984

[OID] S. A. Orszag, M. Israeli and M. Deville, Boundary conditions for incompressible flows. J. Sci. Comput. 1, (1986) 75–111.

[Pe] N. A. Petersson, Stability of pressure boundary conditions for Stokes and Navier-Stokes equations, J. Comp. Phys. 172 (2001) 40-70.

[Te] R. Temam, *Navier-Stokes Equations: Theory and Numerical Analysis.* AMS Chelsea, Providence, 2001.

[TMV] L. J. P. Timmermans, P. D. Minev and F. N. Van De Vosse, An approximate projection scheme for incompressible flow using spectral elements, Int. J. Numer. Methods Fluids 22 (1996) 673–688.

[vK] J. van kan, A second-order accurate pressure-correction scheme for viscous incompressible flow. SIAM J. Sci. Stat. Comput., 7 (3) (1986) 870–891

[WL] C. Wang and J.-G. Liu, Convergence of gauge method for incompressible flow, Math. Comp. 69 (2000) 1385–1407.